



Master of Science in  
Cultural Heritage Materials & Technologies



UNIVERSITY OF THE PELOPONNESE  
DEPARTMENT OF HISTORY, ARCHAEOLOGY  
AND CULTURAL RESOURCES MANAGEMENT



DEMOKRITOS  
NATIONAL CENTER  
FOR SCIENTIFIC RESEARCH  
“DEMOKRITOS”



NATIONAL  
OBSERVATORY  
OF ATHENS

**Master of Science in  
«Cultural Heritage Materials and Technologies»**

**EIRINI MITSI  
(1012202002007)**

**DIPLOMA THESIS:**

**Physico-chemical Characterization of Waterlogged  
Archaeological Wood  
from a Charred Medieval Shipwreck**

**SUPERVISING COMMITTEE:**

- **Prof. Anastasia Pournou**
- **Prof. Stamatios Boyatzis**

**EXAMINATION COMMITTEE:**

- **Prof. Anastasia Pournou**
- **Prof. Stamatios Boyatzis**
- **Prof. Nikolaos Zacharias**

**KALAMATA, FEBRUARY 2023**

## **Acknowledgements**

First, I would like to thank Dr George Koutsouflakis for providing the archaeological material and the *in situ* photos of the wreck.

My supervisors, Prof. Anastasia Pournou for the ongoing assistance throughout the process of conducting this study and the invaluable information and contribution on the material and research, and Prof. Stamatios Boyatzis for the analytical techniques of XRD and FTIR.

I would also like to thank Dr Alexios-Nikolaos Stefanis for running the experiment of Mercury Intrusion Porosimetry, and Athanasios Karampotsos for his technical support with SEM.

Special thanks, to Helen M. Bardas and Celia Valantou for their support.

Finally, I would like to thank the University of West Attica, and the Department of Conservation of Antiquities and Works of Art for providing access to their facilities and equipment for conducting this research.

## **Abstract**

In 2008, a partially burned wooden shipwreck, dating from the 12th century, was discovered off the port of Rhodes, Greece.

The shipwreck timbers presented a varied degree of charring consisting of uncharred, charred and semi-charred material, often encountered on the same piece of wood, which indicates considerably different consolidation requirements and poses a great challenge for their future conservation.

This study was set to characterize the morphology, and the physical, chemical and mechanical properties of the material, in order to assist in the development of an appropriate remedial conservation strategy.

The morphology of the archaeological wood was documented via scanning electron microscopy (SEM). The main physical properties were estimated gravimetrically whereas its porosity was evaluated by mercury intrusion porosimetry (MIP). For the charred and the semi-charred wood, proximate analysis was also undertaken. The mechanical properties were investigated using a modified Janka test and a fruit penetrometer. The chemistry of wood was examined with Fourier transform infrared spectroscopy (FTIR) for the organic part of wood, and energy dispersive spectroscopy (EDS) for its inorganic composition. Alterations on cellulose crystallinity were also assessed with X-ray diffraction (XRD).

Results regarding the morphology, clearly demonstrated the three distinct charring degrees of the material that exhibited significant ultrastructural differences, although the basic cellular anatomy of wood had been preserved. More specifically, the uncharred material showed signs of severe biodeterioration which is typical in waterlogged wood, while the semi-charred and charred wood exhibited alterations mainly owed to thermal exposure rather than bacterial or fungal decay. In addition, the semi-charred samples presented a varied degree of thermal degradation, reflecting its diverse exposure to the fire front, whereas the charred material presented “plastic deformation” that indicated fast pyrolysis of a wet wood, at high temperatures.

Physical properties confirmed that the exposure of wood to heat and its burial in the marine environment, has created three different waterlogged “materials”. In particular among the three charring conditions, the uncharred wood presented the lowest basic density, the highest shrinkage and an increased porosity mainly due to biodeterioration. In contrast, the semi-charred and the charred wood presented extremely low shrinkage, which was even lower than sound wood of the same species, whereas their porosity was only slightly increased.

All three charring conditions showed low hardness compared to sound wood, attributed either to biodeterioration or/and to thermal degradation. Furthermore, hardness values of the semi-charred wood were in accordance with the morphological observations, showing the transitional nature of the material, extending from the charred to the uncharred zone. The results obtained regarding the residual chemistry of the material were highly correlated with its physico-mechanical properties and its morphology. Uncharred wood was found to be chemically similar to biodeteriorated wood, with depleted carbohydrates, increased relative lignin content, and elevated sulfur and iron concentrations. The semi-charred material presented a chemical profile comparable to thermally modified wood where hemicelluloses were reduced, cellulose crystallinity was increased, and lignin was not significantly altered compared to sound wood. In contrast in charred wood, polysaccharides and lignin were almost absent due to pyrolysis, making its organic chemistry similar to charcoals. The inorganic chemistry of the wood exposed to the fire showed that, towards the charred areas, sulfur, iron and oxygen concentrations were decreasing, while the carbon content was increasing.

Based on the results of the present study, it is evident that uncharred wood requires remedial conservation using consolidants, whereas semi-charred and charred wood may be left to air-dry without treatment. Nevertheless, a great challenge arises for conservators as the three charring conditions often coexist and the low porosity of the outer charred layer is not expected to facilitate the penetration of consolidants into the uncharred core of wood and impede its consolidation.

## Table of figures

<b>Fig. 1.1</b> The location of the shipwreck pinned on Google Earth map (Map data: 2017 <sup>©</sup> Google).....	1
<b>Figure 1.2</b> Wooden elements that shows traces of charring (Photo: V Mentogiannis, EUA <sup>©</sup> , with permission from Dr. G. Koutsouflakis) .....	4
<b>Figure 1.3</b> Frames of the west side, where the upper parts are severely charred (Photo: V. Mentogiannis, EUA <sup>©</sup> , with permission from Dr. G. Koutsouflakis).....	4
<b>Figure 2.1</b> Graphic representation of the imprint created by the (a) Brinell and (b) Vickers indenter. For each, the perpendicular diagonals (d1 and d2) are noted. ....	18
where $\pi$ = the mathematical constant ( $\sim 3.14159$ ), and $r$ = the radius of the projected contact area.....	20
<b>Figure 2.2</b> Graphic representation of (a) the ball penetrated at $\frac{1}{2}$ and $\frac{1}{4}$ of its diameter, and (b) their projected contact area with radius $R$ and $r$ respectively. ....	20
<b>Figure 2.3</b> Diagram of the geometrical calculation of the projected contact area's radius ( $r$ ). $R$ = ball radius, $e$ = extension recorded by Instron, and $h = R - e$ . Based on Pythagoras' theorem, $r = \sqrt{R^2 - h^2}$ .....	20
<b>Figure 3.1.</b> (a) earlywood and (b) latewood showing distortion and degradation. Degradation recorded on the secondary cell wall as detachment from the ML [d], thickness reduction [r], and granular texture [gt]. ....	24
<b>Figure 3.2</b> Fungal decay, evident with the presence of fungal hyphae [fg].	25
<b>Figure 3.3</b> Bacterial decay. (a) Rod-shape bacteria [bc]. (b) Bacterial degradation patterns [p] on bordered pits.....	25
<b>Figure 3.4</b> (a) Earlywood and (b) latewood showing only minor alterations. ....	26
<b>Figure 3.5</b> Fungal and bacterial degradation patterns. Rare presence of fungal hyphae (fg) and bacteria (bc) were recorded.....	26
<b>Figure 3.6</b> Different morphology observed in the transverse plane among the semi-charred zone. ....	26
<b>Figure 3.7</b> (a) earlywood and (b) latewood showing coalescence of the ML secondary wall. Distortion was also recorded as a characteristic wavy appearance (a). ....	27
<b>Figure 3.8</b> (a) Bacterial degradation patterns were seen seldom. (b) Bacteria [bc] were rarely detected. Small rounded formations around pit chambers (b,c) or in the tracheid wall (c), possibly attributed to bacillus cross-section or warty layer. ....	27

<b>Figure 3.9</b> Graphic representation of equilibrium moisture content (EMC), moisture content at the waterlogged state (MC), basic density (Rg), and shrinkage ( $\beta_{\text{cross}}$ ) of uncharred, semi-charred and charred wood compared to reference samples of <i>Pinus brutia</i> and <i>Pinus halepensis</i> .....	29
<b>Figure 3.10</b> Histograms of intruded pore volume as a function of the pore radius of the controls of <i>Pinus brutia</i> and <i>Pinus halepensis</i> (left) and the archaeological uncharred, semi-charred and charred wood (right). The IUPAC categorization is presented versus the pore size categorization adopted in the present study.....	30
<b>Figure 3.11</b> Differential pore-size distribution curves and cumulative intrusion curves of controls ( <i>Pinus brutia</i> and <i>Pinus halepensis</i> ) and the three conditions of the archaeological wood (uncharred, semi-charred and charred). .....	31
<b>Figure 3.12</b> End, radial and tangential hardness of the reference <i>Pinus brutia</i> and <i>Pinus halepensis</i> measured at both earlywood and latewood. Results are the average of two replicates.....	33
<b>Figure 3.13</b> End, radial and tangential hardness of waterlogged archaeological uncharred, semi-charred and charred wood on both freeze dried (FD) and waterlogged (W) state. Results are the average of two replicates. * Single value due to material's failure. ....	34
<b>Figure 3.14</b> End, radial and tangential hardness of the archaeological wood, at the freeze-dried (FD) and at the waterlogged (W) state, in comparison to the hardness of <i>Pinus halepensis</i> and <i>Pinus brutia</i> of which EW-LW values were averaged. * Single value due to material's failure. ....	35
<b>Figure 3.15</b> Force-penetration graph of charred wood in freeze-dried and waterlogged state.....	36
<b>Figure 3.16</b> Force-penetration graph of uncharred (a), and semi-charred (b) wood in freeze-dried and waterlogged state.....	36
<b>Figure 3.17</b> Graphic representation of resistance to penetration. Uncharred wood (iii) ranged from 430 to 699 g, semi-charred wood (ii) from 903 to 1156 g, and charred wood (i) from 1147 to 1452 g. ....	38
<b>Figure 3.18</b> Correlation between resistance to penetration and Rg for the three charring conditions of uncharred, semi-charred and charred archaeological wood. Each penetration point is plotted against the average Rg values of each condition calculated using four replicates. The error bars represent the standard deviation of Rg.....	38
<b>Figure 3.19</b> Macroscopic image (a) and SEM micrograph (b) of a sample where charred (i), semi-charred (ii), and uncharred (iii) material coexisted; (c) EDS spectrum of each condition. ....	39

**Figure 3.21** EDS Line-scan and mapping of a sample where all conditions coexisted. (a) Line scan of carbon (yellow) and oxygen (blue) (left to right the transition from charred to uncharred (i–iii); (b) mapping of carbon (yellow) and oxygen (blue). ..... 40

**Figure 3.22** Infrared spectra recorded for reference samples, (a) *Pinus halepensis* Mill. and (b) *Pinus brutia* Ten. (c) uncharred (d) semi-charred, and (e) charred archaeological samples. .... 41

**Figure 3.23** X-ray diffraction pattern of (a) *Pinus halepensis* Mill. and (b) *Pinus brutia* Ten. reference samples in comparison with (c) uncharred, (d) semi-charred, and (e) charred waterlogged samples. The  $2\theta$  values correspond to Cobalt source reflections..... 43

### Table of tables

**Table 3.1** Physical properties recorded for archaeological wood (average of 4 replicates) and controls of *Pinus brutia* and *Pinus halepensis*. <sup>a</sup>:(Glass and Zelinka 2010), <sup>b</sup>: $U_{max}=[(1/Rg)-0,67] \times 100$  (Tsoumis 1991), <sup>c</sup>:(Crivellaro and Schweingruber 2013), <sup>d</sup>:(Tsoumis 1983), Values in brackets represent the standard deviation. .... 28

**Table 3.2** Proximate analysis results for charred and semi-charred samples. Percentages values of moisture content (M), volatile matter (VM), ash content (Ash) and fixed carbon (Fixed C) are the average of 2 replicates. Fixed carbon was calculated on dry basis. .... 31

**Table 3.3** End, radial and tangential hardness measured with the modified Janka test. All values are the average of 4 replicates. Values in brackets represents standard deviation. .... 33

**Table 3.4** Hardness measured with the modified Janka test. Values of reference *Pinus halepensis* and *Pinus brutia* are the average of 8 replicates (4 on EW and 4 on LW), while of archaeological samples of 2 replicates, \*: a single value due to material's failure under testing. Values in brackets represents standard deviation. .... 35

**Table 3.5** Resistance to penetration values recorded on each charring condition..... 37

**Table 3.6.** Band positions of the maximum total intensity (I<sub>200</sub>) and the minimum intensity of the amorphous cellulose (I<sub>am</sub>). CrI represents the crystalline index based on Segal's method and L correspond to the crystallite size..... 43

## **Table of contents**

Acknowledgements .....	i
Abstract .....	ii
Table of figures .....	iv
Table of tables .....	vi
Table of contents .....	vii
1. Introduction .....	1
1.1 The medieval shipwreck discovered in Rhodes harbor.....	1
1.2. Remedial conservation of waterlogged archaeological wood.....	6
1.3 Rationale for the study .....	8
1.4 Aims and Objectives .....	10
2. Materials and Methods .....	12
2.1 Morphological Alterations at a Cellular Level.....	12
2.1.1 Scanning Electron Microscopy (SEM) .....	12
2.2 Physical Properties .....	13
2.2.1 Moisture Content, Density and Shrinkage Determination .....	13
2.2.2 Mercury Intrusion Porosimetry (MIP) .....	14
2.2.3 Proximate Analysis .....	15
2.3 Mechanical Properties .....	16
2.3.1 Force-controlled Hardness Test Methods- Brinell and Vickers..	17
2.3.2 Depth-controlled Hardness Test Method- Janka.....	18
2.3.3 Penetrometer .....	21
2.4 Chemistry .....	21
2.4.1 Energy Dispersive Spectroscopy (EDS) .....	21
2.4.2 Fourier-Transform Infrared Spectroscopy (FTIR) .....	22
2.4.3 X-ray Diffraction (XRD).....	22
3. Results .....	24
3.1 Morphological Alterations at a Cellular Level.....	24
3.1.1 Scanning Electron Microscopy (SEM) .....	24
3.2 Physical Properties .....	27
3.2.1 Moisture Content, Density and Shrinkage Determination .....	27
3.2.2 Mercury Intrusion Porosimetry (MIP) .....	29
3.2.3 Proximate Analysis .....	31



3.3 Mechanical Properties .....	32
3.3.1 Force-controlled Hardness Test Methods- Brinell and Vickers..	32
3.3.2 Depth-controlled Hardness Test Method- Janka.....	32
3.3.3 Penetrometer .....	37
3.4 Chemistry .....	39
3.4.1 Energy Dispersive Spectroscopy (EDS) .....	39
3.4.2 Fourier-Transform Infrared Spectroscopy (FTIR) .....	41
3.4.3 X-ray Diffraction (XRD).....	42
4. Discussion and Conclusions.....	44
4.1 Morphological Alterations at a Cellular Level.....	44
4.1.1 Scanning Electron Microscopy (SEM) .....	44
4.2 Physical Properties .....	45
4.2.1 Moisture Content, Density and Shrinkage Determination .....	45
4.2.2 Mercury Intrusion Porosimetry (MIP) .....	47
4.2.3 Proximate Analysis .....	49
4.3 Mechanical properties .....	51
4.3.1 Force-controlled Hardness Test Methods- Brinell and Vickers..	51
4.3.2 Depth-controlled Hardness Test Method- Janka.....	51
4.3.3 Penetrometer .....	52
4.4 Chemistry .....	53
4.4.1 Energy Dispersive Spectroscopy (EDS) .....	53
4.4.2 Fourier Transform Infrared Spectroscopy (FTIR) .....	54
4.4.3 X-ray Diffraction (XRD).....	56
4.5 Conclusions .....	58
References .....	61
Publications .....	85
<i>Chemical Characterization of Waterlogged Charred Wood: The Case of a Medieval Shipwreck</i> .....	85
<i>Physico-Mechanical Properties of Waterlogged Archaeological Wood: The Case of a Charred Medieval Shipwreck</i> .....	98



despite the risks posed for its preservation due to the high-energy environment.

Five years later, in 2013, an expedition was undertaken under the “MERMAID” project – Saving Wood Shipwrecks in the Mediterranean Marine Ecosystems: Research, Development and Application of Innovative Methods of In Situ Protection’ (Pournou 2016), funded by the European program Thales/NSRF 2007-2013 (Koutsouflakis and Rieth 2021). The project was coordinated by the Department of Conservation of Antiquities and Works of Art of the TEI of Athens, currently University of West Attica, and it was implemented in collaboration with the Institute of Oceanography and Marine Biology of the Hellenic Center for Marine Research (HCMR), the Department of History, Archaeology and Cultural Resources Management of the University of the Peloponnese and the EUA (Pournou 2016; Koutsouflakis and Rieth 2021). During the project, the wreck was partially excavated and reburied with geotextiles for its *in situ* protection (Pournou 2016; Koutsouflakis and Rieth 2021).

The excavated area was of approximately 90 m<sup>2</sup>, covering both sides of the southern end of the hull (Koutsouflakis and Rieth 2021). The exact size of the ship has not been assessed, as during the 2013 season, the northern end, was not visible. Nonetheless, based on the shipbuilding elements of the excavated part, it is believed that the ship could have exceeded 30 m in length (Koutsouflakis 2017b; Koutsouflakis and Rieth 2021). The ship cargo was consisted mostly of the well-known type of “Günsenin 3” amphorae, indicating that it was a merchant ship of the last quarter of the 12th century (Koutsouflakis and Rieth 2021). The excavation in 2013, focused primarily on the structural elements of the wreck, and not on the fragmented cargo, as this would be time-consuming and would not permit a study of the shipbuilding technology (Koutsouflakis and Rieth 2021). The results though

were uncertain, as the limited time of excavation permitted only the partial study of the ship's construction technology (Koutsouflakis and Rieth 2021).

Rhodes wreck No4 is important not only for Rhodes's history and medieval seafaring in the eastern Mediterranean, but also for the naval architecture of this era (Koutsouflakis and Rieth 2021). Based on archaeological data, it seems that Rhodes wreck No4 had probably departed from a major port of mainland Greece for the markets of the southern Aegean and possibly further east, to the direction of Cyprus and the Levant. This ship diversifies from the vessels of the same period as it is of massive construction (Koutsouflakis 2017a), of approximately 35 m long while the known Byzantine vessels of all kinds are up to 15 m (Koutsouflakis and Rieth 2021). Nevertheless, its size is not the only exceptional construction find, as the surviving planking, of 120 mm thickness, appears to be the thicker than that of the known ancient ships (Koutsouflakis and Rieth 2021). Moreover, the shipbuilding of such an enormous vessel is expected to differ from the known shipbuilding technology of smaller vessels, thus requiring further investigation (Koutsouflakis and Rieth 2021).

The west side of the ship was more buried than the east one, thus being preserved to a greater extent (Koutsouflakis and Rieth 2021). However, the preservation of the eastern side is owed not only to the burial conditions but also to a fire event that is believed to have potentially caused the sinking. This is indicated by the charring traces found on the excavated southern end timbers (figure 1.2), as well as by the condition of the majority of the lifted artifacts (Koutsouflakis 2017a; Koutsouflakis and Rieth 2021). The charring of timbers was inhomogeneous, as its extent and depth was shown to be different on the various construction elements of the ship (Mitsi and Pournou 2019; Koutsouflakis and Rieth 2021). More specifically, in the western side,

the charring is obvious at the upper part of the frames (figure 1.3), whereas at their lower parts was superficial.



**Figure 1.2** Wooden elements that shows traces of charring (Photo: V Mentogiannis, EUA<sup>©</sup>, with permission from Dr. G. Koutsouflakis)



**Figure 1.3** Frames of the west side, where the upper parts are severely charred (Photo: V. Mentogiannis, EUA<sup>©</sup>, with permission from Dr. G. Koutsouflakis)

Furthermore, at the eastern side of the ship, the lower parts of the hull were charred; in contrast to the upper parts that were uncharred (Koutsouflakis and Rieth 2021). This diverse degree and extent of charring in the various elements throughout the wreck, could be suggestive of the way that the fire was spread and probably of how the ship was sunk (Mitsi and Pournou 2019; Koutsouflakis and Rieth 2021).

At present, the wreck is reburied with the use of geotextiles (Koutsouflakis 2017a). Nonetheless, its long-term preservation is not secured, even though the performance of geotextiles has been proven successful in preserving wooden shipwrecks *in situ* (Pournou 2018). This is mainly owed to Rhodes's underwater environment, where enormous cruise ships pass and anchor daily near No4 wreck's location (Koutsouflakis and Rieth 2021). This high-energy underwater environment, due mostly to scouring caused by ships' propellers, does not offer stable and protective burial conditions. The periodic movements of the sediment can lead to the uncovering of the wreck, which was the reason of its discovery (Koutsouflakis and Rieth 2021). In such an environment, the integrity of the wreck is in danger (Koutsouflakis and Rieth 2021), as the re-exposure of the wood in the water column is very hazardous, especially in the Mediterranean, as it could lead to the complete loss of the material due to biodeterioration (Pournou et al. 2001; Pournou 2016; Pournou 2018).

The raising of the hull is not possible at present mainly due to the lack of funding. However, even if funding is provided, the peculiar preservation state of the ship that presents various charring conditions (Mitsi and Pournou 2019) is quite problematic as there is also a lack of previous experience in handling and conserving charred waterlogged wood. Therefore, it appears that studying the material in order to develop an adequate remedial conservation plan is very important as the *in situ* protection method appears to be only a temporary

solution due to the high-energy hydrodynamic conditions prevailing at the site (Koutsouflakis and Rieth 2021).

## 1.2. Remedial conservation of waterlogged archaeological wood

Archaeological wood buried in waterlogged anoxic sediments, typically appears intact or in good condition after exposure (Gregory et al. 2012; Broda and Hill 2021). However as the material is usually deteriorated and its physical, mechanical, chemical and structural properties are altered (Hedges 1989; Florian 1990; Schniewind 1990), upon uncontrolled drying, it will undergo permanent deformations caused by collapse and shrinkage, that will threaten its structural integrity (Grattan and Clarke 1987; Gregory et al. 2012; Collis 2015; Broda and Hill 2021). Therefore, remedial conservation treatments are needed in order to remove the water from the material, and concurrently preserve its dimensions and make it durable, in terms of mechanical strength, and resistance to biodeterioration (Grattan and Clarke 1987; Broda and Hill 2021). For choosing the most suitable conservation method, several factors need to be considered. These include, reversibility (Grattan and Clarke 1987; Broda and Hill 2021) or at least re-treatability (Broda and Hill 2021), preservation of color and texture (Gregory et al. 2012; Collis 2015) so that the treated object could be interpretable by the viewer (Grattan and Clarke 1987), factors such as the hazard and the cost (Gregory et al. 2012; Broda and Hill 2021), as well as basic conservation ethics, like the “minimum intervention” principle (Grattan and Clarke 1987).

Remedial conservation treatments are usually grouped into i) impregnation and bulking methods where a consolidation agent penetrates into the wood, ii) drying methods, and iii) combination of both impregnation and drying (Grattan and Clarke 1987; Kaye 1995; Broda and Hill 2021).

The first group includes numerous consolidation agents, but by far the most widely accepted and applied one, is the polyethylene glycol (PEG) of various

molecular weights (MW) (Kaye 1995; Gregory et al. 2012; Collis 2015; Broda and Hill 2021). PEG provides good dimensional stability (Grattan and Clarke 1987; Collis 2015; Broda and Hill 2021), it is low in toxicity, of relatively low cost and it is mostly reversible (Collis 2015; Broda and Hill 2021). However, there are also some concerns such as the hygroscopic nature of its low MW grades and the dark and waxy appearance of the treated wood (Gregory et al. 2012; Collis 2015; Broda and Hill 2021).

Among the impregnation agents used for waterlogged wood it is worth mentioning a) the “alum”, which was the first one used in large scale but is no longer in use (Grattan and Clarke 1987; Kaye 1995), b) the melamine-formaldehyde resin, applied in large-scale projects such as the Pisa wrecks and the Yenikapi wrecks, which despite the dimensional stability and durability that provides it is disputed due to health and safety concerns and irreversibility (Collis 2015; Broda and Hill 2021; Vlata and Pournou 2023) and c) the sugars such as sucrose, trehalose, lactitol, etc. (Grattan and Clarke 1987; Gregory et al. 2012; Broda and Hill 2021) which are of low cost, but of high susceptibility to microbial and insect attack (Gregory et al. 2012; Broda and Hill 2021). Besides the above-mentioned consolidation agents, there are proposals for new consolidants, however the adequate research to consider them reliable for application is lacking (Broda and Hill 2021).

Drying methods on the other hand include a) the air-drying often referred to as slow-drying (Grattan 1982; Grattan and Clarke 1987) or as controlled air-drying (Gregory et al. 2012; Broda and Hill 2021), b) the freeze-drying under vacuum (Grattan 1982; Grattan and Clarke 1987; Kaye 1995; Gregory et al. 2012; Broda and Hill 2021), c) the atmospheric (non-vacuum) freeze drying (Grattan and Clarke 1987; Gregory et al. 2012), d) the supercritical-drying (Kaye 1995; Gregory et al. 2012; Broda and Hill 2021), and e) the solvent-exchange drying (Grattan and Clarke 1987; Broda and Hill 2021).



Usually, a combination of a consolidation and a drying method is adopted with the PEG/controlled air-drying, and the PEG/freeze drying to be the most common ones (Grattan 1982; Hoffmann 1986; Grattan and Clarke 1987; Gregory et al. 2012; Broda and Hill 2021).

Up to now, the majority of shipwrecks and boats' conservation, such as the Vasa, the Mary Rose, the Bremen Cog, the Hasholme logboat, etc. have been conserved with PEG (by spraying or immersion) followed primarily by controlled air-drying, though freeze-drying has been also used (Broda and Hill 2021).

### 1.3 Rationale for the study

*In situ* preservation of wreck sites is the recommended primary option suggested by the 2001 UNESCO Convention for the Protection of the Underwater Cultural Heritage (UCH). However, when *in situ* preservation is not possible the need for a rescue excavation and recovery is recognized (Gregory et al. 2012; Broda and Hill 2021). In case of recovery, the design of the preservation strategy prior to any action is required. For the design of the strategy it is advised to predefine the end use of the UCH (Grattan and Clarke 1987; Gregory et al. 2012; Collis 2015); in the case of wooden shipwrecks, it is mandatory to acknowledge the preservation state of the wood (Gregory et al. 2012), as this will define not only the conservation method but also the raising technique. Furthermore, for all projects a thorough planning of each phase is required and an adequate funding, which is of paramount importance, should be guaranteed (Grattan and Clarke 1987).

Rhodes wreck No 4, as already pointed out, is not expected to survive in foreseeable future, as its burial environment despite the protective action taken, cannot ensure the stability of the site. Thus, in order to preserve the shipwreck, appropriate measures and strategies should be designed such as its lifting followed by remedial conservation (EN 16873 2016), or at least the

reburial of the wreck in a safer marine environment. Examination of the state of preservation of the material is required for both strategies (Jensen and Gregory 2006). The literature regarding charred wood conservation and condition assessment is limited, especially for wet or waterlogged charred wood (Caple and Murray 1994; Triantafyllou et al. 2010). The most commonly applied methods on charred wood, are those typically applied on waterlogged wood, with most frequent the use of PEGs (Caple and Murray 1994; Jover 1994; Triantafyllou et al. 2010).

On this basis, a preliminary investigation on conservation methods for the material was conducted during a BSc final year project entitled “Comparative Study of Conservation Treatments for Charred Waterlogged Wood from Medieval Shipwreck in the Port of Rhodes Island” at the Department of Conservation of Antiquities and Works of Art, at the University of West Attica in 2019 (Mitsi 2020). This work was also partially presented at the 14<sup>th</sup> ICOM-CC Wet Organic Archaeological Materials (WOAM) Conference at Portsmouth, UK in 2019 (Mitsi and Pournou 2019). This work demonstrated that Rhodes wreck timbers presented concurrently charred and uncharred areas and in many cases an inner uncharred core was found surrounded by a charred outer layer (Mitsi and Pournou 2019; Mitsi 2020). Results showed as anticipated that the two charring conditions (uncharred and charred) have different physicochemical properties and also indicated the presence of a third charring condition, mostly located at the charred/uncharred interface (Mitsi and Pournou 2019; Mitsi 2020). Furthermore, results on potential conservation methods, showed that almost all PEG treatments irrespective of the drying method are capable of stabilizing uncharred wood dimensions, except low MW PEG (PEG 400). In contrast, charred material did not require any consolidation. Therefore, timbers with a charred outer layer and uncharred inner core may not permit PEG diffusion, as charred material is expected to have lower porosity. It was also indicated the presence of a third

charring condition, termed semi-charred wood, that existed at the interface of the charred and uncharred material (Mitsi 2020).

Therefore, further research was considered necessary, in order to investigate in-depth, the different properties of the three identified charring conditions (uncharred, semi-charred, and charred), which would permit the design of an efficient conservation plan, capable of conserving all charring conditions concurrently while preserving the historic, aesthetic and physical integrity of the ship.

#### 1.4 Aims and Objectives

The principal aim of this work is to assess the condition of Rhodes medieval shipwreck's timbers in order to enable the development of an effective conservation plan that would be applied if the shipwreck is raised. For achieving this aim the following objectives should be met.

- Characterization of the state of preservation of shipwreck timbers through physicochemical analysis. This will include documentation of the morphological features at a cellular level with scanning electron microscopy (SEM), determination of materials' residual chemistry with Fourier transform infrared spectroscopy (FTIR) for its organic composition, investigation on cellulose crystallinity alterations with X-ray diffraction (XRD), examination of its inorganic chemistry and/or the inorganic elements present with energy dispersive spectroscopy (EDS), and assessment of its physical properties with gravimetric and volumetric methods as well as with proximate analyses for the thermally altered material (semi-charred and charred).
- Assessment of wood properties related to the handling and the employment of remedial conservation treatments such as hardness and porosity.

- Correlating the physicochemical and mechanical characterization of the material with properties related to treatment, in order to resolve practical aspects involved in conservation of waterlogged organics such as impregnation and consolidation.

## 2. Materials and Methods

The waterlogged wood used in the present study came from a frame of the Rhodes wreck No4 that was made of *Pinus halepensis* Mill. (Aleppo pine) or *Pinus brutia* Ten. (Turkish pine) (Koutsouflakis 2017b; Koutsouflakis and Rieth 2021). Samples were produced from a frame part that was retrieved from the wreck in 2013 and it was kept waterlogged at 5°C until investigation. All samples used were taken from the surface of the frame inwards, at least 50 annual rings away from the pith, in order to correspond to the sapwood of the tree trunk, and represented the three different degrees of wood charring that have been identified on the wreck timbers.

The following investigation has been conducted at the facilities of the Department of Conservation of Antiquities and Works of Art, University of West Attica.

### 2.1 Morphological Alterations at a Cellular Level

#### 2.1.1 Scanning Electron Microscopy (SEM)

Uncharred and semi-charred waterlogged archaeological samples were cut in subsamples of approximately 2x2x3 mm using a double-edged razor blade, whereas charred samples were fractured also to ~ 2x2x3 mm subsamples. All samples were then dehydrated in a series of ethanol solutions of increasing concentrations until water-free alcohol was reached and then left to air-dry in a desiccator. They were then mounted on aluminum stubs using a double-sided carbon conductive tape, gold-coated in a sputter coater (Polaron SC7640), and examined at an acceleration voltage of 20 kV under low vacuum (33 Pa) using a JEOL JSM-6510LV scanning electron microscope.

## 2.2 Physical Properties

### 2.2.1 Moisture Content, Density and Shrinkage Determination

For assessing the density of the material, waterlogged samples of uncharred, semi-charred, and charred condition were weighed in air and in water and their relative density (rRg) was estimated according to equation 1. The basic density (Rg) was also calculated according to equation 2, where the waterlogged volume of samples was recorded by water displacement method, and the dry weight by oven-drying the samples at  $103 \pm 2$  °C for 48 h until constant (ASTM D2395-14).

For measuring shrinkage<sup>1</sup> ( $\beta$ ), stainless steel insect pins were placed on the transverse plane to mark the tangential and radial direction, and the distance between the pins was recorded with a vernier caliper (0,02 mm). Samples were then air-dried to a constant weight at  $21 \pm 2$  °C and 45  $\pm$ 5% RH, and the distance between the pins was measured again. The cross-sectional shrinkage ( $\beta_{\text{cross}}$ ) was estimated by summing the tangential and radial shrinkage ( $\beta$ ), which were calculated by equation (3).

Lastly for the equilibrium moisture content (EMC), and the moisture content (MC), waterlogged samples of all charring conditions were first air-dried at  $21 \pm 2$  °C 45  $\pm$ 5% RH and when they reached equilibrium, EMC was estimated based on the equation (4). Following, air-dried samples were oven-dried at  $103 \pm 2$  °C for 48 h until constant (ASTM D2395-14) and MC was calculated based on the equation (5).

For the evaluation of all physical properties, four replicates of each condition were used.

$$\text{rRg.} = 3 \times W_{\text{sub}} / (W_{\text{w}} - W_{\text{sub}}) \quad (\text{Cook and Grattan 1990}) \quad (1)$$

---

<sup>1</sup> In this study, shrinkage refers to the total dimensional reduction measured during drying that includes both cell collapse occurring above the fiber saturation point (FSP) and the cell wall shrinkage occurring below the FSP.

where  $W_{sub}$  = waterlogged weight submerged in water, and  $W_w$  = waterlogged weight in air.

$$Rg = W_o / V \quad (\text{Kollmann and Côté 1968}) \quad (2)$$

where  $W_o$  = oven-dry weight at  $102 \pm 3^\circ\text{C}$  after three consecutive constant measurements, and  $V$  = waterlogged volume measured by water displacement.

$$\beta\% = [(\beta_w - \beta_{A.D.})/\beta_w] \times 100 \quad (\text{Tsoumis 1991}) \quad (3)$$

where  $\beta_w$  = waterlogged dimensions and  $\beta_{A.D.}$  = air-dried dimensions. Shrinkage was calculated for tangential and radial direction and their sum equals the cross-sectional shrinkage.

$$\text{EMC}\% = [(W_{A.D.} - W_o)/W_o] \times 100 \quad (\text{Kollmann and Côté 1968}) \quad (4)$$

where  $W_{A.D.}$  = air-dried weight at  $23 \pm 2^\circ\text{C}$  after three consecutive constant measurements.

$$\text{MC}\% = [(W_w - W_o)/W_o] \times 100 \quad (\text{Grattan 1987}) \quad (5)$$

### 2.2.2 Mercury Intrusion Porosimetry (MIP)

Mercury intrusion porosimetry (MIP) was carried out with a Quantachrome PoreMaster 60, on uncharred, semi-charred and charred samples. Reference samples of *Pinus halepensis* and *Pinus brutia* were also used. The archaeological samples of the three charring conditions that measured  $\sim 5 \times 5 \times 5$  mm, were freeze-dried prior to porosity measurements, as their air drying was anticipated to affect their porosity due to the cell wall collapse and shrinkage (Broda et al. 2021b). Freeze -dried samples were stored in a desiccator until porosity measurements. Low pressure was first applied to 50 MPa and then samples were placed into the high-pressure station where pressure up to 400MPa was and equilibration time of 10s. Surface tension and mercury wetting angle were set at  $0.485 \text{ Nm}^{-1}$  and  $140^\circ$  respectively.

Wood porosity is defined by two size classes of pores, based on the IUPAC classification (Sing et al 1985), the macropores with diameter  $>50$  nm, ( $r >25$  nm) and the mesopores with diameters from 2 nm to 50 nm ( $1 \text{ nm} < r > 25$  nm). Nonetheless, in wood science the pore size distribution is often categorized in relation to wood ultrastructure (Thygesen et al. 2010; Plötze

and Niemz 2011; Zauer et al. 2014; Vitas et al. 2019), thus, an anatomy-based categorization was adopted in this study which is consisted of three pore classes; the macrovoids that include the lumen of tracheids and the resin canals with radii ranging from to 5  $\mu\text{m}$  to  $\sim 200 \mu\text{m}$ , the microvoids that encompass pit apertures, pit chambers and other small voids with radii from 5 nm to  $\sim 5 \mu\text{m}$ , and the nanovoids that comprise the cell wall porosity with radii  $< 5 \text{ nm}$  (Thygesen et al. 2010; Yin et al. 2015).

### 2.2.3 Proximate Analysis

Proximate analysis was implemented on charred and semi-charred wood samples according to ASTM D 1762-84 (2011). Samples were air-dried to a constant weight at  $21 \pm 2 \text{ }^\circ\text{C}$  and  $45 \pm 5\% \text{ RH}$ . They were then grinded with the use of an agate mortar and pestle and sieved to  $\sim 100 \mu\text{m}$  (No 140-mesh size). The determination of moisture content, ash content, volatile matter, and fixed carbon was duplicated. For moisture content (M), approximately 1 g of each charring condition was placed in a porcelain crucible and weighed to the nearest 0.1 mg. Crucibles and covers were previously dried in a muffle furnace at  $750 \text{ }^\circ\text{C}$  for 10 min and cooled in a desiccator for 1 h. Crucibles containing grinded samples were then placed uncovered in an oven at  $105 \text{ }^\circ\text{C}$  for 2 h. Dried samples were cooled covered in a desiccator for 1 h and weighed. Samples were considered oven-dried when the decrease in weight was  $\leq 0.0005 \text{ g}$ . Succeeding drying periods were 1 h. Moisture content was calculated based on Equation (6).

$$M\% = [(A - B)/A] \times 100 \quad (\text{ASTM D 1762-84 2011}) \quad (6)$$

where A = grams of air-dry sample, and B = grams of the sample after drying at  $105 \text{ }^\circ\text{C}$ .

For volatile matter (VM), crucibles with lids in place and containing the samples used for moisture determination were placed in a muffle furnace heated to  $950 \text{ }^\circ\text{C}$ . They were first positioned, with the furnace door open, for 2 min on the outer ledge of the furnace ( $300 \text{ }^\circ\text{C}$ ), and then for 6 min with the



muffle door closed. Samples were then cooled in a desiccator for 1 h and weighed. The percentage of volatile matter in the sample was calculated based on equation (7).

$$\text{VM}\% = [(B - C)/B] \times 100 \quad (\text{ASTM D 1762-84 2011}) \quad (7)$$

where C = grams of the sample after drying at 950 °C.

For ash content, lids and uncovered crucible used for the volatile matter determination containing the samples were placed in a muffle furnace at 750 °C for 6 h. Samples were cooled with lids in place covered in a desiccator for 1 h and weighed. Samples were repeatedly burned with succeeding 1-h periods until results showed a loss of less than 0.0005 g. The percentage of ash content was calculated based on equation (8).

$$\text{Ash}\% = (D/B) \times 100 \quad (\text{ASTM D 1762-84 2011}) \quad (8)$$

where D = grams of residue.

Fixed carbon (Fixed C) was calculated on a dry basis according to ASTM E870–82 based on equation (9).

$$\text{Fixed C}\% = 100 - [\text{VM}\% + \text{Ash}\%] \quad (\text{ASTM D 1762-84 2011}) \quad (9)$$

### 2.3 Mechanical Properties

Based on the literature the most widely applied methods for the determination of wood hardness are i) the “Brinell test”, using a 10 mm ball (Hirata et al. 2001; Skyba et al. 2009; Riggio and Piazza 2010; Lykidis et al. 2016; Sedlar et al. 2019; Sydor et al. 2020; Vörös and Németh 2020) or a 2.5 mm one (Hirata et al. 2001; Stanzl-Tschegg et al. 2009; Babic et al. 2017) and ii) the “Janka test” using a 11.3 mm ball (Green et al. 2006; Riggio and Piazza 2010; Lykidis et al. 2016; Vörös and Németh 2020). Nonetheless, rarely, the “Vickers test”, is also being used for measuring hardness of wood (Li 2015; Aşıkuzun and Karagöz İşleyen 2019).

The hardness of waterlogged archaeological wood is not uniform, as it is dependent on the preservation state (Schniewind 1990), which differentiates greatly with depth (Gregory et al. 2007; High and Penkman 2020). The above-mentioned tests, characterize the “surface” hardness (< 1 cm) and they cannot therefore demonstrate the hardness gradient in deteriorated waterlogged archaeological wood. However, in this work all three methods were trialed, not for recording this decay gradient, but differences among uncharred, semi-charred and charred material. However, only a modified Janka test was found appropriate for the hardness of the material under investigation.

### *2.3.1 Force-controlled Hardness Test Methods- Brinell and Vickers*

Based on the EN 1534 (2000) for the Brinell test, a 10 mm diameter ball indenter with a load of 1 kN (101,972 kgf) is required to produce the calculable indentation on wood. Nonetheless, the dimensions of the archaeological available samples did not permit the use of a ball of this diameter and thus a 2.5 mm Ø ball was used instead. Brinell hardness test was conducted on a Zwick/Roell 8187.5 LKV Universal Hardness Testing Machine. The ISO 6506-1 (2005) issued for metallic materials, specifies that the applied force shall be adjusted to create an indentation with a diameter (d) in the range of 0.24 D and 0.6 D (where D is the diameter of the ball indenter). Thus, several preliminary experiments were run with a full load dwell set to 10 seconds in order to determine the appropriate force that complies with this ISO. Due to the limited range of forces available in the Zwick/Roell machine, these experiments were also conducted on an Instron 3367, dual-column universal testing machine with a 2 kN load cell and compression platens of 100 kN maximum load on both upper and lower connection. On the upper platen a 2.5 mm ball, was attached using a neodymium magnet. After each force loading tested, the diameter (d) of the imprint was measured as the mean

value of two perpendicular diagonals ( $d_1$  and  $d_2$ ) as shown in figure 2.1a, using the built-in microscope of the Zwick/Roell instrument.

Preliminary experiments with the Vickers method were also conducted using the Zwick/Roell 8187.5 LKV Universal Hardness Testing Machine, with the full load dwell mode set to 10 seconds and an applied load of 3 and 10 kgf. After each indentation, the diagonal length of the imprint was measured (figure 2.1b), using the built-in microscope of the instrument.

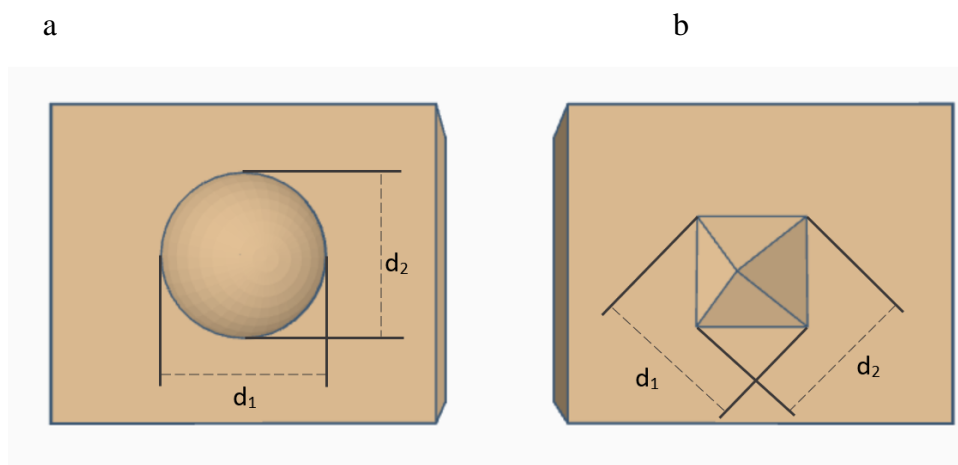


**Figure 2.1** Graphic representation of the imprint created by the (a) Brinell and (b) Vickers indenter. For each, the perpendicular diagonals ( $d_1$  and  $d_2$ ) are noted.

### 2.3.2 Depth-controlled Hardness Test Method- Janka

The Janka hardness test was implemented based on the ASTM D143 and the ASTM D1037. However, a 2.5 mm ball used instead of the typical 11.3 mm due to the limited dimensions of the available archaeological samples. The test was conducted on an Instron 3367, dual-column universal testing machine with a 2 kN load cell and compression platens of 100 kN maximum load on both upper and lower connection. On the upper platen, the 2.5 mm ball was adjusted using 0.6 mm high neodymium ring magnet (outer  $\varnothing$ : 0.8 mm, inner  $\varnothing$ : 1.9 mm). The test speed was set at 0,1 mm/s rate (ASTM D

143 1994) and a 1.2 mm extension was selected to achieve the final penetration of  $\frac{1}{2}$  the ball diameter. The load-extension data were recorded per 0,1 s with the BlueHill 3 software. However, for most of the measurements conducted on the semi-charred and charred samples cracks or/and failure was recorded at a minimum extension of 0.70 mm, and so the data were obtained at the 0.62 mm extension that equals to a penetration of  $\sim \frac{1}{4}$  the ball diameter (Esteves et al. 2011; Esteves et al. 2014).

Hardness test was conducted on all three charring conditions and on reference samples of sound *Pinus halepensis* and *Pinus brutia* for comparative reasons. Measurements were taken on end grain and both side planes (radial and tangential) in order to determine end and side hardness respectively. The use of the 2.5 mm ball allowed on the reference samples the documentation of differences between earlywood and latewood, and thus two replicate measurements were taken per growing period, their average was also calculated for each plane. Two samples from each charring condition were examined. Uncharred, and charred samples measured  $\sim 2T \times 2R \times 2L$  cm (Tangential x Radial x Longitudinal), whereas the semi-charred  $\sim 2T \times 1.5R \times 2L$  cm. For every condition, one sample was tested, at the waterlogged state to acquire knowledge for their handling before and during conservation and the second one at the freeze-dried state, to assess the residual hardness of the material without bi-as by the contained water. Earlywood and latewood were rarely distinguishable in the archaeological material; thus, two replicate measurements were taken per plane.

Hardness is expressed as the ratio of the applied force (F) to the projected area of contact (A) (equation 10), and as was determined under load included both the plastic and elastic deformation of the material (Doyle and Walker 1985; De Assis et al. 2017; Sydor et al. 2020). The projected contact area is treated as the area of a circle created by the ball intender at the wood surface, using equation 11. Typically, in Janka test, the ball is pressed into half its diameter

(ASTM D 143 1994; ASTM D1037 1999), so the radius of the projected area ( $r$ ) equals to the radius of the indenter ( $R$ ), whereas in the modified Janka test, where ball is pressed to the  $\frac{1}{4}$  of its diameter,  $r$  value is lower than ball radius (figure 2.2). Hence, the radius of the projected contact area was geometrically calculated based on scheme of figure 2.3 and the Pythagoras' theorem.

$$\text{Hardness} = F/A \quad (\text{Doyle and Walker 1985}) \quad (10)$$

where  $F$  = the force recorded at 0.62 extension, and  $A$  = the projected contact area

$$A = \pi r^2 \quad (\text{Doyle and Walker 1985}) \quad (11)$$

where  $\pi$  = the mathematical constant ( $\sim 3.14159$ ), and  $r$  = the radius of the projected contact area

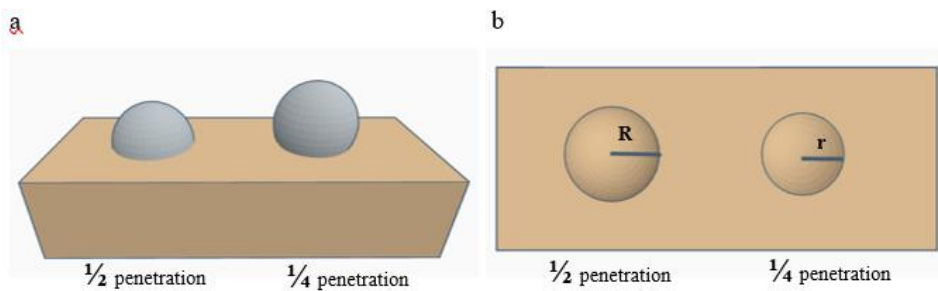


**Figure 2.2** Graphic representation of (a) the ball penetrated at  $\frac{1}{2}$  and  $\frac{1}{4}$  of its diameter, and (b) their projected contact area with radius  $R$  and  $r$  respectively.

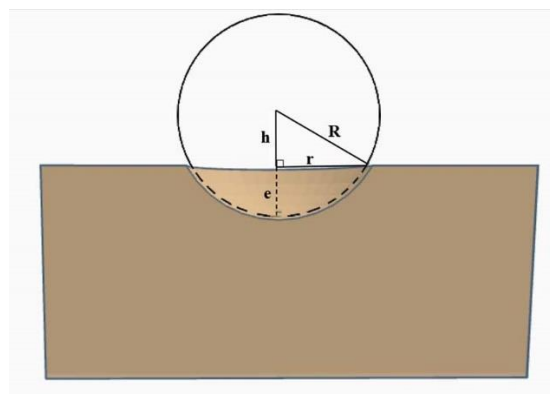


**Figure 2.3** Diagram of the geometrical calculation of the projected contact area's radius ( $r$ ).  $R$  = ball radius,  $e$  = extension recorded by Instron, and  $h = R - e$ . Based on Pythagoras' theorem,  $r = \sqrt{R^2 - h^2}$

### 2.3.3 Penetrometer

For assessing the preservation state of waterlogged wood, the “pin test” is often applied by conservators (Christensen 1970; Hoffmann 1982; Florian 1990; Panter and Spriggs 1997; Schindelholz et al. 2009). This type of manual assessment is rather subjective; therefore wood resistance to penetration can be instead measured with penetrometers (Petrou and Pournou 2018). These instruments can assess the hardness of a material at a given depth and they can also indirectly assess its density. In this work a penetrometer was used for assessing differences in resistance to penetration of the three charring conditions, at a greater depth than Janka permits.

Resistance to penetration was recorded on a part of a shipwreck frame, measuring approximately 9 cm Ø and 15 cm in length, which included all three charring conditions. A Fruit Hardness Tester, FR-5105, with a maximum load capacity up to 5000g was used. The penetrometer was equipped with a needle of 3 cm length and 0.75 mm diameter, of which 1 cm was fasten inside a custom-made holder in order to allow penetration at a constant depth of 2 cm. Six measurements per condition were recorded using the peak hold mode, on the transverse section of the part, as this was the only section, where each charring zone was visible, accessible and could allow penetration into each zone at the same depth without bias.

## 2.4 Chemistry

### 2.4.1 Energy Dispersive Spectroscopy (EDS)

Samples of approximately 1x1x1 cm including all three conditions, were dehydrated in a series of ethanol solutions of increasing concentrations until water-free alcohol was reached and then left to air-dry in a desiccator, prior mounting on aluminum stubs using a double-sided carbon conductive tape. Energy dispersive X-ray spectroscopy (EDS) was performed using a JEOL JSM-6510LV scanning electron microscope, equipped with an Inca x-act

silicon drift detector (SDD) with PentaFET® Precision (Oxford Instruments, Oxford, UK), at an acceleration voltage of 20 kV under low vacuum (33 Pa). The analytical data were obtained with Inca® software. Bulk analysis was applied on every wood charring condition, whereas line scans and mapping were applied on samples where the three charring conditions coexisted.

#### 2.4.2 Fourier-Transform Infrared Spectroscopy (FTIR)

Uncharred, semi-charred, and charred waterlogged archaeological wood were air-dried to a constant weight at  $21 \pm 2$  °C and  $45 \pm 5\%$  RH, and together with reference sound wood samples of *Pinus halepensis* Mill. and *Pinus brutia* Ten., were finely pulverized manually with the use of an agate mortar and pestle to  $\sim 100$   $\mu\text{m}$  (No 140-mesh size). Wood powder was then mixed with potassium bromide powder (KBr, Merck), and pressed into 13 mm discs with a hydraulic press. FTIR analysis was conducted on discs with a Perkin Elmer Spectrum GX spectrometer, equipped with DTGS (deuterated diglycine sulfate) detector. Spectra were recorded and edited with the Perkin Elmer Spectrum v.5.3.1 software.

#### 2.4.3 X-ray Diffraction (XRD)

Uncharred, semi-charred, and charred waterlogged archaeological wood were air-dried to a constant weight at  $21 \pm 2$  °C and  $45 \pm 5\%$  RH, and together with reference sound wood samples of *Pinus halepensis* Mill. and *Pinus brutia* Ten., were finely pulverized manually with the use of an agate mortar and pestle to  $\sim 100$   $\mu\text{m}$  (No140 mesh size). X-ray diffraction spectra of wood powder were recorded with an InXitu BTX II Benchtop X-ray Diffraction/X-ray Fluorescence hybrid system, using a Cobalt source ( $K\alpha_1$  1.78897 Å). All spectra were recorded in duplicate after the completion of  $>1200$  scan cycles from 5 to 50 degrees  $2\theta$ . The crystallinity index (CrI) was calculated based on the method developed by Segal et al. in 1959 (Segal et al. 1958) using the height ratio between the crystalline intensity, expressed as the difference

( $I_{200} - I_{am}$ ) and the total intensity ( $I_{200}$ ), Equation (12). Diffractograms were baseline-corrected with the X Powder software and consequently analyzed using the Perkin Elmer Spectrum v.5.3.1 software with no further processing of peak heights at the (200) plane and at the amorphous region. The total intensity that corresponds to both crystalline and amorphous material ( $I_{200}$ ), is assigned at  $2\theta \sim 25.6^\circ$ , whereas the amorphous intensity ( $I_{am}$ ) is assigned at  $2\theta \sim 20.6^\circ$ , angles corresponding to Cobalt source radiation.

$$\%CrI = (I_{(200)} - I_{(am)}) / I_{(200)} \times 100 \quad (\text{Segal et al. 1958}) \quad (12)$$

The apparent crystallite size  $L$  (nm) was estimated using the Scherrer Equation (13) (Scherrer and Debye 1918), where  $K$  is the Scherrer constant, for which, the value of 0.94 was typically adopted;  $\lambda$  is the X-ray wavelength (1.78897 Å for Co  $K\alpha_1$  radiation);  $b$  is the full width at half maximum (FWHM) of the diffraction band calculated after curve deconvolution using the Thermo GRAMS suite v.9.0 at the  $\sim 11\text{--}30.5$   $2\theta$  range using a 1:1 Gaussian-Lorentzian profile; and  $\theta$  is the Bragg angle corresponding to the (200) plane.

$$L = K \times \lambda / \beta \times \cos\theta \quad (\text{Scherrer and Debye 1918}) \quad (13)$$



### 3. Results

#### 3.1 Morphological Alterations at a Cellular Level

##### 3.1.1 Scanning Electron Microscopy (SEM)

Examination of the morphology demonstrated three distinctly different conditions of wood owed to charring, uncharred, semi-charred and charred.

##### *Uncharred wood*

Examination of the uncharred wood revealed severe decay of the material that was recorded as a wavy appearance of the cells due to distortion (figure 3.1a); and as an extensive degradation of the secondary cell wall layer (figure 3.1 b). The later was demonstrated via i) detachment of the wall from the middle lamella (ML) (figure 3.1 a, b), ii) reduction of its thickness (figure 3.1 a, b) and iii) its granular texture (figure 3.1b). Moreover, biodeterioration was evident with the presence of both fungi (fig. 3.2.) and bacteria (figure 3.3).

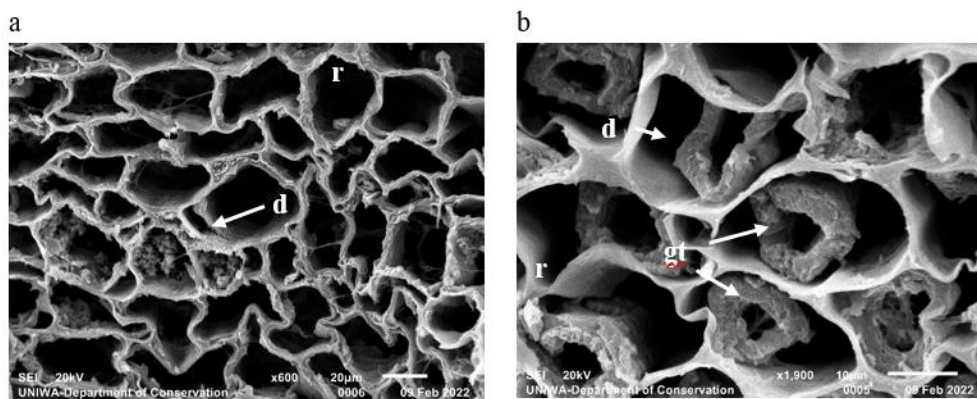


**Figure 3.1.** (a) earlywood and (b) latewood showing distortion and degradation. Degradation recorded on the secondary cell wall as detachment from the ML [d], thickness reduction [r], and granular texture [gt].

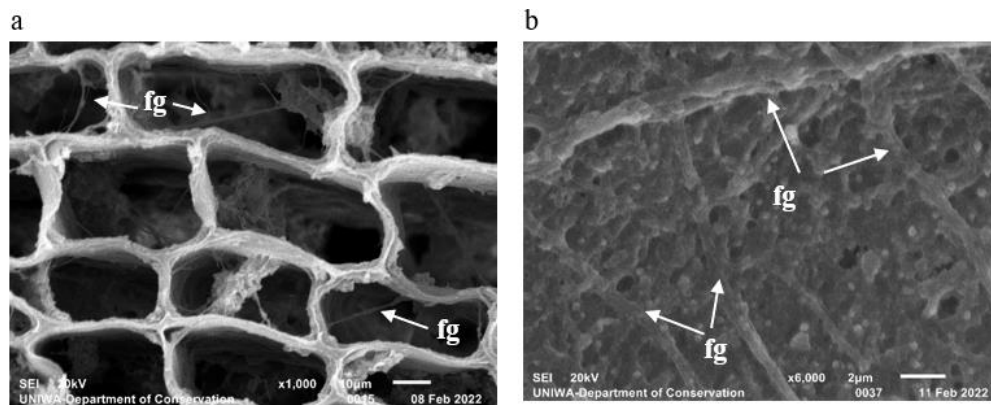


**Figure 3.2** Fungal decay, evident with the presence of fungal hyphae [fg].

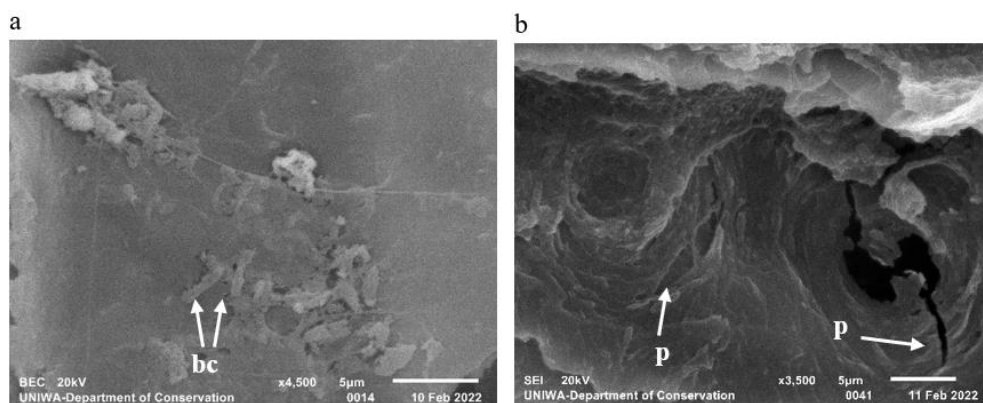


**Figure 3.3** Bacterial decay. (a) Rod-shape bacteria [bc]. (b) Bacterial degradation patterns [p] on bordered pits.

### *Semi-charred wood*

The general typical ultrastructure of the semi-charred wood samples observed, was rather intact. Distortion of cells' shape was limited, detachment of the secondary walls from the ML was rare, whereas the cell boundaries were clearly visible (figure 3.4). Although biodeterioration patterns were evident (figure 3.5 a), microorganisms such as fungal hyphae and bacteria (figure 3.5) were rarely detected. However, the examination of the semi-charred samples revealed a wide variation in the preservation of its morphology (figure 3.6).

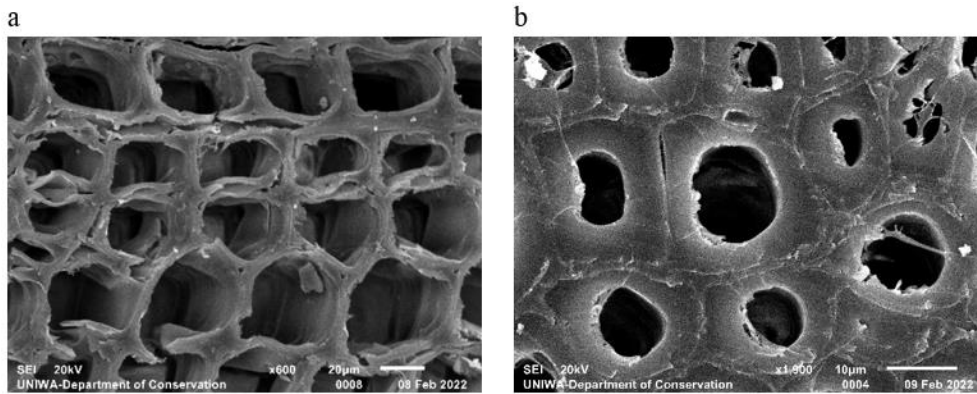


**Figure 3.4** (a) Earlywood and (b) latewood showing only minor alterations.

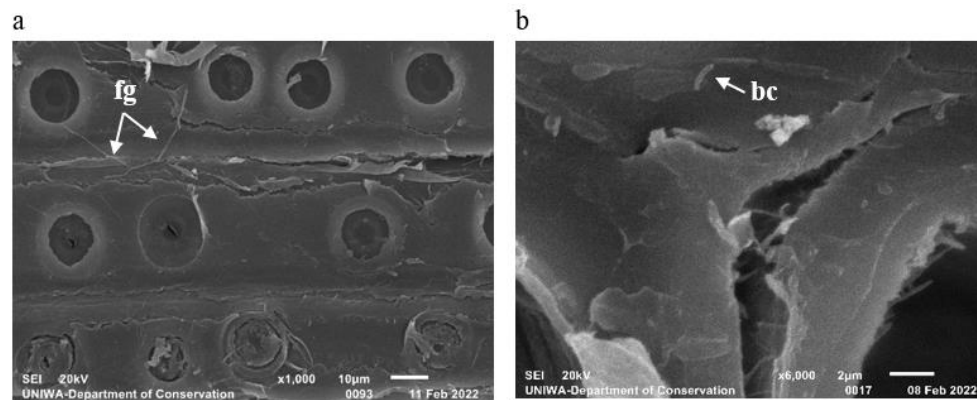


**Figure 3.5** Fungal and bacterial degradation patterns. Rare presence of fungal hyphae (fg) and bacteria (bc) were recorded.

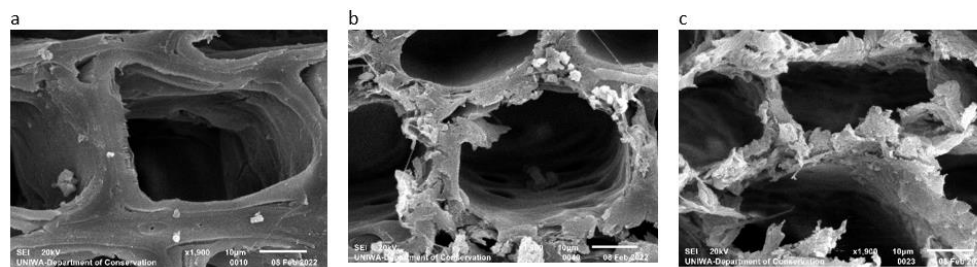


**Figure 3.6** Different morphology observed in the transverse plane among the semi-charred zone.

### ***Charred wood***

Charred wood cells showed severe distortion in both early- and latewood (figure 3.7). The secondary walls appeared to coalesce with the ML and cells demonstrated a distinct vitreous appearance (figure 3.7). Bacterial

deterioration patterns were seen seldom (figure 3.8 a) and were mainly observed around pit membranes (figure 3.8 b). Microorganisms that were rarely spotted, were rod-shape bacteria (figure 3. 8 b) of a  $\sim 0.25 \mu\text{m}$   $\text{\O}$  cross section. Furthermore, numerous small rounded formations, of  $\sim 0.22\text{-}0.28 \mu\text{m}$   $\text{\O}$ , possibly attributed to bacillus cross-section or to warty layer were abundant (figure 3.8 b, c).

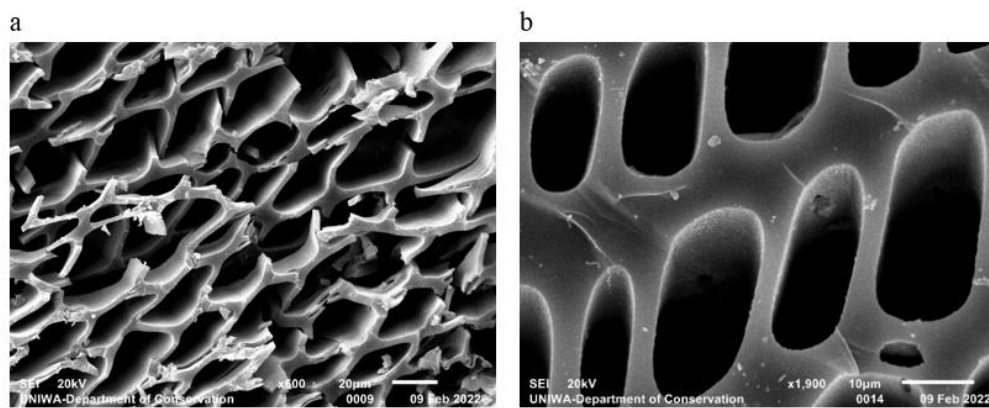


**Figure 3.7** (a) earlywood and (b) latewood showing coalescence of the ML secondary wall. Distortion was also recorded as a characteristic wavy appearance (a).

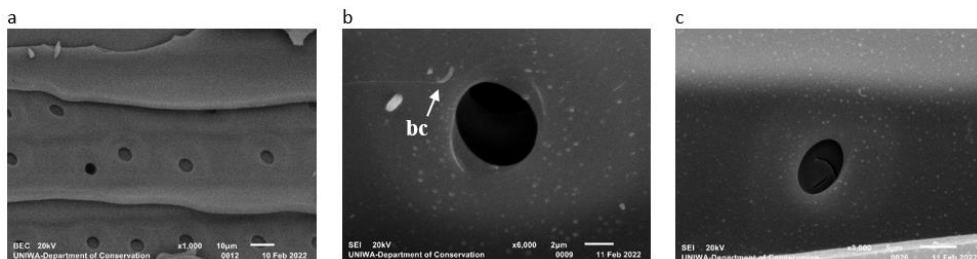


**Figure 3.8** (a) Bacterial degradation patterns were seen seldom. (b) Bacteria [bc] were rarely detected. Small rounded formations around pit chambers (b,c) or in the tracheid wall (c), possibly attributed to bacillus cross-section or warty layer.

## 3.2 Physical Properties

### 3.2.1 Moisture Content, Density and Shrinkage Determination

Results on the physical properties of the archaeological material are presented in table 3.1 and figure 3.9. Archaeological samples of all charring conditions

examined (uncharred, semi-charred, charred) presented lower basic density (Rg) and higher moisture content (MC) compared to the reference samples of sound *Pinus brutia* and *Pinus halepensis*.

Regarding shrinkage ( $\beta_{cross}$ ), uncharred wood was shown to be severely shrank with a  $\beta_{cross}$  value of 81,49%. In contrast, the  $\beta_{cross}$  values recorded for semi-charred and charred samples were even lower than the reference material.

The equilibrium moisture content (EMC) of the uncharred wood was slightly higher compared to the reference samples, whereas the EMC of both the semi-charred and charred wood was significantly lower than the uncharred wood EMC.

Samples	MC (%)	EMC (%)	<i>rRg</i>	Rg	$\beta_{cross}$
		45± 5% RH	(g/cm <sup>3</sup> )	(g/cm <sup>3</sup> )	(%)
<i>Pinus brutia</i>	150 <sup>b</sup>	~8-9 <sup>a</sup>	-	0.46 <sup>c</sup>	12 <sup>d</sup>
<i>Pinus halepensis</i>	150 <sup>b</sup>	~8-9 <sup>a</sup>	-	0.46 <sup>c</sup>	12 <sup>d</sup>
Uncharred	590.46	10.13	0.19	0.15	81.49
	(±28.33)	(±0.58)	(±0.02)	(±0.01)	(±0.15)
Semi-charred	232.48	6.49	0.32	0.33	10.38
	(±28.33)	(±1.88)	(±0.02)	(±0.02)	(±0.33)
Charred	188.23	6.43	0.38	0.40	8.55
	(±24.80)	(±0.47)	(±0.02)	(±0.04)	(±0.40)

**Table 3.1** Physical properties recorded for archaeological wood (average of 4 replicates) and controls of *Pinus brutia* and *Pinus halepensis*. <sup>a</sup>:(Glass and Zelinka 2010), <sup>b</sup>: $U_{max}=[(1/Rg)-0,67] \times 100$  (Tsoumis 1991), <sup>c</sup>:(Crivellaro and Schweingruber 2013), <sup>d</sup>:(Tsoumis 1983), Values in brackets represent the standard deviation.

The basic density (Rg) of the archaeological material varied greatly among the three charring conditions, where the uncharred wood presented the lowest values, followed by the semi-charred and the charred wood. The non-destructive determination of wood's density (rRG) presented similar results

to the destructive calculation (Rg), however for the uncharred wood the rRg calculation gave slightly higher values than the Rg (table 3.1).

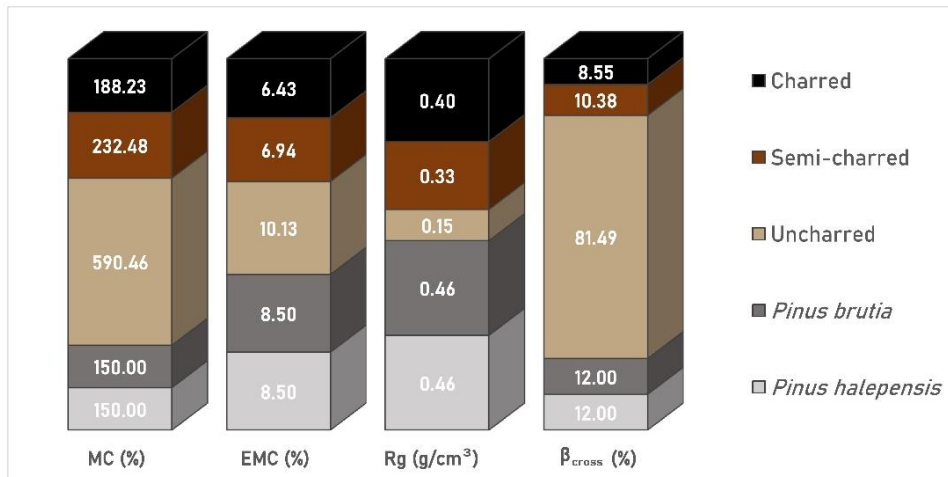


**Figure 3.9** Graphic representation of equilibrium moisture content (EMC), moisture content at the waterlogged state (MC), basic density (Rg), and shrinkage ( $\beta_{cross}$ ) of uncharred, semi-charred and charred wood compared to reference samples of *Pinus brutia* and *Pinus halepensis*

### 3.2.2 Mercury Intrusion Porosimetry (MIP)

The results of MIP are presented in histograms of intruded pore volume as a function of the pore radius for the reference samples of *Pinus brutia* and *Pinus halepensis*, and for the archaeological uncharred, semi-charred and charred wood (figure 3.10). Based on the histograms, it is apparent that the pore size distribution among the archaeological wood and the controls of *Pinus brutia* and *P. halepensis*, is considerably different (figure 3.10). Controls' porosity is mostly constituted by microvoids (5nm -5 $\mu$ m), macrovoids (5  $\mu$ m ~ 200  $\mu$ m) to a much lesser extent, and few nanovoids (< 5 nm). In contrast, in archaeological wood macrovoids prevail noticeably, as the general porosity had shifted towards larger pores > 1 $\mu$ m (dotted line) (figure 3.10). Differences in the pore size distribution as a function of the intruded volume have been

also observed among the three charring conditions (figure 3.10). Uncharred wood demonstrated a similar porosity to semi-charred material, while both showed a higher porosity compared to charred wood that appeared to have few large pores, located mostly at the narrow range of 5 to 15  $\mu\text{m}$ .

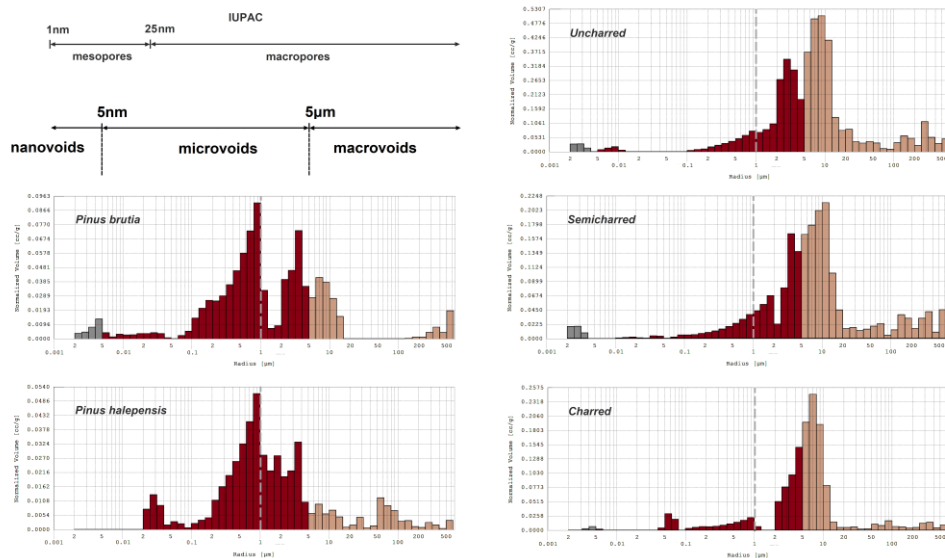


**Figure 3.10** Histograms of intruded pore volume as a function of the pore radius of the controls of *Pinus brutia* and *Pinus halepensis* (left) and the archaeological uncharred, semi-charred and charred wood (right). The IUPAC categorization is presented versus the pore size categorization adopted in the present study.

The increased porosity of the archaeological material compared to fresh reference samples, becomes clearer with the differential pore-size distribution curves and the cumulative intruded volume curves (figure 3.11), in which all three conditions showed a higher total pore volume compared to controls of *Pinus halepensis* (0.50 cc/g), and *Pinus brutia* (0,92 cc/g). Differences, in porosity among the three charring conditions were again evident, as the uncharred wood showed the highest intruded Hg volume (4,45 cc/g) compared to semi-charred (2,05 cc/g) and charred wood (1,40 cc/g) (figure 3.11).

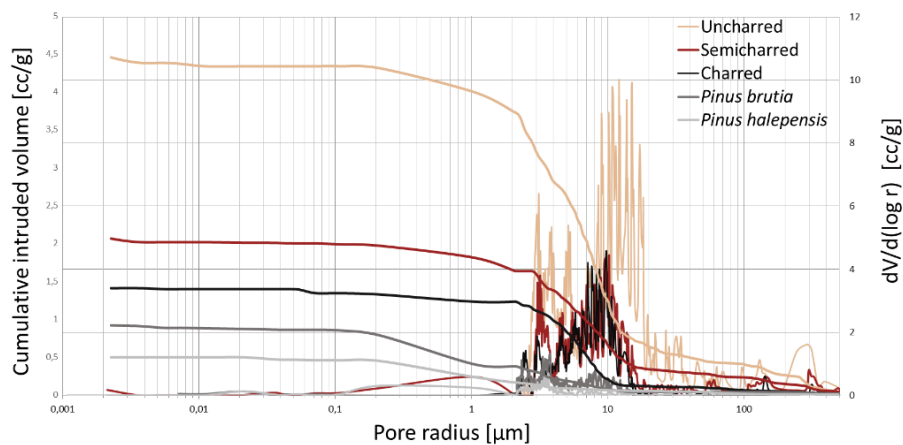


**Figure 3.11** Differential pore-size distribution curves and cumulative intrusion curves of controls (*Pinus brutia* and *Pinus halepensis*) and the three conditions of the archaeological wood (uncharred, semi-charred and charred).

### 3.2.3 Proximate Analysis

The results of proximate analysis conducted on semi-charred and charred wood, for moisture content, volatile matter, ash content, and fixed carbon, are presented in table 3.2. For the moisture content, no difference was recorded among the two charring conditions, while the volatile matter was lower in fully charred material. Additionally, ash and fixed carbon content appeared to increase with combustion.

Sample	M	VM	Ash	Fixed C
Semi-charred	6.53	75.07	1.87	16.51
Charred	6.71	24.16	3.53	65.59

**Table 3.2** Proximate analysis results for charred and semi-charred samples. Percentages values of moisture content (M), volatile matter (VM), ash content (Ash) and fixed carbon (Fixed C) are the average of 2 replicates. Fixed carbon was calculated on dry basis.



### 3.3 Mechanical Properties

#### *3.3.1 Force-controlled Hardness Test Methods- Brinell and Vickers*

The Brinell hardness test, proved not to be suitable for the archaeological material under investigation mainly due to the extremely varied hardness demonstrated by the three charring conditions. More specifically, the force that produced a measurable indentation mark with diameter in the range of 0.24 D and 0.6 D (International Standard 2005) on charred wood, on uncharred wood was penetrating the wood in a depth larger than the ball diameter resulting in an ‘out of travel’ error message. Similarly, the force required to produce an indentation on uncharred wood, meeting the test specifications, was inadequate to create an indentation on charred wood.

The Vickers hardness test, presented similar restrictions to the Brinell hardness test in terms of measurements, as the same force could not produce measurable indentations on all three substrates tested.

#### *3.3.2 Depth-controlled Hardness Test Method- Janka*

Results of end, radial and tangential hardness for the reference *Pinus brutia* and *Pinus halepensis* samples are presented in figure 3.12 and table 3.3. End hardness was higher than side (radial and tangential) hardness in both species. Additionally, latewood hardness, measured on both end and side planes, were higher than the earlywood one. Generally, *Pinus halepensis* presented higher hardness values compared to *Pinus brutia* except for the latewood tangential hardness that appeared slightly lower, though the high standard deviation (table 3.3) exhibited for this result makes this low value questionable.

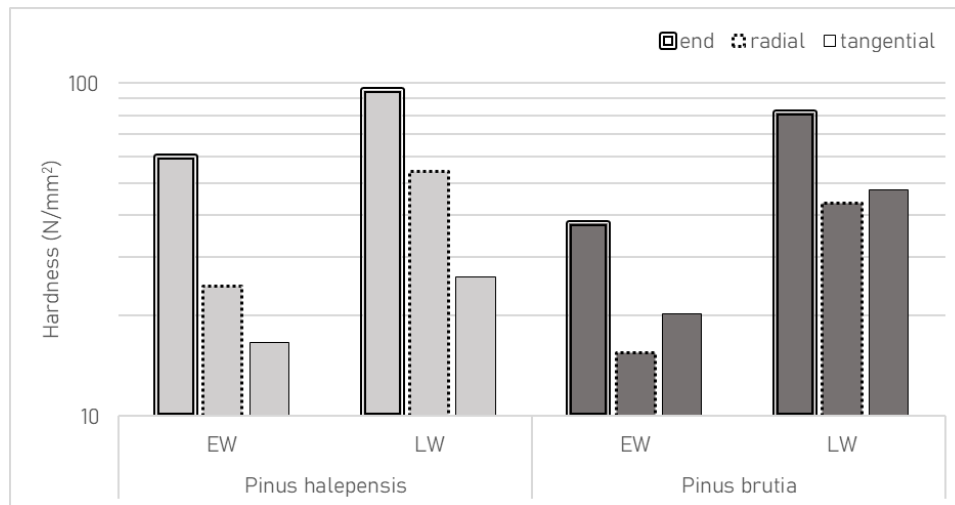


**Figure 3.12** End, radial and tangential hardness of the reference *Pinus brutia* and *Pinus halepensis* measured at both earlywood and latewood. Results are the average of two replicates.

Hardness (N/mm <sup>2</sup> )	End	Radial	Tangential	
<i>Pinus halepensis</i>	EW	60.19 ( $\pm$ 1.26)	24.62 ( $\pm$ 1.33)	16.66 ( $\pm$ 2.33)
	LW	95.16 ( $\pm$ 10.06)	54.04 ( $\pm$ 3.24)	26.19 ( $\pm$ 5.84)
<i>Pinus brutia</i>	EW	37.94 ( $\pm$ 5.87)	15.53 ( $\pm$ 0.67)	20.31 ( $\pm$ 1.22)
	LW	81.58 ( $\pm$ 9.67)	43.53 ( $\pm$ 3.80)	47.87 ( $\pm$ 2.60)

**Table 3.3** End, radial and tangential hardness measured with the modified Janka test. All values are the average of 4 replicates. Values in brackets represents standard deviation.

Regarding the hardness recorded among the three charring conditions (figure 3.13, table 3.4), the obtained results on the freeze-dried (FD) material, showed that the highest hardness was recorded for charred wood, followed by the semi-charred and the uncharred wood for all three planes. However, it has to be noted that both radial and tangential values of uncharred and semi-charred samples were similar.

For the waterlogged (W) material, the highest values were recorded on the semi-charred wood, followed by charred, and uncharred wood. In that state, difference between uncharred and semi-charred wood was significant.

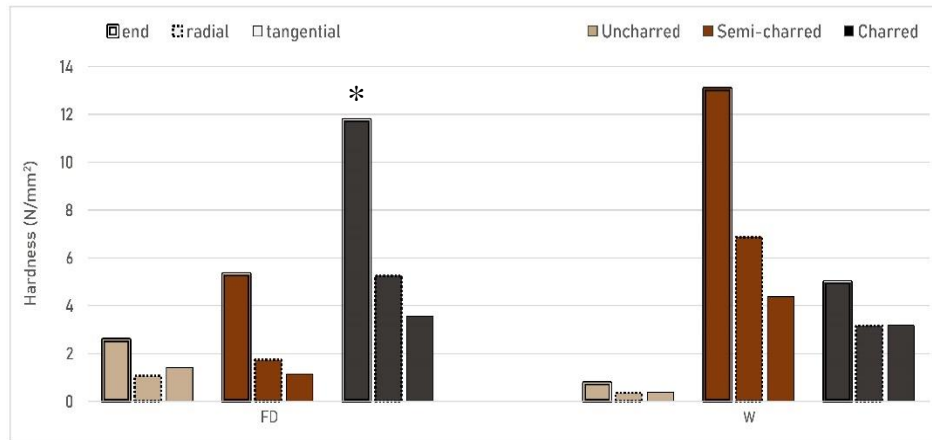


**Figure 3.13** End, radial and tangential hardness of waterlogged archaeological uncharred, semi-charred and charred wood on both freeze dried (FD) and waterlogged (W) state. Results are the average of two replicates. \* Single value due to material's failure.

Hardness values recorded for the archaeological material, irrespective of the containing water, charring condition, and plane were ranging from 0.35 to 13.06 MPa (Table 3.4). On the other hand, hardness respective values of the reference samples were ranging from 15.53 to 60.19 MPa for EW, and from 15.53 to 95.16 MPa for LW (table 3.3). As measurements for the archaeological material were not able to be conducted on a defined growing season, in figure 3.14 and table 3.4, results on the FD and W archaeological material hardness, are presented comparatively to the average hardness of EW-LW of *Pinus brutia* and *Pinus halepensis*. By this comparison, it becomes apparent that all archaeological samples presented significantly lower hardness than references.

The end hardness measurements on charred wood for both moisture content states, were rather problematic as the FD material failed upon testing and the W material presented hardness with extremely high standard deviation. This is more evident in force-penetration graphs presented in figure 3.15.

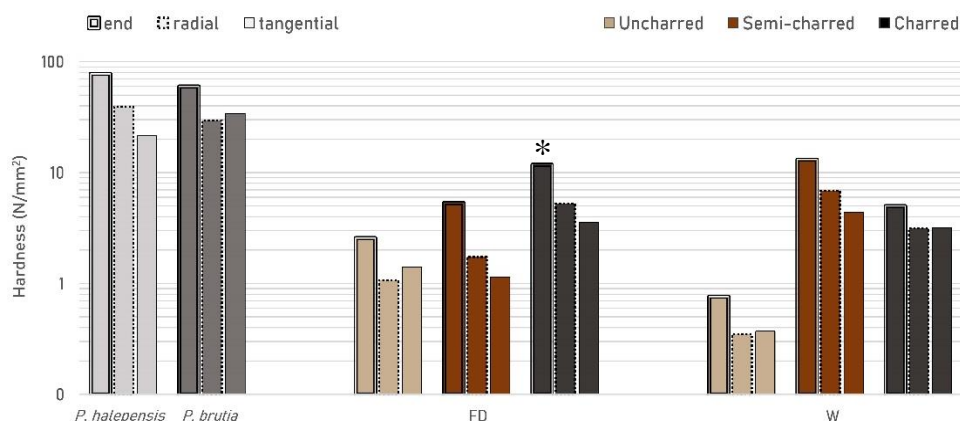


**Figure 3.14** End, radial and tangential hardness of the archaeological wood, at the freeze-dried (FD) and at the waterlogged (W) state, in comparison to the hardness of *Pinus halepensis* and *Pinus brutia* of which EW-LW values were averaged. \* Single value due to material's failure.

Hardness (N/mm <sup>2</sup> )		End	Radial	Tangential
<i>Pinus halepensis</i>		77.68 (± 21.02)	39.33 (± 17.10)	21.43 (± 6.59)
<i>Pinus brutia</i>		59.76 (± 26.02)	29.53 (± 16.32)	34.09 (± 16.00)
Uncharred	FD	2.57 (± 0.87)	1.07 (± 0.26)	1.41 (± 0.07)
	W	0.76 (± 0.18)	0.35 (± 0.02)	0.37 (± 0.00)
Semi-charred	FD	5.32 (± 1.02)	1.73 (± 0.13)	1.14 (± 0.20)
	W	13.06 (± 3.18)	6.86 (± 4.09)	4.37 (± 0.04)
Charred	FD	11.76*	5.25 (± 1.44)	3.55 (± 0.01)
	W	4.98 (± 3.46)	3.16 (± 1.15)	3.17 (± 1.07)

**Table 3.4** Hardness measured with the modified Janka test. Values of reference *Pinus halepensis* and *Pinus brutia* are the average of 8 replicates (4 on EW and 4 on LW), while of archaeological samples of 2 replicates, \*: a single value due to material's failure under testing. Values in brackets represents standard deviation.

Only few samples produced smooth lines with constant slopes (mainly in tangential planes), while the majority of samples presented a fluctuated strength under increasing load. The failure of one of the two end replicates was recorded at the graph as a flat line at zero force after a 0.3 mm penetration.

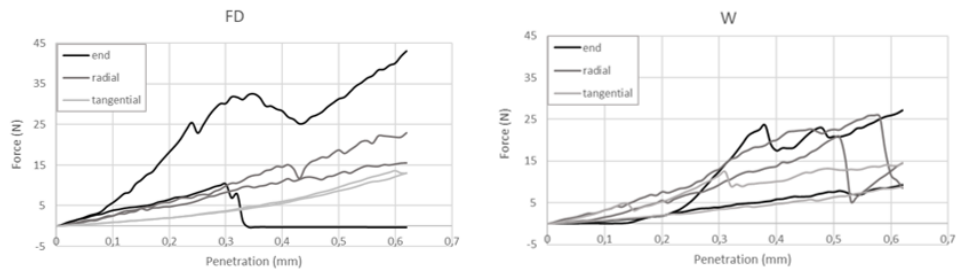


**Figure 3.15** Force-penetration graph of charred wood in freeze-dried and waterlogged state

The respective graphs for uncharred and semi-charred material at both FD and W state are presented in figure 3.16 where it is demonstrated that under load the material produced smoother lines with almost constant slopes. Semi-charred wood at the waterlogged state was also checked at opposite tangential plane than originally tested and presented before, due to the high standard deviation recorded at both end and radial plane. The second tangential conducted at the less charred side and showed significantly lower maximum force than the originally tested side ( $\sim 15$  N), but similar to the tangential of the FD sample ( $\sim 5$  N).

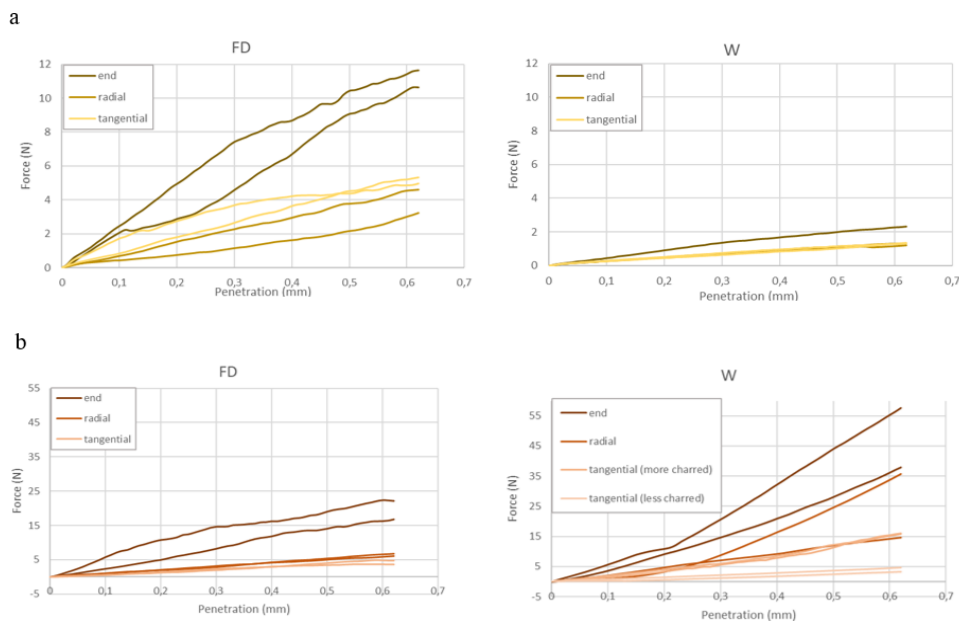


**Figure 3.16** Force-penetration graph of uncharred (a), and semi-charred (b) wood in freeze-dried and waterlogged state

### 3.3.3 Penetrometer

Results obtained with the fruit penetrometer for each charring condition are presented in figure 3.17 and table 3.5. Uncharred wood demonstrated the lowest resistance to penetration (ranged from 430 to 699 g), semi-charred wood presented almost double values (ranged from 903 to 1156 g), whereas charred wood demonstrated the highest resistance to penetration (ranged from 1147 to 1452 g). All measurements indicate the maximum load recorded, which however wasn't documented at the same penetration depth of 2cm as intended, due to materials' limitations. Uncharred wood allowed full penetration of the needle (2cm), whereas in the semi-charred the needle penetrated only partially (~0.5 - 1 cm), and charred wood allowed only superficial penetration the needle penetrated only partially (~0.0 – 0.3 cm). Therefore, results cannot be interpreted as hardness values as in needle hardness test either the force (Vörös and Németh 2020) or the penetration depth (Kollmann and Côté 1968; Vörös and Németh 2020) must be kept stable.

Furthermore, among the three charring conditions, resistance to penetration measurements showed a correlation with the Rg values (figure 3.18). Correlation between Rg and resistance to penetration has been reported for waterlogged archaeological wood (Gregory et al. 2007; Petrou and Pournou 2018), and is also anticipated to exist for semi-charred and charred material. However, further research is required to confirm this assumption.

Charring condition	Replicates					
	1	2	3	4	5	6
Uncharred	430 g	466 g	537 g	561 g	597 g	699 g
Semi-charred	903 g	909 g	1062 g	1101 g	1140 g	1156 g
Charred	1147 g	1152 g	1174 g	1228 g	1310 g	1452 g

**Table 3.5** Resistance to penetration values recorded on each charring condition.



## 3.4 Chemistry

### 3.4.1 Energy Dispersive Spectroscopy (EDS)

Bulk analysis of all charring conditions showed the presence of calcium (Ca), magnesium (Mg), silica (Si), sulfur (S) and iron (Fe), (figure 3.19), while sulfur (S) and iron (Fe) were the most abundant. In terms of topochemistry, it was shown that the concentration of all elements decreased towards the charred areas. Moreover, aluminum (Al) was only detected at uncharred area.

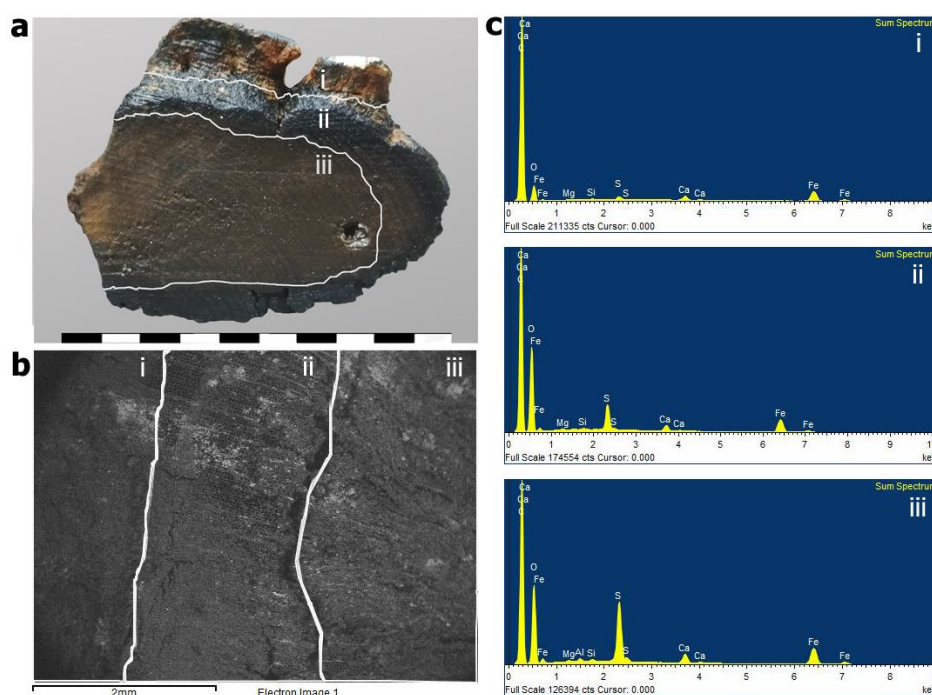


**Figure 3.19** Macroscopic image (a) and SEM micrograph (b) of a sample where charred (i), semi-charred (ii), and uncharred (iii) material coexisted; (c) EDS spectrum of each condition.

Elemental mapping and line scan on samples on which all charring conditions coexisted (figure 3.20) also confirmed that the presence of S and Fe is more pronounced in uncharred areas. Moreover, mapping revealed often the close coexistence of S and Fe. Another finding revealed by EDS was the different concentrations of carbon (C) and oxygen (O<sub>2</sub>) due to charring (Figure 3.21). The C percentage is much higher than O, which is almost depleted in charred



area (Figure 3.21 a). On the other hand, in semi-charred and uncharred area the O to C ratio (O/C) is constant, but relatively low in the latter (Figure 3.21 a).

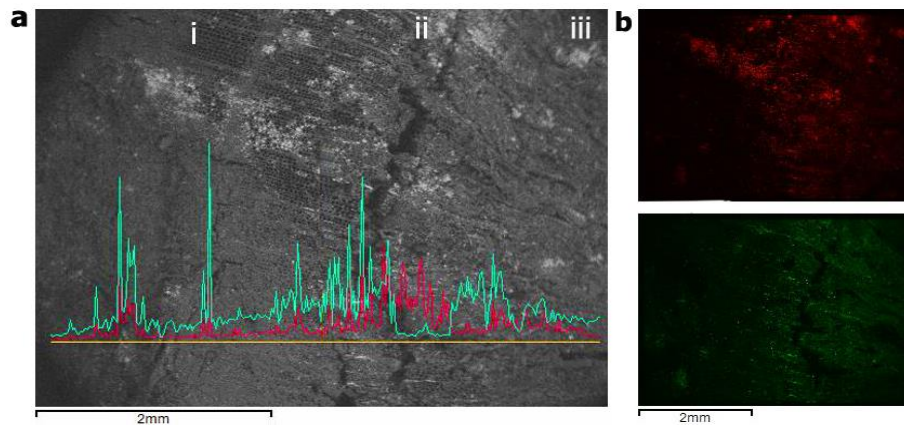


**Figure 3.20** EDS line-scan and mapping of a sample where all conditions coexisted. (a) Line scan of Fe (red) and S (green) (left to right the transition from charred to uncharred (i–iii); (b) mapping of Fe (red) and S (green).

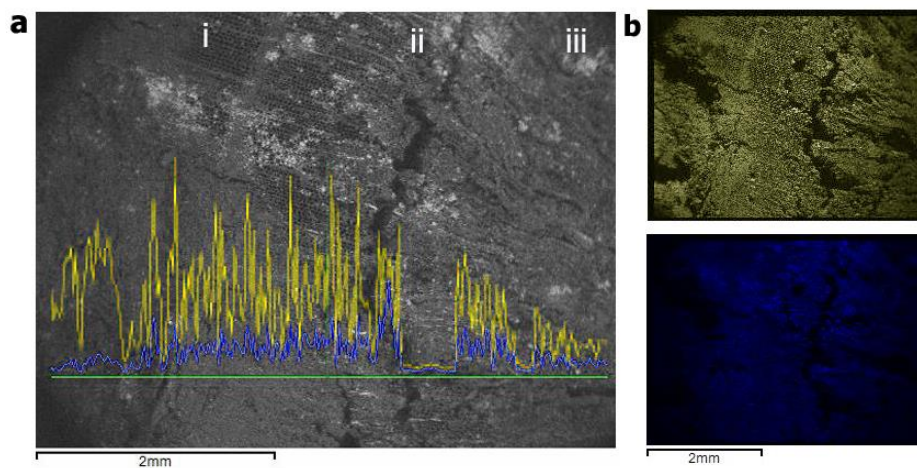


**Figure 3.21** EDS Line-scan and mapping of a sample where all conditions coexisted. (a) Line scan of carbon (yellow) and oxygen (blue) (left to right the transition from charred to uncharred (i–iii); (b) mapping of carbon (yellow) and oxygen (blue).

### 3.4.2 Fourier-Transform Infrared Spectroscopy (FTIR)

Spectra obtained from uncharred, semi-charred, and charred archaeological samples along with reference spectra of *Pinus halepensis* and *Pinus brutia* are presented in Figure 3.22

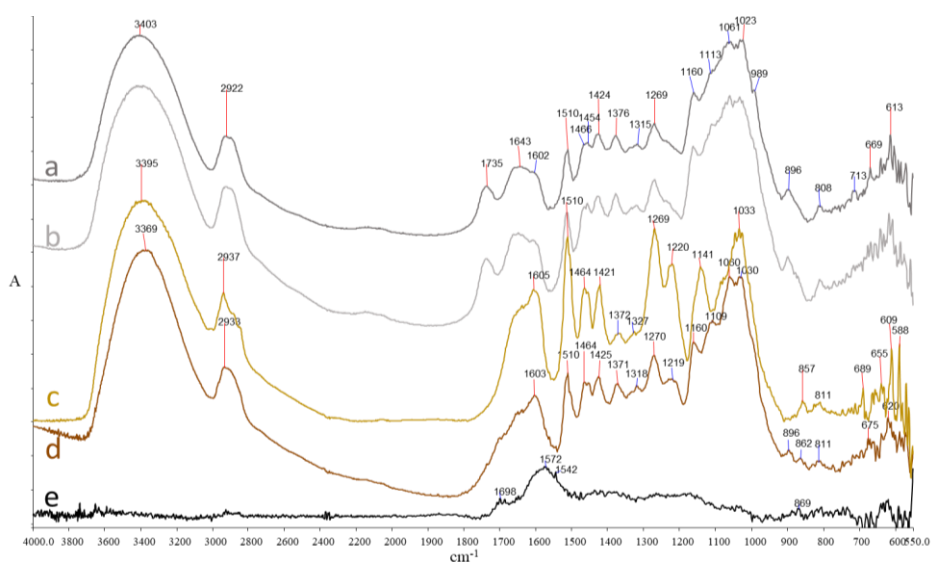


**Figure 3.22** Infrared spectra recorded for reference samples, (a) *Pinus halepensis* Mill. and (b) *Pinus brutia* Ten. (c) uncharred (d) semi-charred, and (e) charred archaeological samples.

In the uncharred wood spectrum (spectrum c, Figure 3.22), the lignin bands at 1605, 1510, 1269, 1220, and 1030  $\text{cm}^{-1}$  are pronounced, in contrast to the carbohydrate bands at 1737, 1370, 1158, 1060, and 895  $\text{cm}^{-1}$ , which are decreased in intensity. Development of new bands at  $\sim 1140$  and 855  $\text{cm}^{-1}$  was also recorded.

On the semi-charred wood spectrum, many carbohydrate bands such as those at  $\sim 1371$ ,  $\sim 1160$ , and 1110  $\text{cm}^{-1}$  showed no significant difference in intensity while the band at 1060  $\text{cm}^{-1}$  was increased. On the other hand, the intensity of hemicelluloses ester carbonyl peak at 1737  $\text{cm}^{-1}$  is evidently decreased as so the cellulose peak at  $\sim 895$   $\text{cm}^{-1}$ . Similarly, the lignin bands, approximately at 1464, 1316, 1269, and 1223  $\text{cm}^{-1}$  showed no intensity differences, whereas

an increase in absorption at 1030 and 1060  $\text{cm}^{-1}$  and also a slight rise of some bands at 1603, 1510, and 1425  $\text{cm}^{-1}$  has been observed.

On the charred wood spectrum, the broad band at 3400–3320  $\text{cm}^{-1}$  represents the –OH stretching vibration of water and the peaks at 3000–2800  $\text{cm}^{-1}$ , due to aliphatic C-H stretching vibration derived from methyl, methylene, and methine group, are absent. Characteristic bands of wood components such as hemicelluloses ( $\sim 1737 \text{ cm}^{-1}$ ), lignin ( $\sim 1510$  and  $1269 \text{ cm}^{-1}$ ), and cellulose (1026 and  $\sim 898 \text{ cm}^{-1}$ ) and roughly all bands of the wood fingerprint region (1500–900  $\text{cm}^{-1}$ ) were also absent. However, broad bands at  $\sim 1708 \text{ cm}^{-1}$  assigned to the acidic C=O groups and 1610–1590  $\text{cm}^{-1}$  assigned to lignin aromatic C=C skeletal vibrations are present.

#### 3.4.3 X-ray Diffraction (XRD)

Diffraction patterns regarding the typical wood cellulose lattice planes reflections ( $1\bar{1}0$ ), (110), (102), (200), and (004) (Anderson et al. 2004; Park et al. 2010; Agarwal et al. 2013) for the two reference samples (*P. halepensis* and *P. brutia*) along with charred, semi-charred, and uncharred archaeological waterlogged samples are shown in figure 3.23. All cellulose reflection peaks were evident at both reference samples, and at the semi-charred diffraction patterns. On the other hand, the uncharred sample diffraction pattern showed a considerably flattened line-shape on the ( $1\bar{1}0$ ) and (110) plane, while a more prominent peak on the (200) plane reflection was observed. Similarly, the charred sample diffraction pattern appeared flattened but with a weak broad peak on the (200) reflection plane and a shifted vague maximum at  $\sim 30^\circ$ .

The crystallinity index (CrI) of the material examined varied greatly (table 3.6). The higher cellulose CrI value was calculated for the uncharred material and followed by semi-charred wood and by the reference samples. For charred wood CrI was not calculated as no cellulose is expected to be

preserved in the material due to the high thermal exposure. Furthermore, CrI values were not in accordance with the respective crystallite sizes (L), as for the uncharred material, L presented the lowest value.

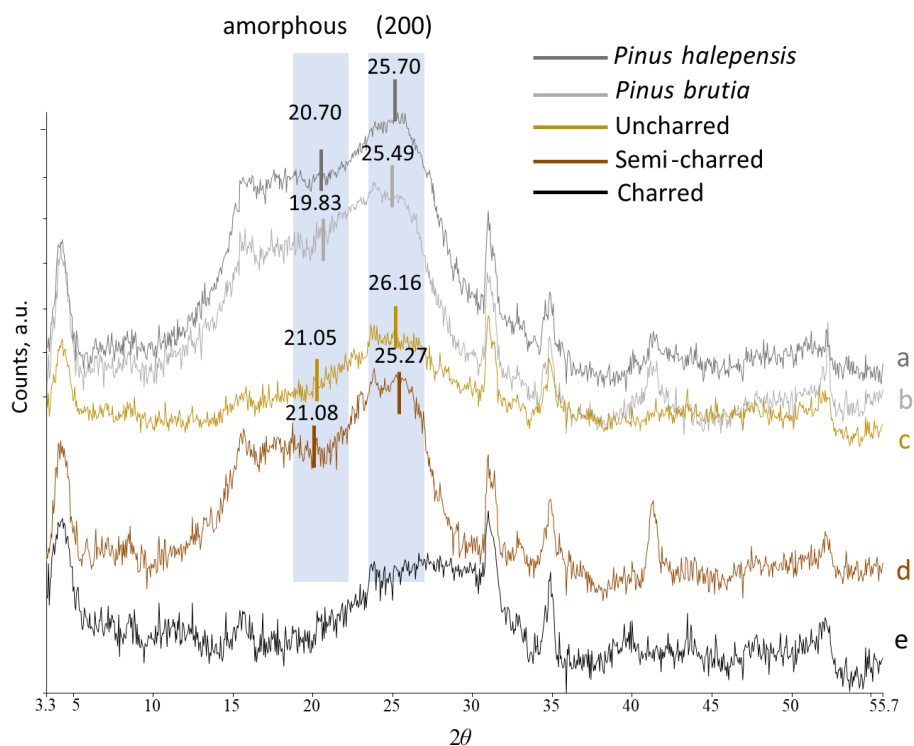


**Figure 3.23** X-ray diffraction pattern of (a) *Pinus halepensis* Mill. and (b) *Pinus brutia* Ten. reference samples in comparison with (c) uncharred, (d) semi-charred, and (e) charred waterlogged samples. The  $2\theta$  values correspond to Cobalt source reflections.

Sample	$2\theta$ (I200) <sup>a</sup>	$2\theta$ (Iam) <sup>a</sup>	CrI	L (nm)
<i>Pinus brutia</i>	25.49	19.83	41.7%	2.29
<i>Pinus halepensis</i>	25.70	20.70	41.8%	2.51
Uncharred	26.16	21.05	53.2%	1.10
Semi-charred	25.27	21.08	47.4%	2.75
Charred <sup>b</sup>	-	-	-	-

**Table 3.6.** Band positions of the maximum total intensity (I200) and the minimum intensity of the amorphous cellulose (Iam). CrI represents the crystalline index based on Segal's method and L correspond to the crystallite size.

<sup>a</sup>  $2\theta$  values are expressed as Co-source, <sup>b</sup> CrI was not calculated as no cellulose is expected to be preserved with charring above 400 °C.

## 4. Discussion and Conclusions

### 4.1 Morphological Alterations at a Cellular Level

#### 4.1.1 Scanning Electron Microscopy (SEM)

The ultrastructure of the archaeological material observed with SEM, demonstrated the existence of three distinctly dissimilar materials, uncharred, semi-charred and charred. Uncharred waterlogged wood appeared to be severely deteriorated, as extensive biodeterioration was documented attributed to fungi and bacteria based on the recorded decay patterns and the identified microorganisms (Pournou 2020).

On the other hand, in semi-charred wood evidence on biodeterioration is rare and its general morphology seems rather intact. This different deterioration degree of the semi-charred wood in comparison to the uncharred material is considered to be more likely owed to the thermal alterations of the former that probably made it less prone to biodeterioration (Li et al. 2017; Gao et al. 2018). However, some of the samples present differences in morphology indicating multiple preservation conditions, most likely related to a different thermal degradation. Although the present study examined the semi-charred wood as a single condition, this should have been expected as wood charring results in a final material organized in layers of descending thermal exposure from the fire front surface towards the inner core (Tsai 2010; Friquin 2011; Bartlett et al. 2019) where some layer can be extremely thin (35 mm) (Friquin 2011). It is though unclear whether this morphology is owed directly to the thermal alterations (Bakar et al. 2013) or to their possible consequences, such as different degree of resistance to biodeterioration (Hill 2006; Kymäläinen et al. 2018b). Further investigation is required in order to clarify this aspect of the morphology.

In charred wood, no biodeterioration patterns were observed, although bacteria were rarely present, indicating a material resistant to

biodeterioration. The small rounded formations that were abundant in the tracheid wall and around the pit chambers it is uncertain if they belong to the warty layer (Liese 1963; Terziev and Daniel 2002), or if they are cross-sections of bacilli. The severe distortion that was observed, resembling a material that had suffer plastic deformation indicating fast pyrolysis of wet wood at high temperatures (Caple and Murray 1994). The recorded coalescence of secondary cell walls with the middle lamella, is a feature commonly reported in chars (Cutter et al. 1980; Connor and Daria 1993; Caple and Murray 1994; Tamburini et al. 2020). This disappearance of the discrete cell wall layers, also referred as amalgamation, has been reported to initiates at temperatures close to 300°C (Boocock and Kosiak 1988). Zickler et al. (2006) reported that above 400°C wood resembles a glass-like carbonaceous residue which may corresponds to the characteristic vitreous appearance observed in SEM results. However the exact temperature on which the material was exposed cannot be defined as amalgamation temperature depends on several factors such as the heating rate (Cutter et al. 1980; Connor and Daria 1993). Nonetheless, it can be safely stated that the ultrastructure of the charred wood corresponds to wood that was subjected to thermal exposure of at least 300°C. Similarly, as both middle lamellae and secondary walls were clearly discrete in semi-charred wood, it is suggested that was exposed at a temperature < 300°C.

## 4.2 Physical Properties

### *4.2.1 Moisture Content, Density and Shrinkage Determination*

Deviation of the physical properties examined among the archaeological uncharred, semi-charred and charred samples was also apparent. The moisture content (MC) values of uncharred, semi-charred, and charred wood showed that they were waterlogged. However, one should expect that MC values of semi-charred and charred samples should be lower than reference ones due to charring (Kamperidou 2019), but after prolonged exposure to wet

conditions, like burial in the marine environment, elevated MC is justified (Ronewicz et al. 2017; Cai 2020). The MC values of uncharred wood (590) were indicating a highly degraded material (De Jong 1977; Florian 1990; McConnachie et al. 2008; Broda and Hill 2021). Lower MC values were recorded for the semi-charred (232.48%) and the charred wood (188.23%), suggesting that their exposure to heat has influence their water holding capacity (Kymäläinen et al. 2018a; Chen et al. 2019).

Equilibrium moisture content (EMC) of the uncharred archaeological wood at  $45 \pm 5\%$  RH was slightly higher compared to the reference samples, which is a find that have been frequently reported for degraded waterlogged archaeological wood (Hoffmann 1985; Schniewind 1990; Esteban et al. 2009; Broda et al. 2019; Han et al. 2020; Cao et al. 2023). This is linked to greater sorption sites availability due to increased cell wall porosity caused by the action of microorganisms, which increases bound water and the fiber saturation point (FSP) of the waterlogged wood (Broda et al. 2019; Han et al. 2020; Broda et al. 2021a; Cao et al. 2023), and/or to cellulose degradation to shorter molecules (Broda et al. 2019; Han et al. 2020).

For the semi-charred and charred wood, the EMC values recorded are in line with the literature regarding wood exposed to temperature up to  $300^{\circ}\text{C}$  (Hill 2006; Esteves et al. 2007; Akyildiz and Ates 2008; Ates et al. 2009; Stanzl-Tschegg et al. 2009; Kymäläinen et al. 2014; Chen et al. 2019; Cai 2020; Nhacila et al. 2020) and above  $300^{\circ}\text{C}$  (Kymäläinen et al. 2014). The primary reason for this is connected with the depletion of hemicelluloses, due to biodeterioration in the marine environment (Pournou 2020) and/or heat exposure (Hill 2006; Kymäläinen et al. 2014) that is negatively correlated to wood EMC in terms of both temperature and duration (Esteves et al. 2007; Akyildiz and Ates 2008; Ates et al. 2009; Kamperidou 2019; Nhacila et al. 2020).

As it was anticipated the uncharred waterlogged samples presented the lowest basic density ( $R_g$ ) due to degradation (Borgin et al. 1979; Grattan 1987; Schniewind 1990; Broda and Hill 2021), which is also negatively correlated to the MC (Hoffmann 1982; Kohdzuma et al. 1996; Broda et al. 2021b). On the other hand, the  $R_g$  values of the semi-charred and charred samples were lower than the reference samples, which however is considered to be mostly due to charring (White and Schaffer 1978; Cutter and McGinnes 1981; Brewer et al. 2014; Ronewicz et al. 2017) and to a lesser extent to biodeterioration as shown by SEM results. The non-destructive determination of relative density ( $rR_g$ ) gave similar results to the basic density ( $R_g$ ) for all three charring conditions, and demonstrated that it can be adopted in cases where the oven dried weight cannot be calculated.

Cross shrinkage ( $\beta_{\text{cross}}$ ) for the uncharred waterlogged wood was high as expected, and negatively correlated with basic density (Borgin et al. 1979; Grattan 1987; Schniewind 1990; Kohdzuma et al. 1996; Broda et al. 2018; Broda et al. 2021b). The same correlation was also recorded for the semi-charred and charred material. However, the  $\beta_{\text{cross}}$  of semi-charred and charred material was found to be lower than uncharred wood, and it was even lower than sound wood, indicating that the charred areas of shipwreck timbers can demonstrate high dimensional stability upon drying, a result that should be considered under the conservation perspective.

#### *4.2.2 Mercury Intrusion Porosimetry (MIP)*

Based on the porosimetry results, it becomes apparent a shifting of porosity towards larger pores ( $> 1 \mu\text{m}$ ) for all charring conditions of the archaeological material. This was rather anticipated, as both charring (Rutherford et al. 2005; Grioui et al. 2007; de Assis et al. 2016) and biodeterioration in the marine environment (Pournou 2020), may increase the total porosity of archaeological wood (Grattan 1987; Florian 1990; Broda et al. 2019; Broda and Hill 2021).



More specifically, uncharred wood showed the highest porosity (total pore volume of 4,45 cc/g), which is more likely due to biodeterioration as was evident by SEM results. In contrast charred wood showed the lowest porosity among the three charring conditions (total pore volume of 1,40 cc/g), but still, an increased porosity compared to controls of *Pinus halepensis* (0,50 cc/g), and *Pinus brutia* (0,92 cc/g). This most likely occurred due to carbonization (Rutherford et al. 2005; Grioui et al. 2007; de Assis et al. 2016), where the main volume of macrovoids with radii  $> 5 \mu\text{m}$  was developed. Similarly, for semi-charred material, the thermal modification also increased its porosity (2,05 cc/g), as upon heat exposure, the porosity augments as a function of temperature (Pfriem et al. 2009; Zauer et al. 2014). Furthermore as shown by SEM results, the semi-charred material was still susceptible to biodeterioration, thus its porosity was most likely increased further during burial. Information on the performance of thermally modified wood in the marine environment is lacking (Godinho et al. 2021), however, there are some studies demonstrating that thermal modification makes the wood more resistant to soft rot (Li et al. 2017; Gao et al. 2018). This may probably explain why the porosity of the semi-charred wood was considerably lower compared to the uncharred material, which presented the highest porosity recorded, principally due to biodeterioration but higher than the charred wood. The porosity of uncharred and semi-charred material is in accordance with physical properties results. However, as porosity greatly affects the impregnation rate (Thanh et al. 2018) and the polymer retention during wood treatments, especially inside pores with diameters  $> 0.1 \mu\text{m}$  (Ding et al. 2008), it is expected that uncharred archaeological wood will be more permeable and will promote diffusion and eventually better consolidation. In contrast, it is considered that charred material will be resistant to diffusion even by low MW polymers.

### 4.2.3 Proximate Analysis

Almost negligible difference was recorded between the moisture content (M) of semi-charred (6.53%) and charred wood (6.71%). These results are almost identical to the previously mentioned results of EMC for semi-charred (6.94%) and charred wood (6.43%). The differences between EMC and M for each charring condition are not statistically significant based on t-test ( $p=0.15$  for semi-charred, and  $p=0.20$  for charred wood), indicating a reduced ability of water absorption after air-drying.

Proximate analysis results showed that the volatile matter values, of charred material (24.16%) was lower than the semi-charred (75.07%) one, as the volatile matter is negatively correlated with temperature (Fuwape 1996; Ruiz-aquino et al. 2019; Dias Junior et al. 2020). This is also supported by the higher volatile matter that have been recorded by Şensöz and Can (2002) for sound samples of *Pinus brutia* (87.04%). Volatile matter differentiates among the species (Ruiz-aquino et al. 2019), and since no volatile matter values for *Pinus halepensis* or *Pinus brutia* charcoals have been detected in the literature, no further conclusions could be driven. However, based on references regarding the volatile matter of *Eucalyptus saligna* which in uncharred state have been reported to be ~ 90% (Senelwa and Sims 1999), while after pyrolysis at 450 °C to be 29.8% (Dias Junior et al. 2020), it could hypothesized the combustion temperature of the charred wood in the present study was at or below 450 °C. Nonetheless, as volatile matter is also temperature and time dependent (FAO 1985), further investigation is required to understand the pyrolysis conditions under which the material of the study produced. The difference of volatile matter estimated between semi-charred and charred condition can be attributed to the presence of the outer charred layer which is commonly produced and acts as a barrier that slows the thermal decomposition of the inner areas (Mikkola 1991; Friquin 2011; Lowden and

Hull 2013). Thus the semi-charred material was protected against thermal exposure and volatile loss by the presence of the charred material.

Ash content is species dependent (FAO 1985; Smółka-Danielowska and Jabłońska 2022). For sound samples of *Pinus brutia* and *Pinus halepensis* an ash content of 0.45% have been recorded for sapwood, and of 0.54% for heartwood (Benouadah et al. 2019), while in another research an ash content of 0.40% and 0.42% have been recorded for sapwood close to the bark at different heights of the log (Antonović et al. 2018). The only available data regarding thermally exposed samples of those species detected at Liodakis et al. (2005) which examined the ash content of both hardwood and softwood species ashes prepared at various temperatures (600°C, 800°C and 1000°C). At 600°C *Pinus brutia* and *Pinus halepensis* presented an ash content of 2.39% and 3.27% respectively (Liodakis et al. 2005). At this study (Liodakis et al. 2005) ash content reduces as temperature increases on all samples examined which is in contrast to other researchers finds for hardwood samples exposed up to 600°C (Fuwape 1996; Ruiz-aquino et al. 2019), which could possibly indicate that up to 600°C the ash content is positively correlated to temperature while above that limit is negatively correlated. In the present study, a positive correlation observed as semi charred wood presented lower ash content (1.87%) than charred wood (3.53%), indicating a thermal exposure up to 600°C. However, it need to be noted that ash content of the samples might be altered by sediment contamination (FAO 1985).

Likewise, fixed carbon content of the charred material was 65.59% while of the semi-charred was 16.51% indicating a positive correlation with combustion temperature. This is in accordance with results of other researchers (Fuwape 1996; Ruiz-aquino et al. 2019; Dias Junior et al. 2020) who also found an increase of fixed carbon at higher temperatures. This increase is suggested to be a result of pyrolytic process which favors the

volatile removal and consequently the elevation of ash-minerals and carbon (Fuwape 1996).

### 4.3 Mechanical properties

#### *4.3.1 Force-controlled Hardness Test Methods- Brinell and Vickers*

The difficulties faced by both Brinell and Vickers tests are attributed to materials' characteristics and methods' principles. As indicated by the conducted preliminary trials, uncharred, semi-charred and charred wood required distinctly dissimilar force in order to acquire data and thus are not appropriate for assessing hardness for the material under investigation. Hence, a depth-controlled method not only better describes the performance of the wood as it determines plastic and elastic deformation (Sydor et al. 2020), but in this case is the only way to acquire comparable results.

#### *4.3.2 Depth-controlled Hardness Test Method- Janka*

Results obtained by employing the modified Janka hardness test on reference samples were rather anticipated, as *Pinus halepensis* demonstrated higher hardness values than *Pinus brutia* (Rousodimos 1997). The only exception observed for the tangential hardness, on both earlywood (EW) and latewood (LW). This was indicating some local anomaly, which was later confirmed by macroscopic observation. Hence this result is not representative of the material's hardness. Moreover, the LW values were found higher than the EW (Wimmer et al. 1997; Hirata et al. 2001; Peng et al. 2016) despite the species and plane examined. It is evident that hardness of archaeological wood was considerably lower compared to the reference samples of *Pinus halepensis* and *P. brutia* as expected. This was rather justified as low hardness is commonly reported for deteriorated waterlogged archaeological wood (Schniewind 1990) and because thermal exposure also reduces wood

hardness (Ates et al. 2009; Kymäläinen et al. 2018a; Kamperidou 2019; Sedlar et al. 2019; de Abreu Neto et al. 2021).

The hardness values recorded for the semi-charred material show to deviated in relation to the other two charring conditions. This is considered to be owed to the multiple layers consisting this charring condition as previously mentioned in the SEM. The resolution of the hardness test applied (~ 1 mm indentation) could demonstrate small hardness differences, and so it revealed changes in respect to the heat source and thus, values varied depending on how far the area tested was from the uncharred or the charred part of the wood.

The highly irregular behavior of charred wood as well as the failure recorded on the end side is indicating a brittle nature which by definition is more favorable along the grain and also increases at increasing temperature (Hughes et al. 2015)

#### *4.3.3 Penetrometer*

Although the penetrometer results cannot be interpreted as hardness, they demonstrated successfully the three distinct charring conditions and thus it is indicated that the fruit penetrometer, if properly calibrated, could be developed in to a useful portable tool for identifying the existence of different charring conditions among the shipwreck timbers. Furthermore, resistance to penetration measurements showed a correlation with the Rg values among the three charring conditions. Correlation between Rg and resistance to penetration is commonly reported for waterlogged archaeological wood (Squirrell and Clarke 1987; Schniewind 1990; Gregory et al. 2007; Petrou and Pournou 2018) and is also anticipated to exist for semi-charred and charred material. However, further research is required to confirm this assumption and potentially implement a curve to assist in the documentation of different charring degrees. This could be very challenging as although

uncharred wood is distinctly differentiated by the other two conditions, the limit between semi-charred and charred wood could not be easily distinguished. This could be owed to the testing procedure, which is not taking into account, the wood depth where data were acquired. Nonetheless, the effect of the semi-charred's transitional nature could not be excluded.

## 4.4 Chemistry

### 4.4.1 Energy Dispersive Spectroscopy (EDS)

All elements detected in bulk analysis (S, Fe, Ca, Si, Al) presented the highest concentration in the uncharred region, the lowest in the charred area, whereas an intermediate concentration has been recorded in semi-charred zone. However, Al was not detected in semi-charred and charred areas. The fact that the Fe and S coexist at the exact same spots, could be owed to the probability that they both belong to the same compound (Fors 2008; Rémazeilles et al. 2013). Except S, which presence is related to the action of sulfate-reducing bacteria (Sandström et al. 2002), all the other elements detected are constituents of the seawater and chemical components of the sediment (Florian 1987; Sandström et al. 2002; Monachon et al. 2020) and thus their high concentration in the uncharred wood is most likely owed to its higher porosity and consequently permeability, that has been documented with MIP. The possible concurrent presence of S and Fe in the material, recorded with EDS, is expected to cause severe post-excavation and post-conservation problems (Fors 2008; Fors et al. 2008; Rémazeilles et al. 2013; Collis 2015; High and Penkman 2021).

Moreover, the concentration of C and O appears also to be charring-dependent. In accordance with the proximate analysis results on fixed carbon content, the C percentage increases with charring (Valenzuela-Calahorro et al. 1987; Rutherford et al. 2005; Todaro et al. 2015), while O decreases (Valenzuela-Calahorro et al. 1987; Rutherford et al. 2005). The

increase/decrease rate of the O/C ratio is also dependent on both temperature and heating duration (Rutherford et al. 2005). Moreover, the relative concentrations of these two elements showed that in charred material carbon is much higher than oxygen, indicating that the oxygen-containing organic moieties such as polysaccharides and lignin are depleted as shown also by other researchers (Inari et al. 2006; Kocaefe et al. 2012). In semi charred areas the O/C ratio is constant, indicating the presence of both carbohydrates and lignin (Kocaefe et al. 2012). Uncharred areas also present a constant O/C ratio which however is relatively low, indicating the presence of organic matter, which most likely attributed to lignin (Kocaefe et al. 2012).

#### *4.4.2 Fourier Transform Infrared Spectroscopy (FTIR)*

Fourier Transform Infrared Spectroscopy demonstrated that the spectrum of the uncharred material is a typical spectrum of a biodeteriorated waterlogged wood, where lignin bands appear pronounced and carbohydrates' bands appeared decreased. This chemical profile is indicative of wood deteriorated by erosion bacteria or/and soft-rot fungi, which thrive in the marine environment (Pournou 2020), as erosion bacteria decay has been often reported to be associated with lignin bands' increment and carbohydrate bands' decrement (Gelbrich et al. 2008; Pedersen et al. 2015) and soft-rotters also degrade carbohydrates in preference to lignin (Pournou 2020). Most of soft-rotters are unable to degrade guaiacyl lignin, found predominantly in softwoods, except for the cavity-forming species (Nilsson et al. 1989). In the uncharred wood, guaiacyl lignin presence is indicated by the newly developed bands at  $\sim 855\text{ cm}^{-1}$  which associated with the C-H out-of-plane vibrations (Traoré et al. 2018), and at  $\sim 1140\text{ cm}^{-1}$  which in combination with the increase at  $1030\text{ cm}^{-1}$  and the decrease in the intensity at  $1060$  is an indication of wood decay (Pandey and Pitman 2003), and is attributable to the relative increase of guaiacyl lignin compared to carbohydrates (C–H deformation in the guaiacyl unit, with C–O deformation in primary alcohol).

The semi-charred material spectrum is very similar to spectra of thermally modified wood as most of the carbohydrate bands show no significant changes except the hemicelluloses' ester carbonyl peak at  $1737\text{ cm}^{-1}$ , and the cellulose peak at  $\sim 895\text{ cm}^{-1}$ , due to C-H deformations at the glycosidic linkage, which were decreased. However, these alterations were also expected as the xylan-linked acetyl groups are commonly cleaved with increasing temperature and time during the burning of wood (Tjeerdsma and Militz 2005; Esteves et al. 2013; Popescu et al. 2013; Özgenç et al. 2018; Kubovsk and Kač 2020), and the cellulose peak at  $\sim 895\text{ cm}^{-1}$ , has been previously connected with thermal exposure (Kotilainen et al. 2000; Esteves et al. 2013; Özgenç et al. 2018). It should be mentioned though, that part of carbohydrates' reduction could be owed to abiotic or biotic processes occurring in the marine environment during the service life of the ship or during burial (Kim 1990; Pedersen et al. 2015; Pournou 2020). The moist environment in which fire occur has also been reported to favors the hydrolysis of hemicelluloses and amorphous cellulose (Hill 2006). Furthermore, the lignin bands showed no intensity difference as reported for thermally modified wood (Özgenç et al. 2018) whereas the slight rise observed for some is mainly due to the increase in relative lignin content (Kotilainen et al. 2000). Nonetheless, the increase in absorption at  $1030$  and  $1060\text{ cm}^{-1}$  has been observed indicating respectively the pronounced aromatic nature of the semi-charred wood, since this absorption band also indicates aromatic in-plane C-H deformation and changes in cellulose structure (Kotilainen et al. 2000; Kubovsk and Kač 2020) along with the formation of aliphatic alcohols during heating (Kotilainen et al. 2000; Popescu et al. 2013).

The charred wood spectrum is typical of charcoals as the bands at  $3400\text{--}3320\text{ cm}^{-1}$  and at  $3000\text{--}2800\text{ cm}^{-1}$  were decreased in intensity, a common chemical effect of increasing temperature (Guo and Bustin 1998; Poletto et al. 2012; Tintner et al. 2018; Constantine et al. 2021) . In addition the reduction of



characteristic bands (e.g.  $\sim 1737\text{ cm}^{-1}$ ,  $\sim 1510$  and  $1269\text{ cm}^{-1}$ ,  $1026$  and  $\sim 898\text{ cm}^{-1}$ ) assigned to wood components such as hemicelluloses, lignin and cellulose (High and Penkman 2021), and the fingerprint region ( $1500\text{--}900\text{ cm}^{-1}$ ) bands (Poletto et al. 2012), indicates the chemical changes caused by pyrolysis (Tintner et al. 2018). Furthermore, the broad band at  $\sim 1708\text{ cm}^{-1}$ , due to the acidic C=O groups, characteristic of low-temperature charcoals' spectra (Guo and Bustin 1998; Constantine et al. 2021) and the broad band at  $1610\text{--}1590\text{ cm}^{-1}$ , due to lignin aromatic C=C skeletal vibrations, which have been also reported to increase in intensity with increasing charring (Tintner et al. 2018), are indicating a relative low charring temperature.

The FTIR results for all three charring conditions are in accordance with O/C ratio observations of EDS. Moreover, the reduced hygroscopicity demonstrated by the physical properties is justified by the depletion of hemicelluloses owed either to the biodeterioration in the marine environment (Pournou 2020) or to the heat exposure (Hill 2006; Kymäläinen et al. 2014), as both temperature and duration are negatively correlated to wood EMC (Esteves et al. 2007; Akyildiz and Ates 2008; Ates et al. 2009; Kamperidou 2019; Nhacila et al. 2020).

FTIR results of uncharred wood are in line with the material ultrastructure observed with SEM, as the lignin-rich middle lamellae is preserved and the cellulose-rich secondary cell walls are degraded by erosion bacteria (Björdal 2012)

#### *4.4.3 X-ray Diffraction (XRD)*

The peaks typical of wood cellulose reflection planes (Anderson et al. 2004; Park et al. 2010; Agarwal et al. 2013) were detected in both reference samples and in the semi-charred material. On the other hand, in uncharred and charred wood only the peak on the (200) plane reflection is more evident for the former, while for the latter exists is broad and weak.

The different crystallinity index (CrI) of the material examined, which was higher than reference samples for both semi-charred and uncharred wood, depends on the charring degree and biodeterioration respectively. However, the considerably high CrI of uncharred material was not anticipated, as in archaeological wood the crystallinity usually decreases with decay (Giachi et al. 2003; Popescu et al. 2010; Zhou et al. 2018; High and Penkman 2021). Nonetheless, crystallinity's increase has been reported by other authors in initial stages of degradation due to the dramatic loss of amorphous cellulose regions (Howell et al. 2009; Popescu et al. 2010; High and Penkman 2021). It is believed however that this explanation does not justify the high CrI values of uncharred material as the diffractogram line-shape, the FTIR results and the lowest crystallite size (L) recorded, indicate that in the material investigated, cellulose is probably completely destroyed. Therefore, it appears that the Segal method for CrI calculation cannot successfully apply to severely deteriorated material. This could be due to several reasons related to the deficiency of the Segal method (Thygesen et al. 2005; Park et al. 2010; French and Santiago Cintrón 2013); nonetheless, it is considered that is principally owed to the highly depleted cellulose fraction. It is recommended for this type of material to examine the use other methods such as the two-dimensional X-ray diffraction.

The relative higher CrI of semi-charred material compared to reference samples of *Pinus brutia* and *Pinus halepensis*, is considered that is due to amorphous cellulose degradation, which occurs during the initial stages of heating and progresses as the heat temperature rises (Sivonen et al. 2002; Esteves and Pereira 2009; Tarmian and Akbar Mastouri 2019). This is in accordance with the high L value that corresponds to relatively larger crystal that the other materials examined. Moreover, indicates that the charring temperature for semi-charred material was lower than  $\sim 300$  °C as above this

threshold, cellulose crystalline part is expected to degrade severely (Kwon et al. 2009; Wang et al. 2017).

The relative increase of CrI recorded for semi-charred wood, due to amorphous cellulose degradation, results in rearrangement of the cellulose molecules and cross-linkage with lignin (Kymäläinen et al. 2018a), thus is possibly connected with low hygroscopicity, which is in accordance with low EMC recorded. Moreover, the small cellulose crystallite length recorded in uncharred wood may also be related to its hygroscopic nature recorded by EMC, as cellulose degradation to shorter polymers creates new sorption sites (Broda et al. 2019; Han et al. 2020).

Both XRD and FTIR results justify the recorded dimensional stability, and reduced hygroscopicity of semi-charred wood due to thermal modification (Esteves et al. 2007; Akyildiz and Ates 2008; Ates et al. 2009; Kymäläinen et al. 2018a; Cai 2020; Nhacila et al. 2020). Similarly, the thermal degradation of carbohydrates in charred wood are reducing the hygroscopicity of the material by limiting the sorption sites mainly to those contained in lignin (Carll and Wiedenhoef 2009; Englund et al. 2013) and hence increase its dimensional stability.

#### 4.5 Conclusions

In the present study, the morphology of the material confirmed the existence of three distinct charring conditions: uncharred, semi-charred and charred wood (Mitsi et al. 2023). Charred wood morphology indicated a material exposed to temperatures exceeding 300°C, while uncharred wood a material severely biodeteriorated in the marine environment. Morphological examination of the semi-charred wood did not show either the biodeterioration patterns observed in uncharred wood, or the amalgamation of the secondary cell walls observed in charred wood. However, semi-charred samples presented great variations in the state of preservation of their cellular

morphology indicating different degrees of charring and biodeterioration, reflecting their different exposure to the fire front.

The three charring conditions presented considerably different physico-mechanical properties (Mitsi et al. 2023). The uncharred wood showed the lowest density, hardness and resistance to penetration, and the highest moisture content, shrinkage and porosity. In contrast, charred wood showed the lowest moisture content, shrinkage and porosity, and the highest density, dry hardness and resistance to penetration. Again, the semi-charred wood demonstrated a transitional character in all abovementioned properties.

Results obtained on the chemistry of the archaeological material (Mitsi et al. 2021), justified the morphological differences observed and the dissimilar physico-mechanical properties recorded. The uncharred wood was chemically similar to biodeteriorated waterlogged wood, as carbohydrates were dramatically decreased and lignin was found increased. The charred wood, was chemically similar to low-temperature charcoals, with both its carbohydrates and lignin almost being completely depleted. The semi-charred wood, presented a transitional chemistry between the charred and uncharred wood, and showed a chemical profile analogous to thermally modified wood heated at temperatures  $< 300^{\circ}\text{C}$ , as all major components of the cell wall were still present (Mitsi et al. 2021).

The abovementioned results on the morphological, chemical and physico-mechanical properties of Rhodes' waterlogged wood, indicated different conservation requirements among the three charring conditions. Uncharred wood is in need of remedial conservation with a consolidating agent, while the charred and the semi-charred wood demonstrated negligible shrinkage values indicating that they might be safely air-dried (Mitsi et al. 2023).

These three dissimilar charring conditions are often coexist in the case of Rhodes' wreck timbers. Therefore, the conservation plan should be

formulated based on the needs of the most vulnerable material to drying, which is the uncharred wood even though this could be a difficult task as it is expected that the charred material will be refractory to impregnation even by low MW polymers.

Moreover, the recorded elemental composition is considered of paramount importance and should be bore in mind while developing the conservation strategy of the wreck, as the presence of Fe and S is associated with post-conservation acidity in wood and degradation of both cellulose and PEG.

The conservation of the semi-charred wood, even if it appears more intricate, is more likely that would not implicate the conservations treatments as it represents a quite narrow transition zone, approximately ranging from ~0.8 to ~1.5 cm, between the charred and uncharred wood. Nonetheless further research is required of this transitional zone in order to enhance understanding of its role and the possible implications it may have on future conservation efforts.

Lastly it is considered necessary to further investigate the penetrability of both charred and semi-charred wood and the diffusion of PEGs into these charring conditions, as well as the efficacy of conservation methods employed via impregnation, in cases when all three charring conditions coexist

## References

- de Abreu Neto, R., Guedes Ramalho, F.M., Ribeiro Costa, L. and Gherardi Hein, P.R. 2021. Estimating hardness and density of wood and charcoal by near-infrared spectroscopy. *Wood Science and Technology* 55(1), pp. 215–230. Available at: <https://doi.org/10.1007/s00226-020-01232-y>.
- Agarwal, U.P., Reiner, R.R., Ralph, S.A., Forest, A., Gi, O. and Drive, P. 2013. Estimation of Cellulose Crystallinity of Lignocelluloses Using Near-IR.
- Akyildiz, M. and Ates, S. 2008. Effect of heat treatment on equilibrium moisture content (EMC) of some wood species in Turkey. *Agriculture and Biological Sciences* 4(6), pp. 660–665. Available at: <http://earsiv.kastamonu.edu.tr/jspui/handle/1/499>.
- Anderson, S., Wikberg, H., Pesonen, E., Maunu, S.L. and Serimaa, R. 2004. Studies of crystallinity of Scots pine and Norway spruce cellulose., pp. 346–353. doi: 10.1007/s00468-003-0312-9.
- Antonović, A., Barčić, D., Kljak, J., Ištvančić, J., Podvorec, T. and Stanešić, J. 2018. The quality of fired aleppo pine wood (*Pinus Halepensis* mill.) biomass for biorefinery products. *Croatian Journal of Forest Engineering* 39(2), pp. 313–324.
- Aşıkuzun, E. and Karagöz İşleyen, Ü. 2019. Determination of Mechanical Properties of Aged Wood Material Using Vickers Microhardness Test. *Kastamonu Univ., Journal of Forestry Faculty* 19(1), pp. 106–115. doi: 10.17475/kastorman.543542.
- De Assis, A.A., Alexandre, R.P. and Ballarin, A.W. 2017. Dynamic hardness of wood-measurements with an automated portable hardness tester. *Holzforschung* 71(5), pp. 383–389. doi: 10.1515/hf-2016-0137.
- de Assis, M.R., Brancheriau, L., Napoli, A. and Trugilho, P.F. 2016. Factors

affecting the mechanics of carbonized wood: literature review. *Wood Science and Technology* 50(3), pp. 519–536. doi: 10.1007/s00226-016-0812-6.

ASTM D 143 1994. Standard Test Methods for Small Clear Specimens of Timber. *ASTM International* , pp. 1–31.

ASTM D 1762-84 2011. Standard Test Method for Chemical Analysis of Wood Charcoal. *ASTM International* 84(Reapproved 2007), pp. 1–2. doi: 10.1520/D1762-84R07.2.

ASTM D1037 1999. Standard Test Methods for Evaluating Properties of Wood-Base Fiber and Particle PART A — General Test Methods for Evaluating the Basic Properties of Wood-base. *ASTM International* (July 1999), pp. 1–31. Available at: <https://www.astm.org/d1037-99.html> [Accessed: 24 May 2022].

ASTM D2395-14 2014. Standard Test Methods for Density and Specific Gravity (Relative Density) of Wood and Wood-Based Materials. *ASTM International* , pp. 1–13. doi: 10.1520/D2395-14.2.

Ates, S., Akyildiz, M.H. and Ozdemir, H. 2009. Effects of heat treatment on calabrian pine (*Pinus brutia* Ten.) wood. *BioResources* 4(3), pp. 1032–1043.

Babic, M., Kocovic, V., Vukelic, D., Mihajlovic, G., Eric, M. and Tadic, B. 2017. Investigation of ball burnishing processing on mechanical characteristics of wooden elements. *Proceedings of the Institution of Mechanical Engineers, Part C: Journal of Mechanical Engineering Science* 231(1), pp. 120–127. doi: 10.1177/0954406216641711.

Bakar, B.F.A., Hiziroglu, S. and Tahir, P.M. 2013. Properties of some thermally modified wood species. *Materials and Design* 43(March 2018), pp. 348–355. Available at: <http://dx.doi.org/10.1016/j.matdes.2012.06.054>.

Bartlett, A.I., Hadden, R.M. and Bisby, L.A. 2019. A Review of Factors

Affecting the Burning Behaviour of Wood for Application to Tall Timber Construction. *Fire Technology* 55(1), pp. 1–49. Available at: <https://doi.org/10.1007/s10694-018-0787-y>.

Benouadah, N., Aliouche, D., Pranovich, A. and Willför, S. 2019. Chemical characterization of *Pinus halepensis* sapwood and heartwood. *Wood Material Science and Engineering* 14(3), pp. 157–164. Available at: <https://doi.org/10.1080/17480272.2018.1448436>.

Björdal, C.G. 2012. Microbial degradation of waterlogged archaeological wood. *Journal of Cultural Heritage* 13(3 SUPPL.), pp. S118–S122. Available at: <http://dx.doi.org/10.1016/j.culher.2012.02.003>.

Boocock, D.G.B. and Kosiak, L. 1988. A scanning electron microscope study of structural changes during the liquefaction of poplar sticks by rapid aqueous thermolysis. *The Canadian Journal of Chemical Engineering* 66(1), pp. 121–126. doi: 10.1002/cjce.5450660117.

Borgin, K., Tsoumis, G. and Passialis, C. 1979. Density and shrinkage of old wood. *Wood Science and Technology* 13:1 13(1), pp. 49–57. Available at: <https://link.springer.com/article/10.1007/BF00350175> [Accessed: 15 July 2022].

Brewer, C.E. et al. 2014. New approaches to measuring biochar density and porosity. *Biomass and Bioenergy* 66, pp. 176–185. Available at: <http://dx.doi.org/10.1016/j.biombioe.2014.03.059>.

Broda, M., Curling, S.F. and Frankowski, M. 2021a. The effect of the drying method on the cell wall structure and sorption properties of waterlogged archaeological wood. *Wood Science and Technology* 55(4), pp. 971–989. Available at: <https://doi.org/10.1007/s00226-021-01294-6>.

Broda, M., Curling, S.F., Spear, M.J. and Hill, C.A.S. 2019. Effect of methyltrimethoxysilane impregnation on the cell wall porosity and water



vapour sorption of archaeological waterlogged oak. *Wood Science and Technology* 53(3), pp. 703–726. Available at: <https://doi.org/10.1007/s00226-019-01095-y>.

Broda, M. and Hill, C.A.S. 2021. Conservation of waterlogged wood—past, present and future perspectives. *Forests* 12(9), pp. 1–55. doi: 10.3390/f12091193.

Broda, M., Majka, J., Olek, W. and Mazela, B. 2018. Dimensional stability and hygroscopic properties of waterlogged archaeological wood treated with alkoxysilanes. *International Biodeterioration and Biodegradation* 133(May), pp. 34–41. doi: 10.1016/j.ibiod.2018.06.007.

Broda, M., Popescu, C.M., Timpu, D.I., Rowiński, D. and Roszyk, E. 2021b. Factors that affect the mechanical strength of archaeological wood—a case study of 18th-century wooden water pipes from Bóźnicza street in Poznań, Poland. *Materials* 14(24). doi: 10.3390/ma14247632.

Cai, C. 2020. *Effects of long-term moisture and weather exposure on the structure and properties of thermally modified wood*. University of Eastern Finland. doi: 10.14214/df.298.

Cao, H., Gao, X., Chen, J., Xi, G., Yin, Y. and Guo, J. 2023. Changes in Moisture Characteristics of Waterlogged Archaeological Wood Owing to Microbial Degradation. *Forests* 14(1), pp. 1–18. doi: 10.3390/f14010009.

Caple, C. and Murray, W. 1994. Characterization of a Waterlogged Charred Wood and Development of a Conservation Treatment. *Studies in Conservation* 39(1), p. 28. doi: 10.2307/1506488.

Carll, C. and Wiedenhoef, A.C. 2009. Moisture-Related Properties of Wood and the Effects of Moisture on Wood and Wood Products. In: Trechsel, H. R. and Bomberg, M. T. eds. *Moisture Control in Buildings: The Key Factor in Mold Prevention*. 2nd ed. ASTM International, pp. 54–79. doi:

10.1520/mnl11544m.

Chen, W.H., Lin, B.J., Colin, B., Pétrissans, A. and Pétrissans, M. 2019. A study of hygroscopic property of biomass pretreated by torrefaction. *Energy Procedia* 158, pp. 32–36. Available at: <https://doi.org/10.1016/j.egypro.2019.01.030>.

Christensen, B.B. 1970. *The conservation of waterlogged wood in the National Museum of Denmark*. Copenhagen: National Museum of Denmark.

Collis, S.N. 2015. Revisiting Conservation Treatment Methodologies for Waterlogged Archaeological Wood: An Australian Study. *AICCM Bulletin* 36(2), pp. 88–96. doi: 10.1080/10344233.2015.1111597.

Connor, M.A. and Daria, V. 1993. Changes in Wood Structure During the Course of Carbonisation. *Advances in Thermochemical Biomass Conversion* , pp. 846–858.

Constantine, M. et al. 2021. Science of the Total Environment Using charcoal , ATR FTIR and chemometrics to model the intensity of pyrolysis : Exploratory steps towards characterising fire events. 783

Cook, C. and Grattan, D.W. 1990. A method of Calculating the Concentration of PEG for Freeze-drying Waterlogged Wood. In: Per Hoffmann ed. *4th ICOM-Group on Wet Organic Archaeological Materials Conference.*, pp. 239–250.

Crivellaro, A. and Schweingruber, F.H. 2013. *Atlas of Wood, Bark and Pith Anatomy of Eastern Mediterranean Trees and Shrubs*. doi: 10.1007/978-3-642-37235-3.

Cutter, B.E., Cumbie, B.G. and McGinnes, E.A. 1980. SEM and shrinkage analyses of Southern Pine wood following pyrolysis. *Wood Science and Technology* 14(2), pp. 115–130. doi: 10.1007/BF00584041.

Cutter, B.E. and McGinnes, E.A. 1981. A note on density change patterns in charred wood. *Wood and Fiber* 13(1), pp. 39–44.

Dias Junior, A.F. et al. 2020. Investigating the pyrolysis temperature to define the use of charcoal. *European Journal of Wood and Wood Products* 78(1), pp. 193–204. Available at: <https://doi.org/10.1007/s00107-019-01489-6>.

Ding, W.D., Koubaa, A., Chaala, A., Belem, T. and Krause, C. 2008. Relationship between wood porosity, wood density and methyl methacrylate impregnation rate. *Wood Material Science and Engineering* 3(1–2), pp. 62–70. doi: 10.1080/17480270802607947.

Doyle, J. and Walker, J. 1985. Indentation hardness of wood. *Wood and Fiber Science* 17(3), pp. 369–376.

EN 1534 2000. EN 1534 Wood and parquet flooring—determination of resistance to indentation (Brinell)—test method. *European Committee for Standardization*

EN 16873 2016. *Conservation of cultural heritage - Guidelines for the management of waterlogged wood on archaeological terrestrial sites*. Available at: <https://standards.iteh.ai/catalog/standards/cen/5022dbc8-04ae-46f4-8247-5a3cbe217f4b/en-16873-2016> [Accessed: 8 December 2022].

Engelund, E.T., Thygesen, L.G., Svensson, S. and Hill, C.A.S. 2013. A critical discussion of the physics of wood-water interactions. *Wood Science and Technology* 47(1), pp. 141–161. doi: 10.1007/s00226-012-0514-7.

Esteban, L.G., De Palacios, P., García Fernández, F., Martín, J.A., Génova, M. and Fernández-Golfín, J.I. 2009. Sorption and thermodynamic properties of buried juvenile *Pinus sylvestris* L. wood aged  $1,170 \pm 40$  BP. *Wood Science and Technology* 43(7–8), pp. 679–690. doi: 10.1007/s00226-009-0261-6.

Esteves, B., Domingos, I. and Pereira, H. 2007. Improvement of technological

quality of eucalypt wood by heat treatment in air at 170-200°C. *Forest Products Journal* 57(1/2), pp. 47–52.

Esteves, B., Marques, A.V. and Pereira, H. 2013. Chemical changes of heat treated pine and eucalypt. 15(2), pp. 245–258. doi: 10.4067/S0718-221X2013005000020.

Esteves, B., Nunes, L., Domingos, I. and Pereira, H. 2014. Improvement of termite resistance, dimensional stability and mechanical properties of pine wood by paraffin impregnation. *European Journal of Wood and Wood Products* 72(5), pp. 609–615. doi: 10.1007/s00107-014-0823-7.

Esteves, B., Nunes, L. and Pereira, H. 2011. Properties of furfurylated wood (Pinus pinaster). *European Journal of Wood and Wood Products* 69(4), pp. 521–525. doi: 10.1007/s00107-010-0480-4.

Esteves, B.M. and Pereira, H.M. 2009. Wood modification by heat treatment: a review. 4(1965), pp. 370–404.

FAO 1985. Wood Carbonisation and The Products It Yields. In: *Industrial Charcoal Making*. Rome: FAO (FOOD AND AGRICULTURE ORGANIZATION OF THE UNITED NATIONS), pp. 7–25. Available at: <https://www.fao.org/3/x5555e/x5555e03.htm#2.9.1.2> volatile matter other than water [Accessed: 19 December 2022].

Florian, M.-L.E. 1987. The underwater environment. *Conservation of Marine Archaeological Objects* , pp. 1–20. doi: 10.1016/B978-0-408-10668-9.50007-1.

Florian, M.-L.E. 1990. Scope and History of Archaeological Wood. In: Rowell, R. and Barbour, J. eds. *Archaeological Wood: Properties, Chemistry, and Preservation*. Washington DC: American Chemical Society, pp. 3–32. doi: 10.1021/ba-1990-0225.ch001.

Fors, Y. 2008. *Sulfur-Related Conservation Concerns for Marine Archaeological Wood*.

Fors, Y., Nilsson, T., Risberg, E.D., Sandström, M. and Torssander, P. 2008. Sulfur accumulation in pinewood (*Pinus sylvestris*) induced by bacteria in a simulated seabed environment: Implications for marine archaeological wood and fossil fuels. *International Biodeterioration and Biodegradation* 62(4), pp. 336–347. doi: 10.1016/j.ibiod.2007.11.008.

French, A.D. and Santiago Cintrón, M. 2013. Cellulose polymorphy, crystallite size, and the Segal Crystallinity Index. *Cellulose* 20(1), pp. 583–588. doi: 10.1007/s10570-012-9833-y.

Friquin, K.L. 2011. Material properties and external factors influencing the charring rate of solid wood and glue-laminated timber. *Fire and Materials* 35(5), pp. 303–327. Available at: <https://onlinelibrary.wiley.com/doi/10.1002/fam.1055> [Accessed: 2 September 2021].

Fuwape, J.A. 1996. Effects of carbonisation temperature on charcoal from some tropical trees. *Bioresource Technology* 57(1), pp. 91–94. doi: 10.1016/0960-8524(96)00027-2.

Gao, J., Kim, J.S., Terziev, N., Cuccui, I. and Daniel, G. 2018. Effect of thermal modification on the durability and decay patterns of hardwoods and softwoods exposed to soft rot fungi. *International Biodeterioration and Biodegradation* 127(November 2017), pp. 35–45. doi: 10.1016/j.ibiod.2017.11.009.

Gelbrich, J., Mai, C. and Militz, H. 2008. Chemical changes in wood degraded by bacteria. *International Biodeterioration and Biodegradation* 61(1), pp. 24–32. doi: 10.1016/j.ibiod.2007.06.007.

Giachi, G., Bettazzi, F., Chimichi, S. and Staccioli, G. 2003. Chemical

characterisation of degraded wood in ships discovered in a recent excavation of the Etruscan and Roman harbour of Pisa. 4, pp. 75–83. doi: 10.1016/S1296-2074(03)00018-9.

Glass, S. V and Zelinka, S.L. 2010. Moisture Relations and Physical Properties of Wood. In: *Wood handbook: wood as an engineering material*. Centennial. Madison, WI: U.S. Dept. of Agriculture, Forest Service, Forest Products Laboratory, pp. 1–19. Available at: <http://www.treearch.fs.fed.us/pubs/37428> [Accessed: 12 June 2022].

Godinho, D., Araújo, S. de O., Quilhó, T., Diamantino, T. and Gominho, J. 2021. Thermally modified wood exposed to different weathering conditions: A review. *Forests* 12(10). doi: 10.3390/f12101400.

Grattan, D.W. 1982. A practical comparative study of several treatments for waterlogged wood. *Studies in Conservation* 27(3), pp. 124–136. doi: 10.1179/sic.1982.27.3.124.

Grattan, D.W. 1987. Waterlogged wood. In: Pearson, C. ed. *Conservation of Marine Archaeological Objects*. Butterworth & Co. (Publishers) Ltd., pp. 55–67. Available at: <http://dx.doi.org/10.1016/B978-0-408-10668-9.50009-5>.

Grattan, D.W. and Clarke, R.W. 1987. Conservation of waterlogged wood. In: *Conservation of Marine Archaeological Objects*. Butterworth & Co. (Publishers) Ltd., pp. 164–206. Available at: <http://dx.doi.org/10.1016/B978-0-408-10668-9.50015-0>.

Green, D.W., Begel, M. and Nelson, W. 2006. Janka hardness using nonstandard specimens. *USDA Forest Products Laboratory, Research Note FPL-RN-0303*. Available at: [www.fpl.fs.fed.us](http://www.fpl.fs.fed.us).

Gregory, D., Jensen, P., Matthiesen, H. and Strætkvern, K. 2007. The correlation between bulk density and shock resistance of waterlogged archaeological wood using the Pilodyn. *Studies in Conservation* 52(4), pp.

289–298. Available at: <http://dx.doi.org/10.1179/sic.2007.52.4.289>.

Gregory, D., Jensen, P. and Strætkevorn, K. 2012. Conservation and in situ preservation of wooden shipwrecks from marine environments. *Journal of Cultural Heritage* 13(3 SUPPL.), pp. S139–S148. Available at: <http://dx.doi.org/10.1016/j.culher.2012.03.005>.

Grioui, N., Halouani, K., Zoulalian, A. and Halouani, F. 2007. Experimental study of thermal effect on olive wood porous structure during carbonization. *Maderas: Ciencia y Tecnologia* 9(1), pp. 15–28. doi: 10.4067/S0718-221X2007000100002.

Guo, Y. and Bustin, R.M. 1998. FTIR spectroscopy and reflectance of modern charcoals and fungal decayed woods: implications for studies of inertinite in coals. *International Journal of Coal Geology* 37(1–2), pp. 29–53. doi: 10.1016/S0166-5162(98)00019-6.

Han, L., Guo, J., Wang, K., Grönquist, P., Li, R., Tian, X. and Yin, Y. 2020. Hygroscopicity of Waterlogged Archaeological Wood Deterioration State. *Polymers* 12(4), p. 834.

Hedges, J.I. 1989. The Chemistry of Archaeological Wood. In: *Archaeological Wood.*, pp. 111–140. Available at: <https://pubs.acs.org/doi/pdf/10.1021/ba-1990-0225.ch005> [Accessed: 20 May 2022].

High, K.E. and Penkman, K.E.H. 2020. A review of analytical methods for assessing preservation in waterlogged archaeological wood and their application in practice. *Heritage Science* 8(83), pp. 1–33. Available at: <https://doi.org/10.1186/s40494-020-00422-y> [Accessed: 28 January 2023].

High, K.E. and Penkman, K.E.H. 2021. Correction to: A review of analytical methods for assessing preservation in waterlogged archaeological wood and their application in practice (*Heritage Science*, (2020), 8, 1, (83),

10.1186/s40494-020-00422-y). *Heritage Science* 9(1), pp. 1–34. doi: 10.1186/s40494-021-00515-2.

Hill, C.A.S. 2006. Modifying the Properties of Wood. In: *Wood Modification: chemical, thermal and other processes*. John Wiley & Sons, pp. 19–44. doi: 10.1002/0470021748.fmatter.

Hirata, S., Ohta, M. and Honma, Y. 2001. Hardness distribution on wood surface. *Journal of Wood Science* 47(1), pp. 1–7. doi: 10.1007/BF00776637.

Hoffmann, P. 1982. Chemical wood analysis as a means of characterizing archaeological wood. In: Grattan, D. W. and McCawley, I. C. eds. *2nd ICOM-CC Group on Wet Organic Archaeological Materials Conference, Ottawa, 1982.*, pp. 73–83.

Hoffmann, P. 1985. On the stabilization of waterlogged oak with PEG- Molecular size versus degree of degradation. In: *2nd ICOM Waterlogged Wood Working Group Conference, Grenoble, 1984.*, pp. 95–115.

Hoffmann, P. 1986. On the stabilization of waterlogged oakwood with PEG. II. Designing a two-step treatment for multi-quality timbers. 31(3), pp. 103–113. Available at: <https://www.tandfonline.com/doi/abs/10.1179/sic.1986.31.3.103> [Accessed: 1 July 2022].

Howell, C., Christine, A., Hastrup, S., Goodell, B. and Jellison, J. 2009. International Biodeterioration & Biodegradation Temporal changes in wood crystalline cellulose during degradation by brown rot fungi. 63, pp. 414–419. doi: 10.1016/j.ibiod.2008.11.009.

Hughes, M., Hill, C.A.S. and Pfriem, A. 2015. The toughness of hygrothermally modified wood – a review. *Holzforschung* 69(7), pp. 851–862. doi: 10.1515/hf-2014-0184.



Inari, G.N., Petrissans, M., Lambert, J., Ehrhardt, J.J. and Erardin, P.G. 2006. XPS characterization of wood chemical composition after heat-treatment. *SURFACE AND INTERFACE ANALYSIS Surf. Interface Anal* 38, pp. 1336–1342. Available at: [www.interscience.wiley.com](http://www.interscience.wiley.com).

International Standard 2005. *ISO 6506-1*.

Jensen, P. and Gregory, D.J. 2006. Selected physical parameters to characterize the state of preservation of waterlogged archaeological wood : a practical guide for their determination. *Journal of Archaeological Science* 33, pp. 551–559. doi: 10.1016/j.jas.2005.09.007.

De Jong, J. 1977. Conservation techniques for old waterlogged wood from shipwrecks found in the Netherlands. In: *Biodeterioration Investigation Techniques.*, pp. 295–338.

Jover, A. 1994. The application of peg 4000 for the preservation of palaeolithic wooden artifacts. *Studies in Conservation* 39(3), pp. 193–198. doi: 10.1179/sic.1994.39.3.193.

Kamperidou, V. 2019. The biological durability of thermally-and chemically-modified black pine and poplarwood against basidiomycetes and mold action. *Forests* 10(12). doi: 10.3390/F10121111.

Kaye, B. 1995. Conservation of waterlogged archaeological wood. *Chemical Society Reviews* 24(1), pp. 35–43. doi: 10.1039/CS9952400035.

Kim, Y.S. 1990. Short Note: Chemical Characteristics of Waterlogged Archaeological Wood. *Holzforschung* 44(3), pp. 169–172. doi: 10.1515/hfsg.1990.44.3.169.

Kocafe, D., Huang, X., Kocafe, Y. and Boluk, Y. 2012. Quantitative characterization of chemical degradation of heat-treated wood surfaces during artificial weathering using XPS. doi: 10.1002/sia.5104.

- Kohdzuma, Y., Minato, K. and Yukio Katayama 1996. Relationships between some properties of waterlogged woods. *Mokuzai gakkaiishi* 42(7), pp. 681–687.
- Kollmann, F.F. and Côté, W.A. 1968. *Principles of wood science and technology. vol. I. Solid Wood*. Heidelberg: Springer-Verlag. doi: 10.1007/978-3-642-87928-9\_3.
- Kotilainen, R.A., Toivanen, T.J. and Alén, R.J. 2000. FTIR monitoring of chemical changes in softwood during heating. *Journal of Wood Chemistry and Technology* 20(3), pp. 307–320. doi: 10.1080/02773810009349638.
- Koutsouflakis, G. 2017a. *Arxaiologikon Deltion*.
- Koutsouflakis, G. 2017b. Three Shipwrecks of the Medieval Era in the Commercial Port of Rhodes. In: Britachta, K., Triantafyllidis, P., and Sarantidis, K. eds. *Archeological Work in Aegean Islands*. Lesvos, pp. 477–500.
- Koutsouflakis, G. and Rieth, E. 2021. A late-12th-century Byzantine Shipwreck in the port of Rhodes A preliminary report. In: Demesticha, S. and Lucy Blue eds. *Under the Mediterranean I: Studies in Maritime Archaeology*. Sidestone Press
- Kubovsk, I. and Kač, D. 2020. Structural Changes of Oak Wood Main Components Caused by Thermal Modification.
- Kwon, S.M., Kim, N.H. and Cha, D.S. 2009. An investigation on the transition characteristics of the wood cell walls during carbonization. *Wood Science and Technology* 43(5–6), pp. 487–498. doi: 10.1007/s00226-009-0245-6.
- Kymäläinen, M. et al. 2018a. Chemical, water vapour sorption and ultrastructural analysis of Scots pine wood thermally modified in high-

pressure reactor under saturated steam. *Journal of Materials Science* 53(4), pp. 3027–3037. doi: 10.1007/s10853-017-1714-1.

Kymäläinen, M., Havimo, M. and Louhelainen, J. 2014. Sorption properties of torrefied wood and charcoal. *Wood Material Science and Engineering* 9(3), pp. 170–178. doi: 10.1080/17480272.2014.916348.

Kymäläinen, M., Turunen, H., Čermák, P., Hautamäki, S. and Rautkari, L. 2018b. Sorption-related characteristics of surface charred spruce wood. *Materials* 11(11). doi: 10.3390/ma11112083.

Li, D. 2015. *Wood Hardness & Elastic Modulus Using Microindentation*.

Li, T., Cheng, D.L., Avramidis, S., Wålinder, M.E.P. and Zhou, D.G. 2017. Response of hygroscopicity to heat treatment and its relation to durability of thermally modified wood. *Construction and Building Materials* 144, pp. 671–676. Available at: <http://dx.doi.org/10.1016/j.conbuildmat.2017.03.218>.

Liese, W. 1963. Tertiary wall and warty layer in wood cells. *Journal of Polymer Science Part C: Polymer Symposia* 2, pp. 213–229. doi: 10.1002/polc.5070020121.

Liodakis, S., Katsigiannis, G. and Kakali, G. 2005. Ash properties of some dominant Greek forest species. *Thermochimica Acta* 437(1–2), pp. 158–167. doi: 10.1016/j.tca.2005.06.041.

Lowden, L.A. and Hull, T.R. 2013. Flammability behaviour of wood and a review of the methods for its reduction., pp. 1–19.

Lykidis, C., Nikolakakos, M., Sakellariou, E. and Birbilis, D. 2016. Assessment of a modification to the Brinell method for determining solid wood hardness. *Materials and Structures/Materiaux et Constructions* 49(3), pp. 961–967. doi: 10.1617/s11527-015-0551-4.

McConnachie, G., Eaton, R. and Jones, M. 2008. A re-evaluation of the use

of maximum moisture content data for assessing the condition of waterlogged archaeological wood. *E-preservation Science* 5, pp. 29–35. Available at: <http://www.morana-rtd.com/e-preservation-science/2008/McConnachie-09-04-2008.pdf>.

Mikkola, E. 1991. Charring Of Wood Based Materials. *Fire Safety Science* 3, pp. 547–556. doi: 10.3801/iafss.fss.3-547.

Mitsi, E. 2020. *Comparative Study of Conservation Treatments for Charred Waterlogged Wood from Medieval Shipwreck in the Port of Rhodes Island*. University of West Attica.

Mitsi, E., Boyatzis, S. and Pournou, A. 2021. Chemical Characterization of Waterlogged Charred Wood: The Case of a Medieval Shipwreck. *Forests* 12(11). doi: 10.3390/F12111594.

Mitsi, E. and Pournou, A. 2019. Conserving a charred medieval shipwreck: A preliminary study. In: *14th ICOM-CC WOAM Conference Portsmouth*.

Mitsi, E., Stefanis, N.-A. and Pournou, A. 2023. Physico-Mechanical Properties of Waterlogged Archaeological Wood: The Case of a Charred Medieval Shipwreck. *Forests* 14(3), p. 560. Available at: <https://www.mdpi.com/1999-4907/14/3/560/htm> [Accessed: 20 May 2023].

Monachon, M., Albelda-Berenguer, M., Pelé, C., Cornet, E., Guilminot, E., Rémazeilles, C. and Joseph, E. 2020. Characterization of model samples simulating degradation processes induced by iron and sulfur species on waterlogged wood. *Microchemical Journal* 155(August 2019), p. 104756. Available at: <https://doi.org/10.1016/j.microc.2020.104756>.

Nhacila, F., Siteo, E., Uetimane, E., Manhica, A., Egas, A. and Möttönen, V. 2020. Effects of thermal modification on physical and mechanical properties of Mozambican *Brachystegia spiciformis* and *Julbernardia globiflora* wood. *European Journal of Wood and Wood Products* 78(5), pp. 871–878.

Available at: <https://doi.org/10.1007/s00107-020-01576-z>.

Nilsson, B.T., Daniel, G., Kirk, T.K., Obst, J.R. and Service, F. 1989. Chemistry and Microscopy of Wood Decay by Some Higher Ascomycetes. *43*(1), pp. 11–18.

Özgenç, Ö., Durmaz, S., Boyacı, İ.H. and Eksi-Koçak, H. 2018. ATR-FTIR spectroscopic analysis of thermally modified wood degraded by rot fungi. *Drewno* 61(201). doi: <https://doi.org/10.12841/wood.1644-3985.247.02>.

Pandey, K.K. and Pitman, A.J. 2003. FTIR studies of the changes in wood chemistry following decay by brown-rot and white-rot fungi. 8305(October). doi: 10.1016/S0964-8305(03)00052-0.

Panter, I. and Spriggs, J. 1997. Condition assessments and conservation strategies for waterlogged wood assemblages. In: *6th ICOM group on wet organic archaeological materials conference, York, 9-13 September 1996.*, pp. 185–200.

Park, S., Baker, J.O., Himmel, M.E., Parilla, P.A. and Johnson, D.K. 2010. Cellulose crystallinity index : measurement techniques and their impact on interpreting cellulase performance., pp. 1–10.

Pedersen, N.B., Gierlinger, N. and Thygesen, L.G. 2015. Bacterial and abiotic decay in waterlogged archaeological *Picea abies* (L.) Karst studied by confocal Raman imaging and ATR-FTIR spectroscopy. *Holzforschung* 69(1), pp. 103–112. doi: 10.1515/hf-2014-0024.

Peng, H., Jiang, J., Zhan, T. and Lu, J. 2016. Influence of density and equilibrium moisture content on the hardness anisotropy of wood. *Forest Products Journal* 66(7–8), pp. 443–452. doi: 10.13073/FPJ-D-15-00072.

Petrou, M. and Pournou, A. 2018. Testing the efficiency of a fruit penetrometer to assess the condition of small waterlogged wooden artifacts.

In: Williams, E. and Hocker, E. eds. *13th ICOM-CC Group on Wet Organic Archaeological Materials Conference*. Florence, pp. 47–53. Available at: [https://www.researchgate.net/profile/Anastasia-Pournou-2/publication/308887290\\_Testing\\_the\\_efficiency\\_of\\_a\\_fruit\\_penetrometer\\_to\\_assess\\_the\\_condition\\_of\\_small\\_waterlogged\\_wooden\\_artifacts/links/6278ee972f9ccf58eb3946cc/Testing-the-efficiency-of-a-fruit-pe](https://www.researchgate.net/profile/Anastasia-Pournou-2/publication/308887290_Testing_the_efficiency_of_a_fruit_penetrometer_to_assess_the_condition_of_small_waterlogged_wooden_artifacts/links/6278ee972f9ccf58eb3946cc/Testing-the-efficiency-of-a-fruit-pe).

Pfriem, A., Zauer, M. and Wagenführ, A. 2009. Alteration of the pore structure of spruce (*Picea abies* (L.) Karst.) and maple (*Acer pseudoplatanus* L.) due to thermal treatment as determined by helium pycnometry and mercury intrusion porosimetry. *Holzforschung* 63(1), pp. 94–98. doi: 10.1515/HF.2009.027.

Poletto, M., Zattera, A.J. and Santana, R.M.C. 2012. Structural Differences Between Wood Species : Evidence from Chemical Composition , FTIR Spectroscopy , and Thermogravimetric Analysis. doi: 10.1002/app.

Popescu, C., Larsson, P.E.R.T., Tibirna, C.M. and Vasile, C. 2010. Characterization of Fungal-Degraded Lime Wood by X-ray Diffraction and Cross-Polarization Magic-Angle-Spinning C-Nuclear Magnetic Resonance Spectroscopy. 64(9), pp. 1054–1060.

Popescu, M., Froidevaux, J., Navi, P. and Popescu, C. 2013. Structural modifications of *Tilia cordata* wood during heat treatment investigated by FT-IR and 2D IR correlation spectroscopy. *Journal of Molecular Structure* 1033, pp. 176–186. Available at: <http://dx.doi.org/10.1016/j.molstruc.2012.08.035>.

Pournou, A. 2016. The MERMAID project: Saving wooden shipwrecks in the Mediterranean marine ecosystem- research , development and application of innovative The MERMAID project : Saving wooden shipwrecks in the Mediterranean marine ecosystem- research , development and app. In: *12th ICOM-CC Group on Wet Organic Archaeological Materials Conference.*, pp. 7–14. Available at:

[https://www.researchgate.net/publication/308887197\\_The\\_MERMAID\\_project\\_Saving\\_wooden\\_shipwrecks\\_in\\_the\\_Mediterranean\\_marine\\_ecosystem\\_-\\_research\\_development\\_and\\_application\\_of\\_innovative\\_methods\\_of\\_in\\_situ\\_protection](https://www.researchgate.net/publication/308887197_The_MERMAID_project_Saving_wooden_shipwrecks_in_the_Mediterranean_marine_ecosystem_-_research_development_and_application_of_innovative_methods_of_in_situ_protection) [Accessed: 19 May 2022].

Pournou, A. 2018. Assessing the Long-Term Efficacy of Geotextiles in Preserving Archaeological Wooden Shipwrecks in the Marine Environment. *Journal of Maritime Archaeology* 13(1), pp. 1–14. Available at: <https://link.springer.com/article/10.1007/s11457-017-9176-9> [Accessed: 19 May 2022].

Pournou, A. 2020. Wood Deterioration by Aquatic Microorganisms. In: *Biodeterioration of Wooden Cultural Heritage: Organisms and Decay Mechanisms in Aquatic and Terrestrial Ecosystems*. Cham: Springer International Publishing, pp. 177–260. Available at: [https://doi.org/10.1007/978-3-030-46504-9\\_4](https://doi.org/10.1007/978-3-030-46504-9_4).

Pournou, A., Jones, A.M. and Moss, S.T. 2001. Biodeterioration dynamics of marine wreck-sites determine the need for their in situ protection. *International Journal of Nautical Archaeology* 30(2), pp. 299–305. doi: 10.1006/ijna.2001.0357.

Rémazeilles, C., Tran, K., Guilminot, E., Conforto, E. and Refait, P. 2013. Study of Fe(II) sulphides in waterlogged archaeological wood. *Studies in Conservation* 58(4), pp. 297–307. doi: 10.1179/2047058412Y.0000000071.

Riggio, M. and Piazza, M. 2010. Hardness Test. In: Kasal, B. and Tannert, T. eds. *In Situ Assessment of Structural Timber, State of the Art Report of the RILEM Technical Committee 215-AST*. Springer, Dordrecht, pp. 87–97. Available at: [https://link.springer.com/chapter/10.1007/978-94-007-0560-9\\_10](https://link.springer.com/chapter/10.1007/978-94-007-0560-9_10) [Accessed: 11 June 2022].

Ronewicz, K., Kluska, J., Heda, Ł. and Kardaś, D. 2017. Chemical and Physical Properties of Pine Wood during Pyrolysis. *Drvna Industrija* 68(1), pp. 29–36. doi: 10.5552/drind.2017.1617.

Rousodimos, G. 1997. *Physical and Mechanical wood properties of Greek wood species (Φυσικές και Μηχανικές ιδιότητες του ξύλου Ελληνικών δασοπονικών ειδών)*.

Ruiz-aquino, F., Ruiz-ángel, S. and Sotomayor-castellanos, J.R. 2019. Energy characteristics of wood and charcoal of selected tree species in Mexico. 64(1), pp. 71–82.

Rutherford, D., Wershaw, R. and Cox, L. 2005. Changes in Composition and Porosity Occurring During the Thermal Degradation of Wood and Wood Components: U.S. Geological Survey Scientific Investigations Report 2004-5292., p. 79.

Sandström, M. et al. 2002. The sulphur threat to marine archaeological artefacts: acid and iron removal from the Vasa. *Conservation Science 2002: papers from the conference held in Edinburgh, Scotland, 22-24 May 2002* (November 2014), pp. 79–87.

Scherrer, P. and Debye, P. 1918. Bestimmung der Grösse und der inneren Struktur von Kolloidteilchen mittels Röntgenstrahlen [Determination of the size and internal structure of colloidal particles using X-rays]. *Nachr. Ges. Wiss. Göttingen, Math.-physik. Klasse 2*, pp. 101–120. Available at: <http://eudml.org/doc/59018>.

Schindelholz, E. et al. 2009. An evaluation of supercritical drying and PEG/freeze drying of waterlogged archaeological wood. In: Strætkvern, K. and Huisman, D. G. eds. *10th ICOM Group on Wet Organic Archaeological Materials Conference: Amsterdam 2007*. ICOM CC, pp. 399–316.

Schniewind, A.P. 1990. Physical and Mechanical Properties of



Archaeological Wood. In: Rowell, R. and Barbour, J. eds. *Archaeological Wood: Properties, Chemistry, and Preservation*. Washington DC: American Chemical Society, pp. 87–109.

Sedlar, T., Šefc, B., Stojnić, S., Jarc, A., Perić, I. and Sinković, T. 2019. Hardness of Thermally Modified Beech Wood and Hornbeam Wood. *Šumarski list* 143(9–10), pp. 433–433. Available at: <https://hrcak.srce.hr/227252>.

Segal, L., Creely, J.J., A. E. Martin and Conrad, M. 1958. Empirical Method for Estimating the Degree of Crystallinity of Native Cellulose Using the X-Ray Diffractometer. *Textile Research Journal*, pp. 786–794.

Senelwa, K. and Sims, R.E.H. 1999. Fuel characteristics of short rotation forest biomass. *Biomass and Bioenergy* 17(2), pp. 127–140. doi: 10.1016/S0961-9534(99)00035-5.

Şensöz, S. and Can, M. 2002. Pyrolysis of pine (*Pinus Brutia* Ten.) chips: 2. Structural analysis of bio-oil. *Energy Sources* 24(4), pp. 357–364. doi: 10.1080/00908310252888736.

Sivonen, B.H., Maunu, S.L., Sundholm, F., Jämsä, S. and Viitaniemi, P. 2002. Magnetic Resonance Studies of Thermally Modified Wood. 56, pp. 648–654.

Skyba, O., Schwarze, F.W.M.R. and Niemz, P. 2009. Physical and mechanical properties of Thermo-hygro-mechanically (THM) - Densified wood. *Wood Research* 54(2), pp. 1–18.

Smołka-Danielowska, D. and Jabłońska, M. 2022. Chemical and mineral composition of ashes from wood biomass combustion in domestic wood-fired furnaces. *International Journal of Environmental Science and Technology* 19(3), pp. 5359–5372. Available at: <https://doi.org/10.1007/s13762-021-03506-9> [Accessed: 19 December 2022].

Squirrell, J.P. and Clarke, R.W. 1987. An investigation into the condition and conservation of the hull of the Mary Rose. part I: Assessment of the hull timbers. *Studies in Conservation* 32(4), pp. 153–162. doi: 10.1179/sic.1987.32.4.153.

Stanzl-Tschegg, S., Beikircher, W. and Loidl, D. 2009. Comparison of mechanical properties of thermally modified wood at growth ring and cell wall level by means of instrumented indentation tests. *Holzforschung* 63(4), pp. 443–448. doi: 10.1515/HF.2009.085.

Sydor, M., Pinkowski, G. and Jasińska, A. 2020. The Brinell method for determining hardness of wood flooring materials. *Forests* 11(8). doi: 10.3390/f11080878.

Tamburini, D., Cartwright, C.R., Gasson, P., Jacqueline, J., Luizon, C. and Leme, D. 2020. Using analytical pyrolysis and scanning electron microscopy to evaluate charcoal formation of four wood taxa from the caatinga of north-east Brazil. *Journal of Analytical and Applied Pyrolysis journal* 151, p. 114. doi: 10.1016/j.jaap.2020.104909.

Tarmian, A. and Akbar Mastouri 2019. Changes in moisture exclusion efficiency and crystallinity of thermally modified wood with aging. *iForest-Biogeosciences and Forestry* 12(1), pp. 92–97. doi: 10.3832/ifer2723-011.

Terziev, N. and Daniel, G. 2002. Industrial kiln drying and its effect on microstructure, impregnation and properties of Scots pine timber impregnated for above ground use. Part 2. Effect of drying on microstructure and some mechanical properties of Scots pine wood. *Holzforschung* 56(4), pp. 434–439. doi: 10.1515/HF.2002.067.

Thanh, N.D., Wakiya, S., Matsuda, K., Ngoc, B.D., Sugiyama, J. and Kohdzuma, Y. 2018. Diffusion of chemicals into archaeological waterlogged hardwoods obtained from the Thang Long Imperial Citadel site, Vietnam.

*Journal of Wood Science* 64(6), pp. 836–844. Available at: <http://dx.doi.org/10.1007/s10086-018-1754-4>.

Thygesen, A., Oddershede, J., Lilholt, H., Thomsen, A.B. and Ståhl, K. 2005. On the determination of crystallinity and cellulose content in plant fibres. *Cellulose* 12(6), pp. 563–576. doi: 10.1007/s10570-005-9001-8.

Tintner, J. et al. 2018. Impact of pyrolysis temperature on charcoal characteristics University of Natural Resources and Life Sciences , Department of Material Sciences and University of Natural Resources and Life Sciences , Department of Civil Engineering and. doi: 10.1021/acs.iecr.8b04094.

Tjeerdsma, B.F. and Militz, H. 2005. Chemical changes in hydrothermal treated wood: FTIR analysis of combined hydrothermal and dry heat-treated wood. *Holz als Roh - und Werkstoff* 63(2), pp. 102–111. doi: 10.1007/s00107-004-0532-8.

Todaro, L., Rita, A., Cetera, P. and Auria, M.D. 2015. Thermal treatment modifies the calorific value and ash content in some wood species. *FUEL* 140, pp. 1–3. Available at: <http://dx.doi.org/10.1016/j.fuel.2014.09.060>.

Traoré, M., Kaal, J. and Martínez Cortizas, A. 2018. Differentiation between pine woods according to species and growing location using FTIR-ATR. *Wood Science and Technology* 52, pp. 487–504.

Triantafyllou, M., Papachristodoulou, P. and Pournou, A. 2010. Wet charred wood: A preliminary study of the material and its conservation treatments. *Journal of Archaeological Science* 37(9), pp. 2277–2283. Available at: <http://dx.doi.org/10.1016/j.jas.2010.03.025>.

Tsai, W.K. 2010. *Charring Rates for Different Cross Sections of Laminated Veneer Lumber ( LVL )*. University of Canterbury.

- Tsoumis, G. 1983. *Structure, Properties and Utilization of Wood (in Greek)*. Thessaloniki: Aristotelian University of Thessaloniki.
- Tsoumis, G. 1991. *Science and Technology of Rubber*. Verlag Kessel. doi: 10.1016/c2009-0-21288-8.
- Valenzuela-Calahorro, C., Gmez-Serrano, B.-G. and A V Bernalte-Garcia, J. 1987. *Influence of particle size and pyrolysis conditions on yield, density and some textural parameters of chars prepared from holm-oak wood*.
- Vlata, M. and Pournou, A. 2023. Melamine-formaldehyde versus freeze-drying: A comparative evaluation of treatments. In: *15th ICOM-CC Wet Organic Archaeological Materials (WOAM)*., pp. 106–114.
- Vörös and Németh, R. 2020. The History of Wood Hardness Tests. *IOP Conference Series: Earth and Environmental Science* 505(1), p. 012020. Available at: <https://iopscience.iop.org/article/10.1088/1755-1315/505/1/012020> [Accessed: 11 June 2022].
- Wang, S., Dai, G., Ru, B., Zhao, Y., Wang, X., Xiao, G. and Luo, Z. 2017. Influence of torrefaction on the characteristics and pyrolysis behavior of cellulose. *Energy* 120, pp. 864–871. doi: 10.1016/j.energy.2016.11.135.
- White, R.H. and Schaffer, E.L. 1978. Application of CMA program to wood charring. *Fire Technology* 14(4), pp. 279–290. doi: 10.1007/BF01998387.
- Wimmer, R., Lucas, B.N., Tsui, T.Y. and Oliver, W.C. 1997. Longitudinal hardness and Young's modulus of spruce tracheid secondary walls using nanoindentation technique. *Wood Science and Technology* 31(2), pp. 131–141. doi: 10.1007/s002260050022.
- Zauer, M., Hempel, S., Pfriem, A., Mechtcherine, V. and Wagenführ, A. 2014. Investigations of the pore-size distribution of wood in the dry and wet state by means of mercury intrusion porosimetry. *Wood Science and*

*Technology* 48(6), pp. 1229–1240. doi: 10.1007/s00226-014-0671-y.

Zhou, Y., Wang, K. and Hu, D. 2018. Degradation features of archaeological wood surface to deep inside a case study on wooden boards of marquis of Haihun's outer coffin. 63(3), pp. 419–430.

Zickler, G.A., Schöberl, T. and Paris, O. 2006. Mechanical properties of pyrolysed wood: A nanoindentation study. *Philosophical Magazine* 86(10), pp. 1373–1386. doi: 10.1080/14786430500431390.


## **Publications**

### **Paper #1**

*Chemical Characterization of Waterlogged Charred Wood: The  
Case of a Medieval Shipwreck*

## Article

# Chemical Characterization of Waterlogged Charred Wood: The Case of a Medieval Shipwreck

Eirini Mitsi <sup>1</sup>, Stamatis Boyatzis <sup>2</sup> and Anastasia Pournou <sup>2,\*</sup>

<sup>1</sup> Department of History, Archaeology and Cultural Resources Management, University of the Peloponnese, 24100 Kalamata, Greece; eir.mitsi@gmail.com

<sup>2</sup> Department Conservation of Antiquities & Works of Art, University of West Attica, Ag. Spyridonos Str., Aegaleo, 12243 Athens, Greece; sboyatzis@uniwa.gr

\* Correspondence: pournou@uniwa.gr

**Abstract:** In 2008, a medieval wooden shipwreck was discovered at the port of Rhodes, Greece. The shipwreck was partly burned, presenting a challenge for conservators, as uncharred, semi-charred and charred waterlogged wood were often encountered on the same piece of timber. In seeking the most appropriate conservation method for this unusual material, its chemical characterization was considered necessary. This study examined the chemistry of the three dominant wood conditions found in the wreck. Fourier transform infrared spectroscopy and X-ray diffraction analysis were implemented in comparison to reference samples. Energy dispersive analysis was also used for assessing the inorganic composition of each condition. Moreover, for charred and semi-charred wood, proximate analysis was undertaken. Results obtained regarding the organic moieties of the waterlogged archaeological material, demonstrated that charred samples were chemically comparable to charcoals, semi-charred material showed similarity to thermally modified wood, whereas uncharred waterlogged wood was proven to have an analogous chemistry to biodeteriorated wood. Elemental analysis results also diversified among the three shipwreck's conditions. Sulfur, iron, and oxygen decreased in charred areas, whereas carbon increased. Proximate analysis showed that ash and fixed carbon content increased with charring, whereas volatile matter decreased. This work proved major chemical differences among shipwreck timbers' conditions owing to different degree of charring. These are anticipated to influence not only conservation methods' efficacy, but also the post-treatment behavior of the material. Further investigation is needed for correlating the chemistry of the archaeological material to its physical properties in order to contribute to practical aspects of conservation.

**Keywords:** medieval shipwreck; waterlogged wood; charred wood; chemical analysis; EDS; FTIR; XRD; proximate analysis



**Citation:** Mitsi, E.; Boyatzis, S.; Pournou, A. Chemical Characterization of Waterlogged Charred Wood: The Case of a Medieval Shipwreck. *Forests* **2021**, *12*, 1594. <https://doi.org/10.3390/f12111594>

Academic Editors: Magdalena Broda and Callum A. S. Hill

Received: 9 October 2021

Accepted: 17 November 2021

Published: 19 November 2021

**Publisher's Note:** MDPI stays neutral with regard to jurisdictional claims in published maps and institutional affiliations.



**Copyright:** © 2021 by the authors. Licensee MDPI, Basel, Switzerland. This article is an open access article distributed under the terms and conditions of the Creative Commons Attribution (CC BY) license (<https://creativecommons.org/licenses/by/4.0/>).

## 1. Introduction

During a routine survey in 2008, a late-12th-century ship was discovered at the commercial port of Rhodes by the Greek Ephorate of Underwater Antiquities [1,2]. The shipwreck lay at a maximum depth of 13–14 m and was found half-buried in muddy sediment [1].

In 2013, a partial excavation of the shipwreck revealed that it was a merchant ship loaded with a cargo of amphorae and made apparent that a fire event took place before the vessel sunk [1]. Extensive or superficial traces of burning were recorded on many constructional elements of the ship, such as frames, ceiling planking, and stringers, and almost on every artifact recovered [1,2].

Excavated wooden hull members, identified as *Pinus halepensis* Mill. or *Pinus brutia* Ten. [1], showed a varied preservation state, as the degree and depth of charring was not homogenous among ship timbers due to the fire progression [3]. The coexistence of uncharred, semi-charred, and charred wood, often encountered on the same timber,

poses a great challenge for the ship's future conservation as wood responds differently to impregnation and drying, depending on its charring degree [3]. However, literature on the conservation of waterlogged charred wood is scarce and there are no studies associating the conservation requirements with material's physical and chemical properties. Nonetheless, it is well known that thermal decomposition of wood is accompanied by major chemical changes in hygroscopicity, viscosity, cell wall structure, color, density, and loss of mass and strength [4–8]. Moreover, it is also documented that these alterations depend on variables related not only on the wood, such as density, moisture content, permeability, species, size, grain direction, and surface protection [7,9], but also on the heating scenario, which incorporates the heat flux (temperature and duration) and the environment surrounding the wood like the oxygen concentration [7,9–13]. All these factors which influence pyrolysis, combustion, and the charring rate of wood justify the coexistence of charred, semi-charred, and uncharred wood in the shipwreck.

Preliminary experiments undertaken for the conservation of this material with polyethylene glycol followed by air or freeze drying have demonstrated a very dissimilar response to consolidation [3]. This was rather anticipated because as wood reaches elevated temperatures, the thermally degraded structural and chemical components affect greatly its behavior [4–6,12,14].

Therefore, this study was set to characterize the chemistry of this dissimilarly charred material in order to help understand its behavior and provide insights towards the development of a successful conservation method.

## 2. Materials and Methods

Waterlogged wood examined in this study belonged to a wreck's frame made of *Pinus halepensis* Mill. (Aleppo pine) or *Pinus brutia* Ten. (Turkish pine) [1]. Part of the frame was retrieved in 2013, and was kept waterlogged at 5 °C until sampling. The material presented a varied degree of charring, as its outer surface was charred, its inner core was uncharred, and layers in between were semi-charred [3]. Samples used for the chemical characterization were taken from the surface inwards, at least 50 annual rings away from the pith, to correspond to the sapwood of the mature pine, and contained all three charring conditions.

### 2.1. Energy Dispersive Analysis (EDS)

Uncharred and semi-charred waterlogged archaeological samples were cut in subsamples using a double-edged razor blade, whereas charred samples were fractured. Subsamples were then dehydrated in a series of ethanol solutions of increasing concentrations until water-free alcohol was reached and left to air-dry in a desiccator. They were then mounted on aluminum stubs using a double coated carbon conductive tape and energy dispersive X-ray spectroscopy (EDS) was performed at an acceleration voltage of 20 kV under low vacuum (33 Pa) using a JEOL JSM-6510LV scanning electron microscope, equipped with an Inca x-act silicon drift detector (SDD) with PentaFET<sup>®</sup> Precision (Oxford Instruments, Oxford, UK). The analytical data were obtained with Inca<sup>®</sup> analysis software. Bulk analysis was applied on every wood condition, whereas line scans and mapping were applied on samples where all conditions coexisted.

### 2.2. Fourier Transform Infrared Spectroscopy (FTIR)

Uncharred, semi-charred, and charred waterlogged archaeological wood was air-dried, and along with sapwood of sound wood of mature *Pinus halepensis* Mill. and *Pinus brutia* Ten. were finely grounded manually with the use of an agate mortar and pestle to ~100 µm (No 140-mesh size). Wood powder was then mixed with potassium bromide powder (KBr, Merck), and pressed into 13 mm discs with a hydraulic press. Disc samples were placed in the FTIR system sample chamber for analysis.



All samples were analyzed with a Perkin Elmer Spectrum GX spectrometer, equipped with DTGS (deuterated diglycine sulfate) detector. Spectra were recorded and edited with the Perkin Elmer Spectrum v.5.3.1 software.

### 2.3. X-Ray Diffraction Analysis (XRD)

Air-dried uncharred, semi-charred, and charred, waterlogged archaeological samples along with sapwood of sound wood of mature *Pinus halepensis* Mill. and *Pinus brutia* Ten. were finely grounded manually with the use of an agate mortar and pestle to ~100 µm (No 140 mesh size).

X-ray diffraction spectra of wood powdered samples were recorded with the help of InXitu BTX II Benchtop X-ray Diffraction/X-ray Fluorescence hybrid system using a Cobalt source ( $K\alpha_1$  1.78897 Å). All spectra were recorded in duplicate after the completion of >1200 scan cycles from 5 to 50 degrees  $2\theta$ .

The crystallinity index (CrI) was calculated based on the method developed by Segal et al. in 1959 [15] using the height ratio between the crystalline intensity, expressed as the difference ( $I_{200} - I_{am}$ ) and the total intensity ( $I_{200}$ ), Equation (1). Diffractograms were baseline-corrected with the X Powder software and consequently analyzed using the Perkin Elmer Spectrum v.5.3.1 software with no further processing of peak heights at the (200) plane and at the amorphous region. The total intensity that corresponds to both crystalline and amorphous material ( $I_{200}$ ), is assigned at  $2\theta \sim 25.60^\circ$ , whereas the amorphous intensity ( $I_{am}$ ) is assigned at  $2\theta \sim 20.60^\circ$ , angles corresponding to Cobalt source radiation.

$$\%CrI = \frac{I_{(200)} - I_{am}}{I_{(200)}} \times 100 \quad (1)$$

The apparent crystallite size  $L$  (in nm) was estimated using the Scherrer Equation (2) [16], where  $K$  is the Scherrer constant, for which, the value of 0.94 was typically adopted;  $\lambda$  is the X-ray wavelength (1.78897 Å for Co  $K\alpha_1$  radiation);  $\beta$  is the full width at half maximum (FWHM) of the diffraction band calculated after curve deconvolution using the Thermo GRAMS suite v.9.0 at the ~11–30.5  $2\theta$  range using a 1:1 Gaussian-Lorentzian profile; and  $\theta$  is the Bragg angle corresponding to the (200) plane.

$$L = \frac{K \times \lambda}{\beta \times \cos\theta} \quad (2)$$

### 2.4. Proximate Analysis

Proximate analysis was implemented on charred and semi-charred wood samples according to ASTM D1762-84. Samples were air-dried to a constant weight at 21 °C and 65% RH. They were then grounded manually with the use of an agate mortar and pestle, to ~100 µm (No 140-mesh size). Determination of moisture, ash, volatile matter, and fixed carbon was duplicated.

For moisture, approximately 1 g of each condition was placed in a porcelain crucible and weighed to the nearest 0.1 mg. Crucibles and covers were previously dried in a muffle furnace at 750 °C for 10 min and cooled in a desiccator for 1 h. Crucibles containing grounded samples were then placed uncovered in an oven at 105 °C for 2 h. Dried samples were cooled covered in a desiccator for 1 h and weighed. Samples were considered oven-dried when the decrease in weight was  $\leq 0.0005$  g. Succeeding drying periods were 1 h. Moisture content was calculated based on Equation (3).

$$\text{Moisture\%} = [(A - B)/A] \times 100 \quad (3)$$

where  $A$  = grams of air-dry sample used, and  $B$  = grams of sample after drying at 105 °C.

For volatile matter, crucibles with lids in place and containing the samples used for moisture determination were placed in a muffle furnace heated to 950 °C. They were first positioned, with the furnace door open, for 2 min on the outer ledge of the furnace (300 °C),

then for 3 min on the edge of the furnace (500 °C) and finally to the rear of the furnace for 6 min with the muffle door closed. Samples were then cooled in a desiccator for 1 h and weighed. The percentage of volatile matter in the sample was calculated based on the Equation (4)

$$\text{Volatile matter}\% = [(B - C)/B] \times 100 \quad (4)$$

where C = grams of sample after drying at 950 °C.

For ash, lids and uncovered crucible used for the volatile matter determination containing the samples were placed in a muffle furnace at 750 °C for 6 h. Samples were cooled with lids in place covered in a desiccator for 1 h and weighed. Samples were repeatedly burned with succeeding 1-h periods until results showed loss of less than 0.0005 g.

The percentage of ash content was calculated based on the Equation (5)

$$\text{Ash}\% = (D/B) \times 100 \quad (5)$$

where D = grams of residue.

Fixed carbon was calculated on a dry basis according to ASTM E870–82 based on the Equation (6).

$$\text{Fixed Carbon}\% = 100 - [\text{Volatile Matter}\% + \text{Ash}\%] \quad (6)$$

### 3. Results and Discussion

#### 3.1. EDS

Bulk analysis of uncharred, semi-charred, and charred material (Figure 1a,b) showed the presence of aluminum (Al), calcium (Ca), magnesium (Mg), and silica (Si) (Figure 1c). Moreover, both sulfur (S) and iron (Fe) concentrations were shown to decrease in charred areas. This is more likely owed to the different porosity/permeability of the material, which is charring-dependent [17] and that did not allow Fe found in the burial environment [18,19] and S produced by the action of sulfate-reducing bacteria [18] to penetrate into the material uniformly.

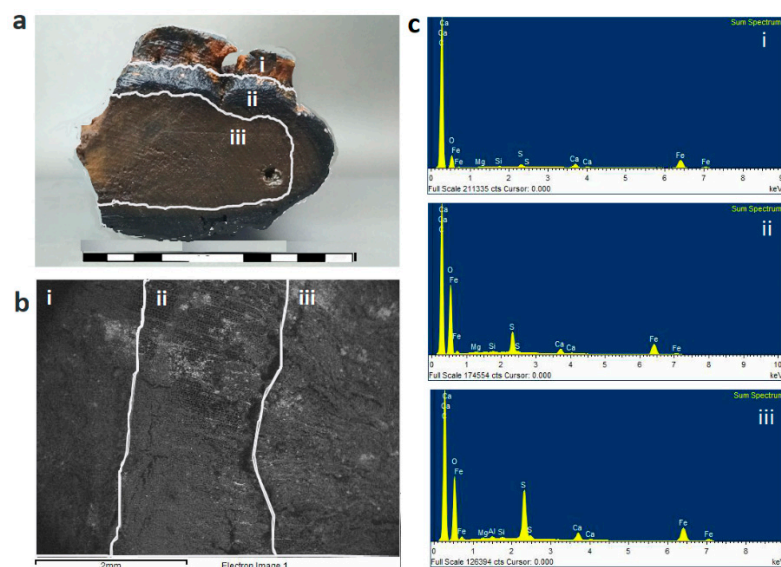


**Figure 1.** Macroscopic image (a) and SEM micrograph (b) of a sample where charred (i), semi-charred (ii), and uncharred (iii) material coexisted; (c) EDS spectrum of each condition.

Elemental mapping and line scans on samples where all conditions coexisted (Figure 2) also confirmed that the presence of S and Fe is more intense in uncharred areas. Moreover, mapping revealed the coexistence of S and Fe in some spots, which possibly indicates their co-occurrence in the same compound [20,21]. This concurrent presence of S and

Fe in the material is expected to cause severe post-excavation and post-conservation problems [20–23].

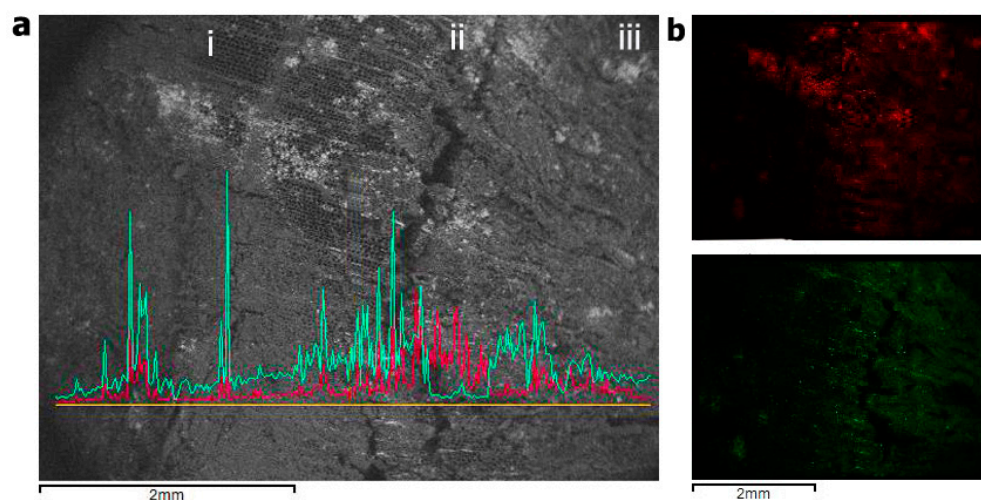


**Figure 2.** EDS line-scan and mapping of a sample where all conditions coexisted. (a) Line scan of Fe (red) and S (green) (left to right the transition from charred to uncharred, i–iii); (b) mapping of Fe (red) and S (green).

Another find revealed by EDS was the different concentration of carbon (C) and oxygen ( $O_2$ ) due to charring (Figure 3). As expected, C percentage increases in charred material [17,24,25] while O decreases [17,24]. The increase/decrease rate of C and O is dependent on both temperature and heating duration [17]. Moreover, the relative concentrations of these two elements (Figure 3a) showed that in charred material carbon is much higher than oxygen, indicating that oxygen-containing organic moieties such as polysaccharides and lignin are depleted [26,27]. In contrast, in uncharred areas the ratio of O to C is constant but relatively low, indicating the presence of organic matter, most likely lignin [27], which is in accordance with FTIR results.

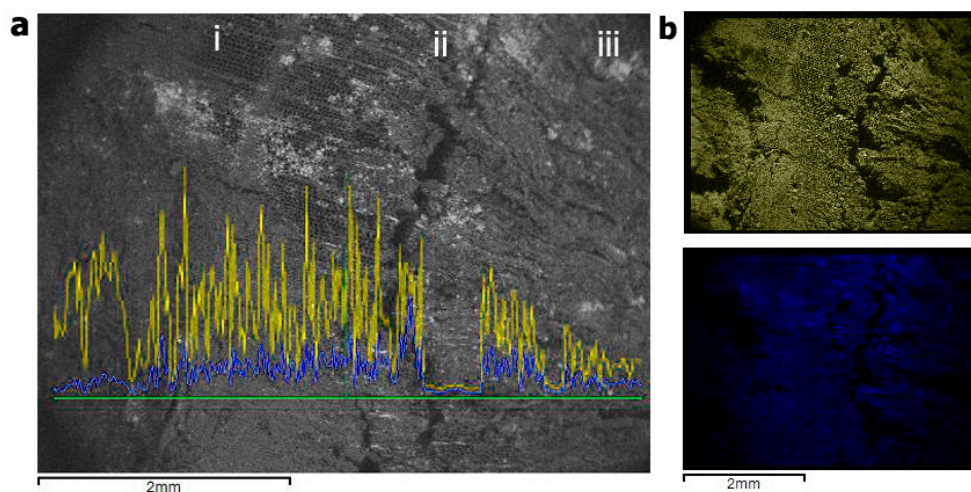


**Figure 3.** EDS Line-scan and mapping of a sample where all conditions coexisted. (a) Line scan of carbon (yellow) and oxygen (blue) (left to right the transition from charred to uncharred, i–iii); (b) mapping of carbon (yellow) and oxygen (blue).

### 3.2. FTIR

Spectra obtained from uncharred, semi-charred, and charred archaeological samples along with reference spectra of *Pinus halepensis* and *Pinus brutia* are presented in Figure 4.

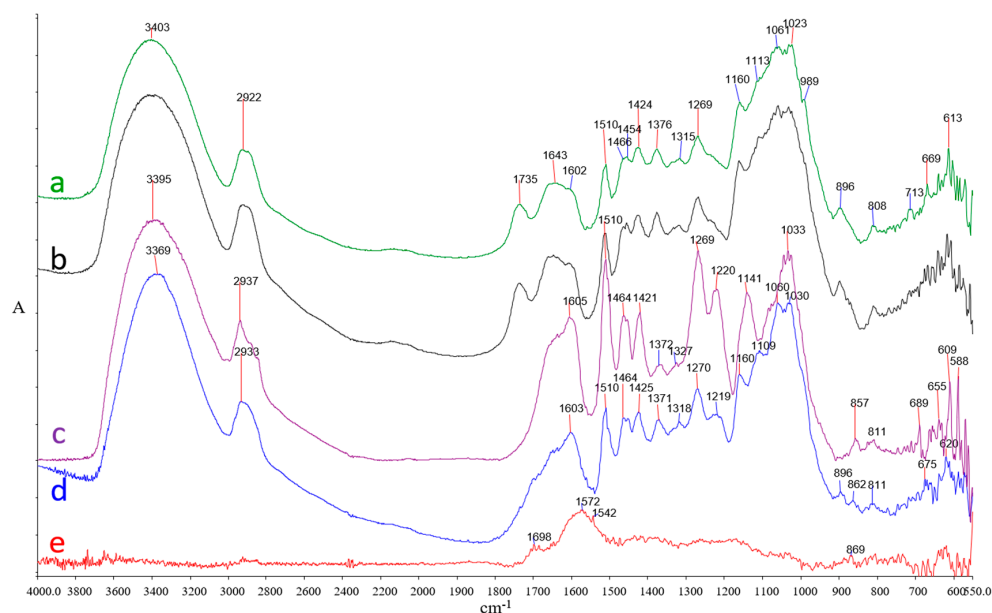


**Figure 4.** Spectra obtained for reference samples, (a) *Pinus halepensis* and (b) *Pinus brutia* (c) uncharred (d) semi-charred, and (e) charred archaeological samples.

The charred archaeological sample infrared spectrum (Figure 4e) appears typical to charcoals where the broad band at 3400–3320  $\text{cm}^{-1}$  representing the –OH stretching vibration of water and the peaks at 3000–2800  $\text{cm}^{-1}$ , due to aliphatic C–H stretching vibration derived from methyl, methylene, and methine group, are absent, as these bands decrease in intensity with increasing temperature [11,13,28,29]. Moreover, specific bands assigned to wood components such as hemicelluloses ( $\sim 1737 \text{ cm}^{-1}$ ), lignin ( $\sim 1510$  and  $1269 \text{ cm}^{-1}$ ) and cellulose (1026 and  $\sim 898 \text{ cm}^{-1}$ ) [23] and generally all bands in the “fingerprint” region 1500–900  $\text{cm}^{-1}$  [23,28] are absent, displaying the chemical changes caused by pyrolysis as well [29]. Nonetheless, the charred sample spectrum presents broad bands at  $\sim 1708 \text{ cm}^{-1}$ , due to the acidic C=O groups, characteristic of low temperature charcoals’ spectra [11,13] and a broad band at 1610–1590  $\text{cm}^{-1}$  due to lignin aromatic C=C skeletal vibrations, which have been also reported to increase in intensity with increasing charring [29].

Semi-charred material spectrum appears comparable to spectra of thermally modified wood. The intensity of hemicelluloses ester carbonyl peak at  $1737 \text{ cm}^{-1}$  is evidently decreased, as most of the xylan-linked acetyl groups are expected to be cleaved with increasing temperature and time during the burning of wood [30–34]. The cellulose peak at  $\sim 895 \text{ cm}^{-1}$  due to C–H deformations at the glycosidic linkage was also decreased, which has been reported to occur when wood is exposed to heat [32,33,35]. It should be mentioned though, that part of carbohydrates’ reduction could be owed to abiotic or biotic processes occurring in the marine environment during the service life of the ship or during burial [36–38]. Other carbohydrate bands at  $\sim 1371$ ,  $\sim 1160$ , and  $1110 \text{ cm}^{-1}$  showed no significant difference in intensity. Similarly, the major lignin bands, approximately at 1603, 1510, 1464, 1425, 1371, 1316, 1269, and  $1223 \text{ cm}^{-1}$  showed no intensity differences as reported for thermally modified wood [33] whereas the slight rise observed for some (1603, 1510, and  $1425 \text{ cm}^{-1}$ ) is mainly due to the increase in relative lignin content [35]. Nonetheless, an increase in absorption at 1030 and  $1060 \text{ cm}^{-1}$  has been observed indicating respectively the pronounced aromatic nature of the semi-charred wood, since this absorption band also indicates aromatic in-plane C–H deformation and changes in cellulose structure [34,35] along with the formation of aliphatic alcohols during heating [31,35].

The spectrum of uncharred waterlogged wood appears typical of biodeteriorated waterlogged wood, where significantly pronounced lignin bands 1605, 1510, 1269, and  $1220 \text{ cm}^{-1}$  appear with a corresponding decrease in the intensities of carbohydrate bands at 1737, 1370, 1158, and  $895 \text{ cm}^{-1}$ . More specifically, it is indicated that shipwreck timbers

have been deteriorated by erosion bacteria or/and soft-rot fungi, which thrive in the marine environment [37]. Erosion bacteria decay has been often reported to be associated with lignin bands' increment and carbohydrates bands' decrement [38,39]. Soft-rotters also degrade carbohydrates in preference to lignin [37] and most of them are unable to degrade guaiacyl lignin, found predominantly in softwoods, with the exception of the cavity-forming species [40]. This probably explains the new band developed at  $\sim 1140\text{ cm}^{-1}$ , which in combination with the decrease in the intensity at 1060 and the increase at  $1030\text{ cm}^{-1}$ , may be attributable to the guaiacyl lignin relative increase compared to carbohydrates [41] (C–H deformation in the guaiacyl unit, with C–O deformation in primary alcohol). This is also in accordance with another band present in uncharred wood sample at  $\sim 855\text{ cm}^{-1}$  that is associated with the C–H out-of-plane vibrations in guaiacyl lignin [42].

### 3.3. XRD

Diffractograms regarding the (110), (110), (102), (200), and (004) reflections of the two reference samples (*P. halepensis* and *P. brutia*) along with charred, semi-charred, and uncharred archaeological waterlogged samples are shown in Figure 5. Both reference samples and semi-charred diffractograms showed all peaks typical of reflection planes of wood cellulose [43–45]. In contrast, the uncharred sample diffractogram showed a considerably flattened line-shape; nonetheless, it showed a more prominent peak on the (200) plane reflection with respect to the (110) and (110). The charred sample diffractogram, as reported by other researchers [46], appeared also flattened with a weak and broad peak regarding the (200) reflection plane, with a shifted vague maximum at  $\sim 30^\circ$ .

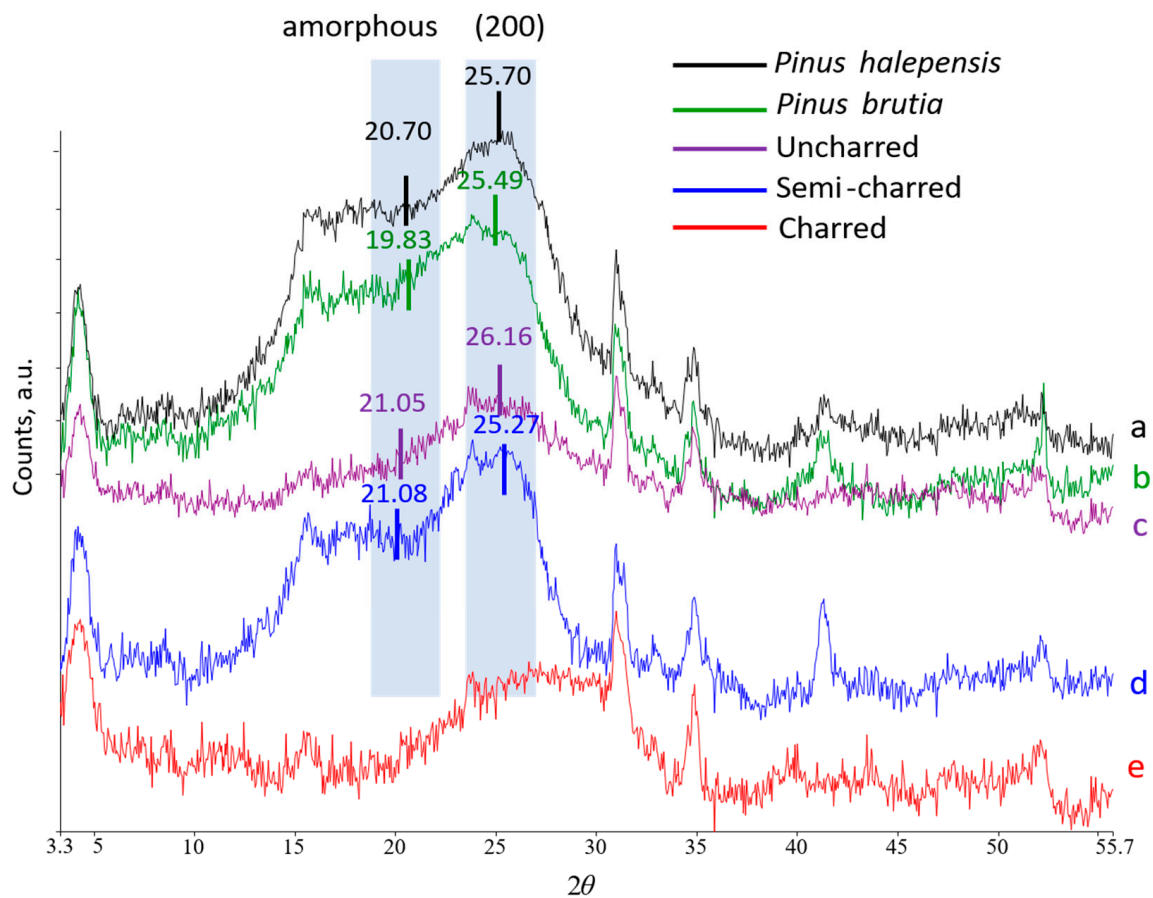


**Figure 5.** X-ray diffraction pattern of (a) *Pinus halepensis* and (b) *Pinus brutia* reference samples in comparison with (c) uncharred, (d) semi-charred, and (e) charred waterlogged samples. The  $2\theta$  values correspond to Cobalt source reflections.

Crystallinity index (CrI) of the material examined varied greatly depending on the charring degree (Table 1). The higher cellulose CrI value was calculated for the uncharred material, and followed by semi-charred wood and by controls. However, CrI values were not in accordance with the respective crystallite sizes ( $L$ ), as for the uncharred material,  $L$  presented the lowest value.

**Table 1.** Band positions of the maximum total intensity ( $I_{200}$ ) and the minimum intensity of the amorphous cellulose ( $I_{am}$ ). CrI represents the crystalline index based on Segal's method and  $L$  correspond to the crystallite size.

Sample	$2\theta$ ( $I_{200}$ ) <sup>a</sup>	$2\theta$ ( $I_{am}$ ) <sup>a</sup>	CrI	$L$ (nm)
<i>Pinus brutia</i>	25.49	19.83	41.7%	2.29
<i>Pinus halepensis</i>	25.70	20.70	41.8%	2.51
Semi-charred	25.27	21.08	47.4%	2.75
Uncharred	26.16	21.05	53.2%	1.10
Charred <sup>b</sup>	-	-	-	-

<sup>a</sup>  $2\theta$  values are expressed as Co-source. <sup>b</sup> CrI was not calculated as no cellulose is expected to be preserved with charring above 400 °C.

The considerably high CrI of uncharred material was not anticipated, as in archaeological wood the crystallinity usually decreases with decay [23,47–49]. Nonetheless, crystallinity's increase has been reported by other authors in initial stages of degradation due to the dramatic loss of amorphous cellulose regions [23,48,50]. It is believed though that this explanation does not justify the high CrI values of uncharred material as the diffractogram line-shape, the FTIR results and the lowest crystallite size ( $L$ ) recorded point out to a material in which cellulose is probably completely destroyed. Therefore, it appears that the Segal method for CrI calculation cannot successfully apply to severely deteriorated material. This could be due to several reasons related to the deficiency of the Segal method [44,51,52]; nonetheless, it is considered that is principally owed to the highly depleted cellulose fraction. It is recommended for this type of material to use other methods such as the two-dimensional X-ray diffraction.

The relative higher CrI of semi-charred material compared to references is considered that is due to amorphous cellulose degradation, which occurs during the initial stages of heating and progresses as the heat temperature rises [53–55]. This is in accordance with the high  $L$  value that corresponds to relatively larger crystal that the other materials examined. Moreover, indicates that the charring temperature for semi-charred material was lower than ~300 °C as above this threshold, cellulose crystalline part is expected to degrade severely [46,56].

### 3.4. Proximate Analysis

Proximate analysis' results on moisture content, volatile matter, ash content and fixed carbon are presented in Table 2 for both semi-charred and charred conditions. For the moisture content, no difference was recorded among samples. As it was anticipated, the volatile matter was lower in fully charred material as it is negatively correlated with temperature [57–59]. Similar values for volatile matter have been recorded by Dias Junior et al. (2020) [59] indicating combustion at/over 450 °C. The difference of volatile matter between the two conditions can be attributed to the barrier role of charred layer over the inner areas [60,61].

**Table 2.** Proximate analysis results for charred and semi-charred samples. Percentages values of moisture content, volatile matter, ash content and fixed carbon are the average of 2 replicates. Fixed carbon was calculated on dry basis.

Sample	Moisture Content	Volatile Matter	Ash Content	Fixed Carbon
Semi-charred	6.53	75.07	1.87	16.51
Charred	6.71	24.16	3.53	65.59

Ash content appears to increase with combustion as expected [57,58]. Likewise, fixed carbon content appears to increase as combustion progresses and it is in accordance with results of other researchers [57–59] and with the EDS results obtained in the present study. This increase is suggested to be a result of pyrolytic process which favors the volatile removal and consequently the elevation of ash-minerals and carbon [57].

#### 4. Conclusions

This work demonstrated major chemical differences among shipwreck timbers' due to charring. Three distinct conditions, consisting of uncharred, semi-charred, and charred wood, were documented which were directly related to the fire heat flux (temperature and duration) and the surrounding oxygen concentration.

Regarding the organic chemistry of the archaeological material, charred samples showed an analogous profile to charcoals, where both polysaccharides and lignin were almost absent due to pyrolysis. Semi-charred material showed a chemical similarity to thermally modified wood, where hemicelluloses were reduced, cellulose crystallinity was increased, and lignin showed no large differences compared to sound wood. Uncharred waterlogged wood chemistry was analogous to biodeteriorated wood, as carbohydrates were dramatically depleted, and the relative lignin content appeared increased.

The inorganic chemistry of the archaeological wood, based on elements' concentrations and topography also varied among the three conditions. Sulfur and iron concentrations were found increased in uncharred areas and their topochemistry indicated their possible co-existence in the same compounds. This concurrent presence of S and Fe it is considered that has the potential to cause severe post-excavation problems.

Finally, proximate analysis also demonstrated differences among conditions, as ash content and fixed carbon was higher in charred compared to semi-charred samples.

All chemical differences documented are awaited to be taken into consideration when developing the conservation plan of this shipwreck, as it is anticipated to influence not only conservation methods' efficacy but also the post-treatment behavior of the material.

It is believed, however, that further investigation is required in order to correlate this diverse chemistry to physical properties such as porosity, permeability, density, and shrinkage, in order to provide a more practical contribution to the shipwreck conservation.

**Author Contributions:** Conceptualization: A.P.; data curation: E.M., S.B. and A.P.; formal analysis: E.M. and S.B.; investigation: E.M., S.B. and A.P.; methodology: E.M., S.B. and A.P.; Supervision: A.P. All authors have read and agreed to the published version of the manuscript.

**Funding:** This research received no external funding.

**Acknowledgments:** The authors would like to thank G. Koutsouflakis, for providing the archaeological material and A. Karabotsos for his assistance with the SEM-EDS analysis.

**Conflicts of Interest:** The authors declare no conflict of interest.

## References

1. Koutsouflakis, G.; Rieth, E. A late-12th-century byzantine shipwreck in the port of Rhodes A preliminary report. In *Under the Mediterranean I Studies in Maritime Archaeology*; Demesticha, S., Blue, L., Eds.; Sidestone Press: Leiden, The Netherlands, 2021.
2. Koutsouflakis, G. Three shipwrecks of the medieval era in the commercial port of Rhodes. In *Proceedings of the Archeological Work in Aegean Islands, Lesbos, Greece, 27 November–1 December 2013*; Birtacha, K., Triantaphyllidis, P., Sarantidis, K., Eds.; pp. 477–500.
3. Mitsi, E.; Pournou, A. Conserving a charred medieval shipwreck: A preliminary study. In *Proceedings of the 14th ICOM-CC WOAM Conference, Portsmouth, UK, 20–24 May 2019*.
4. Stamm, A.J. Thermal degradation of wood and cellulose. *Ind. Eng. Chem.* **1956**, *48*, 413–417. [[CrossRef](#)]
5. Shafizadeh, F. The chemistry of pyrolysis and combustion. *Adv. Chem.* **1984**, *207*, 489–529.
6. Meincken, M.; Smit, N.H.; Steinmann, D. Physical properties of burnt timber, with special focus on the drying performance. *Eur. J. Wood Wood Prod.* **2015**, *68*, 455–461. [[CrossRef](#)]
7. Bartlett, A.I.; Hadden, R.M.; Bisby, L.A. A review of factors affecting the burning behaviour of wood for application to tall timber construction. *Fire Technol.* **2019**, *55*, 1–49. [[CrossRef](#)]
8. Kollmann, F.F.; Côté, W.A. *Principles of Wood Science and Technology. Vol. I. Solid Wood*; Springer: Berlin/Heidelberg, Germany, 1968; ISBN 9783642879302.
9. Friquin, K.L. Material properties and external factors influencing the charring rate of solid wood and glue-laminated timber. *Fire Mater.* **2011**, *35*, 303–327. [[CrossRef](#)]
10. Liu, Q.; Wang, S.R.; Fang, M.X.; Luo, Z.Y.; Cen, K.F.; Chow, W.K. Bench-scale studies on wood pyrolysis under different environments. *Fire Saf. Sci.* **1994**, *7*, 94.
11. Guo, Y.; Bustin, R. FTIR spectroscopy and reflectance of modern charcoals and fungal decayed woods: Implications for studies of inertinite in coals. *Int. J. Coal Geol.* **1998**, *37*, 29–53. [[CrossRef](#)]
12. White, R.H.; Dietsberger, M. Wood products: Thermal degradation and fire. *Encycl. Mater. Sci. Technol.* **2001**, 9712–9716. [[CrossRef](#)]
13. Constantine, M.; Mooney, S.; Hibbert, B.; Marjo, C.; Bird, M.; Cohen, T.; Forbes, M.; Mcbeath, A.; Rich, A.; Stride, J. Science of the Total Environment Using charcoal, ATR FTIR and chemometrics to model the intensity of pyrolysis: Exploratory steps towards characterising fire events. *Sci. Total Environ.* **2021**, *783*, 147052. [[CrossRef](#)]
14. Hill, C.A.S. Modifying the properties of wood. In *Wood Modification: Chemical, Thermal and Other Processes*; John Wiley & Sons: Hoboken, NJ, USA, 2006; pp. 19–44. ISBN 9780470021729.
15. Segal, L.; Creely, J.J.; Martin, A.E., Jr.; Conrad, C.M. An empirical method for estimating the degree of crystallinity of native cellulose using the X-ray diffractometer. *Text. Res. J.* **1959**, *29*, 786–794. [[CrossRef](#)]
16. Scherrer, P.; Debye, P. Bestimmung der grösse und der inneren struktur von kolloidteilchen mittels röntgensahlen [determination of the size and internal structure of colloidal particles using X-rays]. *Nachr. Ges. Wiss. Göttingen Math.-Physik. Kl.* **1918**, *2*, 101–120.
17. Rutherford, D.; Wershaw, R.; Cox, L. *Changes in Composition and Porosity Occurring during the Thermal Degradation of Wood and Wood Components: U.S. Geological Survey Scientific Investigations Report 2004-5292*; U.S. Geological Survey: Reston, VA, USA, 2005; Volume 79.
18. Sandström, M.; Jalilvand, F.; Persson, I.; Fors, Y.; Damian, E.; Gelius, U.; Hall-Roth, I.; Dal, L.; Richards, V.L.; Godfrey, I. The sulphur threat to marine archaeological artefacts: Acid and iron removal from the Vasa. In *Proceedings of the Conservation Science 2002, Edinburgh, UK, 22–24 May 2002*; pp. 79–87.
19. Monachon, M.; Albelda-Berenguer, M.; Pelé, C.; Cornet, E.; Guilminot, E.; Rémazeilles, C.; Joseph, E. Characterization of model samples simulating degradation processes induced by iron and sulfur species on waterlogged wood. *Microchem. J.* **2020**, *155*, 104756. [[CrossRef](#)]
20. Fors, Y. Sulfur-Related Conservation Concerns for Marine Archaeological Wood. Ph.D. Thesis, Stockholm University, Stockholm, Sweden, 2008.
21. Rémazeilles, C.; Tran, K.; Guilminot, E.; Conforto, E.; Refait, P. Study of Fe (II) sulphides in waterlogged archaeological wood. *Stud. Conserv.* **2013**, *58*, 297–307. [[CrossRef](#)]
22. Fors, Y.; Nilsson, T.; Risberg, E.D.; Sandström, M.; Torssander, P. Sulfur accumulation in pinewood (*Pinus sylvestris*) induced by bacteria in a simulated seabed environment: Implications for marine archaeological wood and fossil fuels. *Int. Biodeterior. Biodegrad.* **2008**, *62*, 336–347. [[CrossRef](#)]
23. High, K.E.; Penkman, K.E.H. A review of analytical methods for assessing preservation in waterlogged archaeological wood and their application in practice. *Herit. Sci.* **2020**, *8*, 1–34. [[CrossRef](#)]
24. Valenzuela-Calahorra, C.; Bernalte-García, A.; Gómez-Serrano, V.; Bernalte-García, M.J. Influence of particle size and pyrolysis conditions on yield, density and some textural parameters of chars prepared from holm-oak wood. *J. Anal. Appl. Pyrolysis* **1987**, *12*, 61–70. [[CrossRef](#)]
25. Todaro, L.; Rita, A.; Cetera, P.; D’Auria, M. Thermal treatment modifies the calorific value and ash content in some wood species. *Fuel* **2015**, *140*, 1–3. [[CrossRef](#)]
26. Inari, G.N.; Petrissans, M.; Lambert, J.; Ehrhardt, J.J.; Gérardin, P. XPS characterization of wood chemical composition after heat-treatment. *Surf. Interface Anal.* **2006**, *38*, 1336–1342. [[CrossRef](#)]



27. Kocaefe, D.; Huang, X.; Kocaefe, Y.; Boluk, Y. Quantitative characterization of chemical degradation of heat-treated wood surfaces during artificial weathering using XPS. *Surf. Interface Anal.* **2013**, *45*, 639–649. [[CrossRef](#)]
28. Poletto, M.; Zattera, A.J.; Santana, R.M.C. Structural differences between wood species: Evidence from chemical composition, FTIR spectroscopy, and thermogravimetric analysis. *J. Appl. Polym. Sci.* **2012**, *126*, E336–E343. [[CrossRef](#)]
29. Tintner, J.; Preimesberger, C.; Pfeifer, C.; Soldo, D.; Ottner, F.; Wriessnig, K.; Rennhofer, H.; Lichtenegger, H.; Novotny, E.H.; Smidt, E. Impact of pyrolysis temperature on charcoal characteristics. *Ind. Eng. Chem. Res.* **2018**, *57*, 15613–15619. [[CrossRef](#)]
30. Tjeerdsma, B.F.; Militz, H. Chemical changes in hydrothermal treated wood: FTIR analysis of combined hydrothermal and dry heat-treated wood. *Holz Roh-Und Werkst.* **2005**, *63*, 102–111. [[CrossRef](#)]
31. Popescu, M.-C.; Froidevaux, J.; Navi, P.; Popescu, C.-M. Structural modifications of *Tilia cordata* wood during heat treatment investigated by FT-IR and 2D IR correlation spectroscopy. *J. Mol. Struct.* **2013**, *1033*, 176–186. [[CrossRef](#)]
32. Esteves, B.; Marques, A.V.; Domingos, I.; Pereira, H. Chemical changes of heat treated pine and eucalypt wood monitored by FTIR. *Maderas. Cienc. Tecnol.* **2013**, *15*, 245–258. [[CrossRef](#)]
33. Özgenç, Ö.; Durmaz, S.; Boyacı, İ.H.; Eksi-Koçak, H. ATR-FTIR spectroscopic analysis of thermally modified wood degraded by rot fungi. *Drewno* **2018**, *61*. [[CrossRef](#)]
34. Kubovsk, I.; Ka, D. Structural changes of oak wood main components caused by thermal modification. *Polymers* **2020**, *12*, 485. [[CrossRef](#)]
35. Kotilainen, R.A.; Toivanen, T.-J.; Alén, R.J. FTIR monitoring of chemical changes in softwood during heating. *J. Wood Chem. Technol.* **2000**, *20*, 307–320. [[CrossRef](#)]
36. Kim, Y.S. Short note: Chemical characteristics of waterlogged archaeological wood. *Holzforschung* **1990**, *44*, 169–172. [[CrossRef](#)]
37. Pournou, A. Wood deterioration by aquatic microorganisms. In *Biodeterioration of Wooden Cultural Heritage: Organisms and Decay Mechanisms in Aquatic and Terrestrial Ecosystems*; Pournou, A., Ed.; Springer International Publishing: Cham, Switzerland, 2020; pp. 177–260. ISBN 978-3-030-46504-9.
38. Pedersen, N.B.; Gierlinger, N.; Thygesen, L.G. Bacterial and abiotic decay in waterlogged archaeological *Picea abies* (L.) Karst studied by confocal Raman imaging and ATR-FTIR spectroscopy. *Holzforschung* **2015**, *69*, 103–112. [[CrossRef](#)]
39. Gelbrich, J.; Mai, C.; Militz, H. Chemical changes in wood degraded by bacteria. *Int. Biodeterior. Biodegrad.* **2008**, *61*, 24–32. [[CrossRef](#)]
40. Nilsson, B.T.; Daniel, G.; Kirk, T.K.; Obst, J.R.; Service, F. Chemistry and microscopy of wood decay by some higher ascomycetes. *Holzforschung* **1989**, *43*, 11–18. [[CrossRef](#)]
41. Pandey, K.; Pitman, A. FTIR studies of the changes in wood chemistry following decay by brown-rot and white-rot fungi. *Int. Biodeterior. Biodegrad.* **2003**, *52*, 151–160. [[CrossRef](#)]
42. Traoré, M.; Kaal, J.; Cortizas, A.M. Differentiation between pine woods according to species and growing location using FTIR-ATR. *Wood Sci. Technol.* **2018**, *52*, 487–504. [[CrossRef](#)] [[PubMed](#)]
43. Andersson, S.; Wikberg, H.; Pesonen, E.; Maunu, S.L.; Serimaa, R. Studies of crystallinity of Scots pine and Norway spruce cellulose. *Trees* **2004**, *18*, 346–353. [[CrossRef](#)]
44. Park, S.; Baker, J.O.; Himmel, M.E.; Parilla, P.A.; Johnson, D.K. Cellulose crystallinity index: Measurement techniques and their impact on interpreting cellulase performance. *Biotechnol. Biofuels* **2010**, *3*, 10. [[CrossRef](#)]
45. Agarwal, U.P.; Reiner, R.R.; Ralph, S.A.; Forest, A.; Gi, O.; Drive, P. Estimation of cellulose crystallinity of lignocelluloses using near-IR. *J. Agric. Food Chem.* **2013**, *61*, 103–113. [[CrossRef](#)]
46. Kwon, S.-M.; Kim, N.-H.; Cha, D.-S. An investigation on the transition characteristics of the wood cell walls during carbonization. *Wood Sci. Technol.* **2009**, *43*, 487–498. [[CrossRef](#)]
47. Giachi, G.; Bettazzi, F.; Chimichi, S.; Staccioli, G. Chemical characterisation of degraded wood in ships discovered in a recent excavation of the Etruscan and Roman harbour of Pisa. *J. Cult. Herit.* **2003**, *4*, 75–83. [[CrossRef](#)]
48. Popescu, C.-M.; Larsson, P.T.; Tibirna, C.M.; Vasile, C. Characterization of fungal-degraded lime wood by X-ray diffraction and cross-polarization magic-angle-spinning <sup>13</sup>C-nuclear magnetic resonance spectroscopy. *Appl. Spectrosc.* **2010**, *64*, 1054–1060. [[CrossRef](#)]
49. Zhou, Y.; Wang, K.; Hu, D. Degradation features of archaeological wood surface to deep inside a case study on wooden boards of marquis of Haihun’s outer coffin. *Wood Res.* **2018**, *63*, 419–430.
50. Howell, C.; Hastrup, A.C.S.; Goodell, B.; Jellison, J. Temporal changes in wood crystalline cellulose during degradation by brown rot fungi. *Int. Biodeterior. Biodegrad.* **2009**, *63*, 414–419. [[CrossRef](#)]
51. Thygesen, A.; Oddershede, J.; Lilholt, H.; Thomsen, A.B.; Ståhl, K. On the determination of crystallinity and cellulose content in plant fibres. *Cellulose* **2005**, *12*, 563–576. [[CrossRef](#)]
52. French, A.D.; Cintron, M.S. Cellulose polymorphism, crystallite size, and the segal crystallinity index. *Cellulose* **2013**, *20*, 583–588. [[CrossRef](#)]
53. Sivonen, H.; Maunu, S.L.; Sundholm, F.; Jämsä, S.; Viitaniemi, P. Magnetic resonance studies of thermally modified wood. *Holzforschung* **2002**, *56*, 648–654. [[CrossRef](#)]
54. Esteves, B.M.; Pereira, H.M. Wood modification by heat treatment: A review. *BioResources* **2009**, *4*, 370–404. [[CrossRef](#)]
55. Tarmian, A.; Mastouri, A. Changes in moisture exclusion efficiency and crystallinity of thermally modified wood with aging. *iFor.-Biogeosci. For.* **2019**, *12*, 92–97. [[CrossRef](#)]

- 
56. Wang, S.; Dai, G.; Ru, B.; Zhao, Y.; Wang, X.; Xiao, G. Influence of torrefaction on the characteristics and pyrolysis behavior of cellulose. *Energy* **2017**, *120*, 864–871. [[CrossRef](#)]
  57. Fuwape, J.A. Effects of carbonisation temperature on charcoal from some tropical trees. *Bioresour. Technol.* **1996**, *57*, 91–94. [[CrossRef](#)]
  58. Ruiz-aquino, F.; Ruiz-ángel, S.; Sotomayor-castellanos, J.R. Energy characteristics of wood and charcoal of selected tree species in Mexico. *Wood Res.* **2019**, *64*, 71–82.
  59. Dias Junior, A.F.; Esteves, R.P.; Da Silva, Á.M.; Sousa Júnior, A.D.; Oliveira, M.P.; Brito, J.O.; Napoli, A.; Braga, B.M. Investigating the pyrolysis temperature to define the use of charcoal. *Eur. J. Wood Wood Prod.* **2020**, *78*, 193–204. [[CrossRef](#)]
  60. Mikkola, E. Charring of Wood Based Materials. *Fire Saf. Sci.* **1991**, *3*, 547–556. [[CrossRef](#)]
  61. Lowden, L.A.; Hull, T.R. Flammability behaviour of wood and a review of the methods for its reduction. *Fire Sci. Rev.* **2013**, *2*, 4. [[CrossRef](#)]

Paper #2

*Physico-Mechanical Properties of Waterlogged Archaeological*

*Wood: The Case of a Charred Medieval Shipwreck*

## Article

# Physico-Mechanical Properties of Waterlogged Archaeological Wood: The Case of a Charred Medieval Shipwreck

Eirini Mitsi <sup>1</sup>, Nikolaos-Alexios Stefanis <sup>2</sup> and Anastasia Pournou <sup>2,\*</sup>

<sup>1</sup> Department of History, Archaeology, and Cultural Resources Management, University of the Peloponnese, 24100 Kalamata, Greece; eir.mitsi@gmail.com

<sup>2</sup> Department of Conservation of Antiquities and Works of Art, University of West Attica, Ag. Spyridonos Str., Aegaleo, 12243 Athens, Greece

\* Correspondence: pournoua@uniwa.gr

**Abstract:** In 2008, a late-12th-century merchant ship was discovered off the commercial port of Rhodes. The vessel caught fire before sinking and thus numerous hull timbers were found charred. Three main degrees of charring have been recorded that presented major chemical differences which indicated different conservation requirements. This study investigated the correlation between the chemistry of the waterlogged timbers and their physico-mechanical properties, to assist in the development of an appropriate conservation strategy. Scanning electron microscopy documented the morphology of charred, semi-charred and uncharred samples. Moisture content and density were measured gravimetrically, while porosity was evaluated using mercury intrusion porosimetry. Hardness was assessed using a modified Janka test and a penetrometer. The results obtained showed that differences in chemistry were highly correlated to the physico-mechanical properties of the timbers. The charred wood presented the lowest moisture content, shrinkage and porosity among the three charring conditions and it also had the highest density, Janka hardness and resistance to penetration. The exact reverse properties were recorded for the uncharred material, which was typical of badly preserved, waterlogged wood. The semi-charred wood presented transitional features. These results indicate that the uncharred wood is in need of consolidation, in contrast to the charred and semi-charred material, which may be left to air-dry untreated.



**Citation:** Mitsi, E.; Stefanis, N.-A.; Pournou, A. Physico-Mechanical Properties of Waterlogged Archaeological Wood: The Case of a Charred Medieval Shipwreck. *Forests* **2023**, *14*, 560. <https://doi.org/10.3390/f14030560>

Academic Editors: Yoon Soo Kim and Adya P. Singh

Received: 15 February 2023

Revised: 9 March 2023

Accepted: 10 March 2023

Published: 12 March 2023



**Copyright:** © 2023 by the authors. Licensee MDPI, Basel, Switzerland. This article is an open access article distributed under the terms and conditions of the Creative Commons Attribution (CC BY) license (<https://creativecommons.org/licenses/by/4.0/>).

**Keywords:** waterlogged wood; charred wood; pyrolysis; thermal degradation; physical properties; porosimetry; Janka hardness; SEM

## 1. Introduction

In 2008, during an underwater survey conducted by the Greek Ephorate of Underwater Antiquities, a late-12th-century merchant ship was discovered off the commercial port of Rhodes, at a depth of ~14 m [1]. Excavation of the shipwreck revealed that the vessel caught fire before sinking, as evidence of burning was recorded on almost every recovered artifact and on numerous construction elements of the ship [1,2].

The excavated elements of the wooden hull presented a varied state of preservation [3,4], as the fire affected differently the degree and depth of wood charring. Thus, coexistence of uncharred, semi-charred and charred wood was often encountered even on the same timber element [3].

This inhomogeneous charring of the wreck is due to several parameters including fire factors, such as the heat flux, temperature and duration [5–11]; the ambient parameters surrounding the wood [5,8,9,12]; and wood variables, such as density, moisture content, permeability, species, size, grain direction and surface protection [5,8,13–15], which also influence the charring rate and depth.

Chemical analysis conducted by Mitsi et al. [4] on the main three charring conditions of the timbers, demonstrated that the charred areas are chemically similar to charcoals, semi-charred parts to thermally modified wood and the uncharred material to biodeteriorated

waterlogged wood. Furthermore, Mitsi et al. [4] showed that in charred areas opposed to uncharred ones, elements such as sulfur, iron and oxygen decrease, while carbon increases.

This dissimilar chemistry of the material is principally due to differing exposure to the fire, which, in addition to the chemistry, is likely to have affected the structure and properties of the wood [7,16–18]. Therefore, it is anticipated that the three main charring conditions identified on the Rhodes shipwreck will also present dissimilar physical and mechanical properties and consequently will have quite different conservation requirements.

This study was set up to investigate the physico-mechanical properties of the Rhodes shipwreck timbers in order to further assess their degree of degradation and contribute to the development of a successful conservation strategy.

## 2. Materials and Methods

The waterlogged wood examined in this study came from one frame of the Rhodes wreck, which was made of *Pinus halepensis* Mill. (Aleppo pine) or *Pinus brutia* Ten. (Turkish pine) [1]. The outer layer of the frame was charred, the inner core was uncharred and in between there was a semi-charred zone. The part of the frame used (Figure 1) measured  $\sim 9$  cm  $\varnothing \times 15$  cm length. It was retrieved in 2013 and since then it had been kept waterlogged at 5 °C. Samples produced corresponded to sapwood and represented the three main charring conditions.

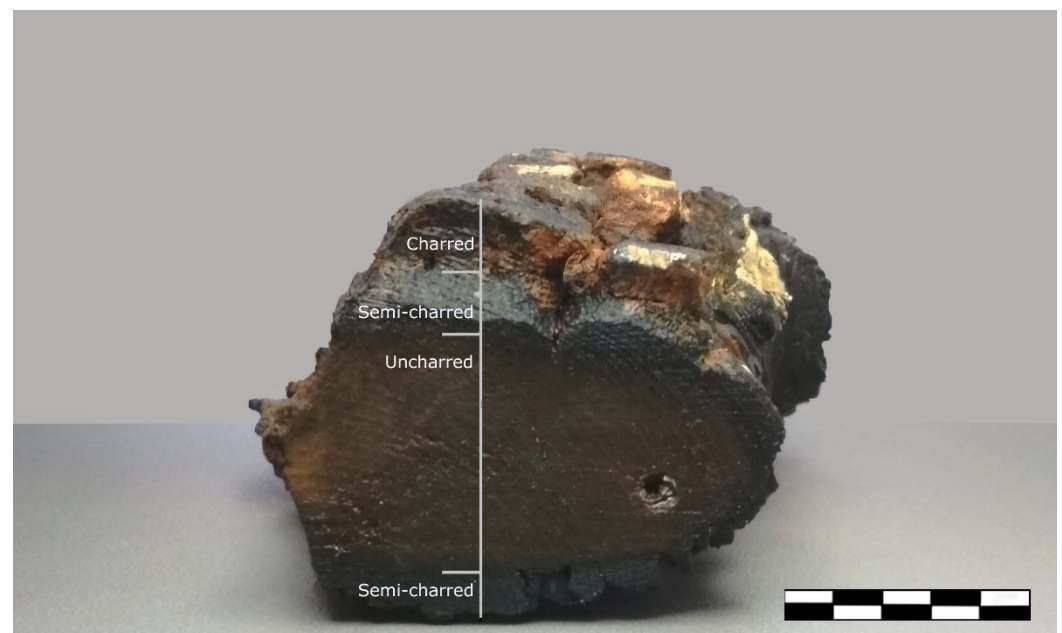


**Figure 1.** The frame part used, presenting an outer charred layer, an uncharred inner core and a semi-charred zone in between.

### 2.1. Morphological Alterations at a Cellular Level Scanning Electron Microscopy (SEM)

Uncharred and semi-charred waterlogged wood was cut into samples measuring  $\sim 0.2$  cm  $\times$  0.2 cm  $\times$  0.3 cm using a double-edged razor blade, whereas charred wood was fractured to produce samples of the same dimensions. Four samples per plane of each charring condition were investigated. All samples were dehydrated in a series of ethanol solutions of increasing concentrations until water-free alcohol was acquired and then left to air-dry in a desiccator. They were then mounted on aluminum stubs using a double-sided carbon conductive tape, gold-coated in a sputter coater (Polaron SC7640) and examined at an acceleration voltage of 20 kV under low vacuum (33 Pa) using a JEOL JSM-6510LV scanning electron microscope.

## 2.2. Physical Properties

### 2.2.1. Moisture Content, Density and Shrinkage Determination

Waterlogged samples,  $\sim 2 \text{ cm} \times 2 \text{ cm} \times 2 \text{ cm}$  (tangential (T)  $\times$  radial (R)  $\times$  longitudinal (L)), of uncharred, semi-charred and charred wood were used for the determination of moisture content, density and shrinkage.

For the moisture content (MC), samples were weighed in their waterlogged state and oven-dried at  $103 \pm 2 \text{ }^\circ\text{C}$  to constant weight [19]. The MC was calculated based on Equation (1) [20].

For the equilibrium moisture content (EMC), the waterlogged samples were air-dried at  $21 \pm 2 \text{ }^\circ\text{C}$  and  $45 \pm 5\% \text{ RH}$  until they reached equilibrium. The EMC was then calculated based on Equation (2) [21].

The basic density (Rg) of the material was calculated according to Equation (3) [21], based on its constant oven-dry weight, at  $103 \pm 2 \text{ }^\circ\text{C}$ , and its waterlogged volume, recorded by water displacement [19]. Relative density (rRg) was estimated based on the weight in air and in water of the waterlogged material according to Equation (4) [22].

For measuring shrinkage, stainless steel insect pins were placed on the transverse plane to mark the tangential and radial direction, and the distance between the pins was recorded with a Vernier caliper (0.02 mm). Samples were then air-dried to constant weight at  $21 \pm 2 \text{ }^\circ\text{C}$  and  $45 \pm 5\% \text{ RH}$ , and the distance between the pins was measured again. The cross-sectional shrinkage ( $\beta_{\text{cross}}$ ) was estimated by summing the tangential and radial shrinkage ( $\beta$ ), which had been calculated with Equation (5) [23]. It has to be noted that shrinkage in this study refers to the total reduction of dimensions measured upon air-drying, which includes both cell collapse and cell wall shrinkage.

For evaluating the above-mentioned physical properties, four replicates of each charring condition were used.

$$\text{MC (\%)} = [(W_W - W_{\text{OD}})/W_{\text{OD}}] \times 100 \quad (1)$$

where MC = moisture content,  $W_W$  = waterlogged weight and  $W_{\text{OD}}$  = oven-dry weight at  $102 \pm 3 \text{ }^\circ\text{C}$  after three consecutive constant measurements.

$$\text{EMC (\%)} = [(W_{\text{AD}} - W_{\text{OD}})/W_{\text{OD}}] \times 100 \quad (2)$$

where EMC = equilibrium moisture content,  $W_{\text{AD}}$  = air-dried weight at  $21 \pm 2 \text{ }^\circ\text{C}$  and  $45 \pm 5\% \text{ RH}$  after three consecutive constant measurements and  $W_{\text{OD}}$  = oven-dry weight at  $102 \pm 3 \text{ }^\circ\text{C}$  after three consecutive constant measurements.

$$\text{Rg (g/cm}^3\text{)} = W_{\text{OD}}/V \quad (3)$$

where Rg = basic density,  $W_{\text{OD}}$  = oven-dry weight at  $102 \pm 3 \text{ }^\circ\text{C}$  after three consecutive constant measurements and  $V$  = waterlogged volume measured by water displacement.

$$\text{rRg} = 3 \times W_{\text{sub}}/(W_{\text{air}} - W_{\text{sub}}) \quad (4)$$

where rRg = relative density,  $W_{\text{sub}}$  = waterlogged weight in water and  $W_{\text{air}}$  = waterlogged weight in air.

$$\beta (\%) = [(l_W - l_{\text{AD}})/l_W] \times 100 \quad (5)$$

where  $\beta$  = shrinkage,  $l_W$  = waterlogged distance between pins and  $l_{\text{AD}}$  = air-dried distance.

Shrinkage was calculated for the tangential ( $\beta_t$ ), and for the radial ( $\beta_r$ ) direction; for the cross-sectional shrinkage ( $\beta_{\text{cross}}$ ), the sum,  $\beta_t + \beta_r$ , was calculated.

### 2.2.2. Mercury Intrusion Porosimetry (MIP)

Mercury intrusion porosimetry (MIP) was carried out with a Quantachrome PoreMaster 60 on uncharred, semi-charred and charred samples. The archaeological samples of the three charring conditions, measuring approximately  $0.5 \text{ cm} \times 0.5 \text{ cm} \times 0.5 \text{ cm}$  (T  $\times$  R  $\times$  L),

were freeze-dried prior to porosity measurements. This was decided to maintain as much as possible the “original” waterlogged pore structure, as air drying would greatly affect the wood porosity due to collapse and shrinkage. Reference samples of *P. halepensis* and *P. brutia* of the same dimensions were also examined. All samples were stored in a desiccator prior to porosity measurements. Low pressure was first applied at 50 MPa and then samples were placed in the high-pressure station, where pressure up to 400 MPa was employed in equilibration time of 10 s. Surface tension and mercury wetting angle were set at  $0.485 \text{ Nm}^{-1}$  and  $140^\circ$ , respectively.

### 2.3. Mechanical Properties

#### 2.3.1. Janka Hardness Test

The methods commonly used for assessing the “surface” hardness (< 1 cm) of wood and especially of thermally-modified wood, are the “Brinell” and the “Janka”, which are force- and depth-controlled ball tests, respectively [24–30]. The Brinell test was found inappropriate for the material under investigation as the same force could not produce measurable indentations for all three charring conditions. Therefore, a Janka test was adopted in order to investigate differences in the “surface” hardness for uncharred, semi-charred and charred material.

The Janka hardness test was implemented based on the ASTM D143 [31] and the ASTM D1037 [32], with a modification on the ball diameter, using a 2.5 mm ball instead of the standard 11.3 mm, due to the limited size of the available archaeological material. The test was conducted on an Instron 3367 dual-column universal testing machine, with a 2 kN load cell and compression platens of 100 kN maximum load on upper and lower connections. On the upper platen, the 2.5 mm ball was adjusted using a cylindrical neodymium magnet (outer  $\varnothing$ : 0.8 mm, inner  $\varnothing$ : 1.9 mm) of 0.6 mm length. The test speed was set at 0.1 mm/s rate and a 0.62 mm extension was selected to achieve a final ball penetration into the specimen equal to  $\sim \frac{1}{4}$  of the ball diameter (D). The load-extension data were recorded per 0.1 s with Bluehill 3 software.

A hardness test was conducted for all three charring conditions and on reference samples of sound *P. halepensis* and *P. brutia* for comparison. Measurements were conducted on end grain and at both radial and tangential planes. The use of the 2.5 mm ball on the sound reference samples allowed documentation of differences between earlywood and latewood, and thus, two replicate measurements were taken per growing period and their average was calculated for each plane. Two samples from each charring condition were examined. Uncharred and charred samples measured  $\sim 2 \text{ cm} \times 2 \text{ cm} \times 2 \text{ cm}$  (T  $\times$  R  $\times$  L), whereas the semi-charred measured  $\sim 2 \text{ cm} \times 1.5 \text{ cm} \times 2 \text{ cm}$  (T  $\times$  R  $\times$  L). For every condition, one sample was tested at the waterlogged state to acquire knowledge on the handling of the material before and during conservation and a second one at the freeze-dried state to assess the residual hardness of the material without bias by the water presence. Earlywood and latewood were rarely distinguishable in the archaeological material; thus, two replicate measurements were taken per plane.

Hardness is expressed as the ratio of the applied force to the projected area of contact and it was calculated based on Equation (6) [33]. The projected contact area is treated as the area of a circle created by the ball indenter at the wood surface, and as is typical in the Janka test, the ball is pressed into half of its diameter [31,34]; the radius of the projected area (r) equals the radius of the indenter (R). In the modified Janka test used, the ball was pushed to a depth of  $\frac{1}{4}$  of the ball’s diameter (Figure 2a), because beyond this limit many of the charred wood samples cracked or/and failed. As the r value is lower than ball radius (Figure 2b), the radius of the projected contact area was geometrically calculated based on the scheme of Figure 2b and Pythagoras’ theorem.

$$\text{Hardness} = F/\pi r^2 \quad (6)$$

where F = the force recorded at 0.62 extension,  $\pi$  = the mathematical constant ( $\sim 3.14159$ ) and r = the radius of the projected contact area.

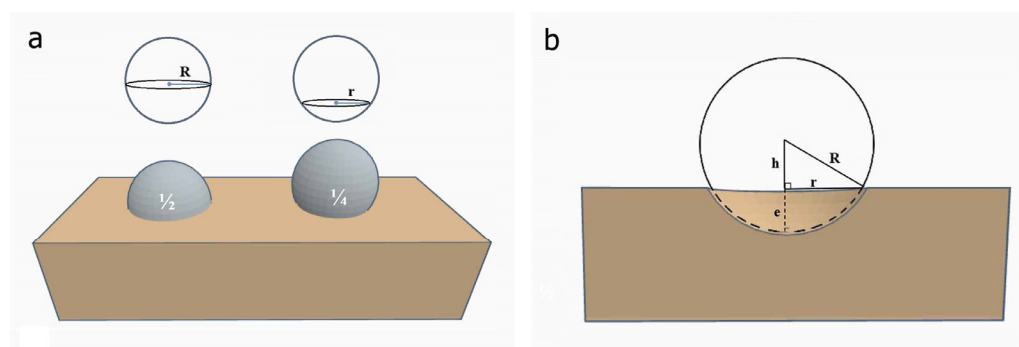


**Figure 2.** (a) Graphic representation of the ball penetrated into a depth of  $\frac{1}{2}$  and  $\frac{1}{4}$  of its diameter, and (b) the radius ( $r$ ) of projected contact area that based on Pythagoras' theorem is equal to  $r = \sqrt{(R^2 - h^2)}$ , where  $R$  = ball radius,  $h = R - e$ , and  $e$  = extension recorded by Instron.

### 2.3.2. Penetrometer

For assessing the state of preservation of waterlogged archaeological wood, conservators often use the “pin test” [35–39]. This type of manual evaluation is rather subjective; therefore, wood resistance to penetration can be measured with penetrometers instead [40]. These instruments using a minimally invasive procedure can in situ assess the hardness of a material at a given depth and can also indirectly assess its density. In this work, a penetrometer was used for assessing differences in resistance to penetration of the three charring conditions.

Resistance to penetration was recorded on the part of the shipwreck frame (~9 cm  $\varnothing$ , 15 cm length) which included all three charring conditions. A Fruit Hardness Tester, FR- 5105, with a maximum load capacity up to 5000 g was used. The penetrometer was equipped with a needle of 3 cm length and 0.75 mm diameter, of which 1 cm was fasten inside a custom-made holder in order to allow penetration at a constant depth of 2 cm. Six measurements per condition were recorded using the “peak hold” mode on the transverse section of the part, as this was the only section where all charring zones were visible, accessible and could allow discrete penetration into each zone at the same depth without bias.

## 3. Results and Discussion

### 3.1. Morphological Alterations at a Cellular Level

#### Scanning Electron Microscopy (SEM)

The morphology of the archaeological wood observed with SEM demonstrated the existence of three distinctly dissimilar materials, the uncharred (Figure 3a–c), the semi-charred (Figure 3d–f) and the charred wood (Figure 3g–i). Uncharred waterlogged wood appeared to be severely deteriorated as cells were deformed, while their secondary wall layer presented a granular texture and was commonly detached from the middle lamellae (Figure 3a). In addition, in both tangential (Figure 3b) and radial (Figure 3c) sections, extensive biodeterioration was documented, caused by marine fungi and bacteria, based on the recorded decay patterns [41].

The semi-charred wood was found to be rather intact. Cells appeared to retain their structural integrity and no deformation in their general anatomy was observed (Figure 3d). Cell wall layers were discrete and detachment fissures alongside the middle lamella were rarely detected (Figure 3d). Occasionally, and mostly in longitudinal sections patterns attributed to bacterial and fungal decay were detected (Figure 3e,f).

The differences in the degree of deterioration between uncharred and semi-charred wood are probably because ‘thermal modification’ of the latter rendered the material less prone to biodeterioration by soft rotters [42,43].



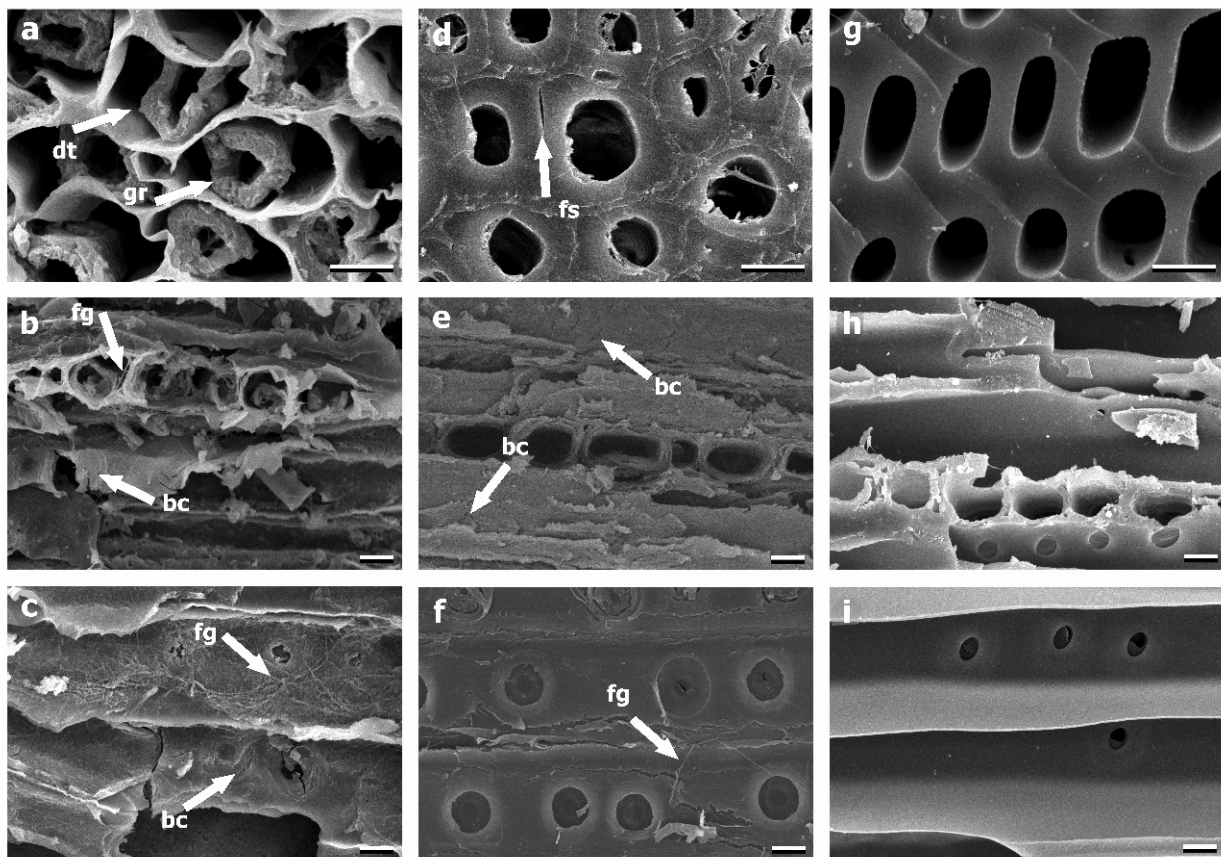


**Figure 3.** SEM micrographs of uncharred, semi-charred and charred wood. Uncharred material (a–c) presented a granular texture (gr) of the secondary cell walls, which were often detached (dt) from the middle lamellae; semi-charred wood (d–f) showed intact cell walls with rare detachment fissures (fs); and charred wood (g–i) presented a vitreous appearance without evident biodeterioration signs. On both uncharred (b,c) and semi-charred (e,f) material, biodeterioration patterns caused by bacteria (bc) and fungi (fg) were recognized. All bars are 10 µm.

Lastly, the morphological features observed in charred wood differed greatly from both the uncharred and the semi-charred material. The wood appeared “vitreous” with no signs of deterioration caused by fungi or bacteria (Figure 3g–i). The latter was anticipated, as due to charring most of the organic part of the material had been depleted and thus during burial very few organisms could utilize it. In the transverse section (Figure 3g), cells were slightly distorted possibly indicating fast combustion of wet wood at high temperatures [44]. The middle lamellae appeared to coalesce with the secondary cell walls, a feature that is commonly reported in charred wood [44–50]. This coalescence, also referred to as amalgamation, has been reported to initiate at approximately 300 °C [46,51]. The amalgamation temperature of the material investigated cannot be defined with certainty as it depends on several factors [45–47], nonetheless, it can be safely stated that the charred wood examined has been subjected to temperature  $\geq 300$  °C. Furthermore, as this feature was absent in the semi-charred material, it could be hypothesized that the exposure temperature was  $<300$  °C, an assumption which is in accordance with its chemical profile studied by Mitsi et al. [4].

### 3.2. Physical Properties

#### 3.2.1. Moisture Content, Density and Shrinkage Determination

Results for the physical properties of the archaeological material are presented in Figure 4 and Table 1 along with reference values of sound *P. brutia* and *P. halepensis*.

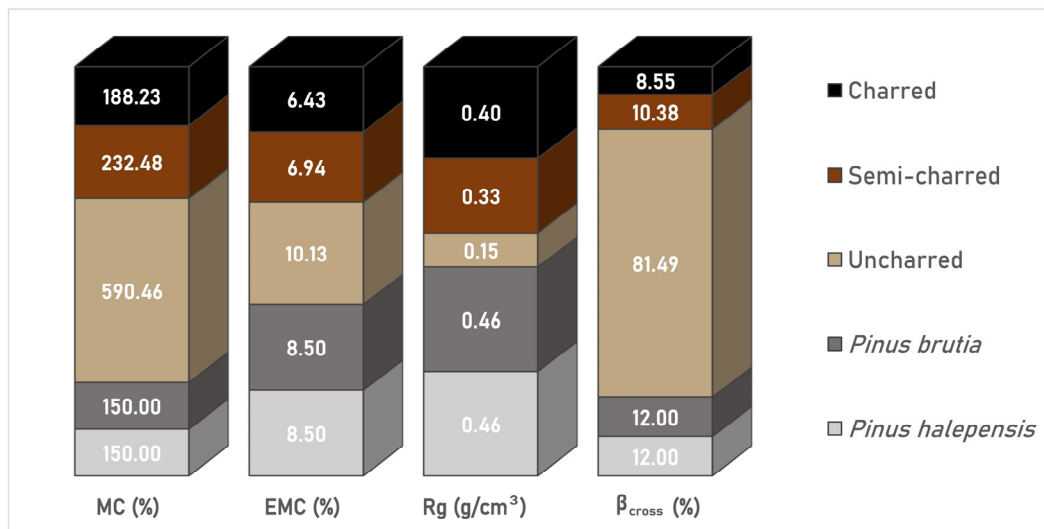


**Figure 4.** Moisture content (MC), equilibrium moisture content (EMC), basic density (Rg) and cross shrinkage ( $\beta_{cross}$ ) values recorded for uncharred, semi-charred and charred archaeological material, juxtaposed to controls of *P. brutia* and *P. halepensis*.

**Table 1.** Moisture content (MC), equilibrium moisture content (EMC), relative density (rRg), basic density (Rg) and cross shrinkage ( $\beta_{cross}$ ) recorded on the archaeological wood and the reference sound wood of *P. brutia* and *P. halepensis*. Values for the archaeological samples are the averages of four replicates. Values in brackets represent the standard deviation.

Samples	MC (%)	EMC (%)	rRg	Rg (g/cm <sup>3</sup> )	$\beta_{cross}$ (%)
Uncharred	590.46 ( $\pm 28.33$ )	10.13 ( $\pm 0.58$ )	0.19 ( $\pm 0.02$ )	0.15 ( $\pm 0.01$ )	81.49 ( $\pm 0.15$ )
Semi-charred	232.48 ( $\pm 20.58$ )	6.94 ( $\pm 1.88$ )	0.31 ( $\pm 0.02$ )	0.33 ( $\pm 0.02$ )	10.38 ( $\pm 0.33$ )
Charred	188.23 ( $\pm 24.80$ )	6.43 ( $\pm 0.47$ )	0.38 ( $\pm 0.02$ )	0.40 ( $\pm 0.04$ )	8.55 ( $\pm 0.40$ )
<i>Pinus brutia</i>	150.00 <sup>a</sup>	8.00–9.00 <sup>b</sup>	-	0.46 <sup>c</sup>	12.00 <sup>d</sup>
<i>Pinus halepensis</i>	150.00 <sup>a</sup>	8.00–9.00 <sup>b</sup>	-	0.46 <sup>c</sup>	12.00 <sup>d</sup>

$$^a U_{max} = [(1/Rg) - 0.67] \times 100 [23]; ^b [52]; ^c [53]; ^d [54].$$

The MC of uncharred, semi-charred and charred wood (Table 1) confirmed the waterlogged nature of the material. Furthermore, the values of uncharred wood (590%) were indicative of a highly degraded material [37,55–57]. The values of the semi-charred (232.48%) and the charred wood (188.23%) were lower in comparison to the uncharred material, suggesting that their different exposure to heat had influenced their water holding capacity. More specifically for the semi charred material, the lower MC may partially be attributed to the reduction of hemicelluloses caused by its thermal degradation [4], as the hygroscopicity of wet wood subjected to heat-treatment may be irreversibly reduced [58–61]. Similarly, for the charred material the reduced moisture uptake could be also attributed to the physicochemical alterations caused by the pyrolytic process [62–65].

The equilibrium moisture content (EMC) of the uncharred archaeological wood, at  $45 \pm 5\%$  RH, was slightly higher compared to the reference samples. In contrast the EMC of both the semi-charred and charred wood was lower than reference samples (Figure 4). High EMC values have been frequently reported for degraded waterlogged archaeological wood [66–71]. This can be justified by the increased cell wall porosity caused by the action of microorganisms, which increases the bound water of wood [68–70] and consequently the measured values of the “fiber saturation point” (FSP) of waterlogged wood [70]. Furthermore, the small cellulose crystallite length of the material [4] could also be related to a greater availability of sorption sites and thus to the higher EMC values [68,69].

For the semi-charred and charred wood, the reduction of EMC recorded is in line with the reduced water holding capacity of wood exposed to temperatures up to 300 °C [17,72–79]

and above 300 °C [75]. This could be due to the depletion of hemicelluloses, either by biodeterioration in the marine environment [41] or by the heat exposure [17,80], which is negatively correlated to wood EMC as a function of both temperature and duration [72–74,77,81,82]. Nonetheless, it has been shown in heat-treated wood that the EMC reduction is owed to additional mechanisms in addition to the reduced accessibility of OH groups in the cell wall matrix [59,60,83].

Basic density (Rg) values (Table 1) were found to be very low for the uncharred waterlogged samples due to degradation in the marine environment [20,57,66,84]. As anticipated, Rg was also negatively correlated to the MC [36,57,70]. The Rg values of the semi-charred and charred samples were also lower than the references, which is considered to be due principally to the thermal decomposition of the materials at elevated temperatures [27,73,85–88] and to a lesser extent to biodeterioration.

The non-destructive determination of relative density (rRg) gave similar results to the basic density (Rg) for all three charring conditions, and demonstrated that it can be successfully adopted in cases where the oven-dried weight cannot be measured.

Cross shrinkage ( $\beta_{\text{cross}}$ ) values for the uncharred waterlogged wood were extremely high (Figure 4), as expected, and negatively correlated with basic density [20,66,84,89]. The same correlation was also recorded for the semi-charred and charred material (Figure 4). However, their shrinkage values were found to be much lower than the uncharred wood values, and to be even lower than the sound reference wood values. This dimensional behavior of the semi-charred wood is more likely to be associated with the low MC of the material that has resulted from thermal degradation.

The results on shrinkage indicate that the semi-charred and charred areas of the wreck are dimensionally stable upon drying, an outcome that should be seriously considered in the conservation strategy of the shipwreck timbers.

### 3.2.2. Mercury Intrusion Porosimetry (MIP)

The pore size distribution recorded according to the IUPAC classification [90] indicates two size classes of pores: the macropores with diameter > 50 nm, ( $r > 25$  nm) and the mesopores with diameters from 2 nm to 50 nm ( $1 \text{ nm} < r < 25$  nm) (Figure 5). Nonetheless, in wood science the pore size distribution is often categorized in relation to wood structure [91–94]. Therefore, for the softwoods investigated, an anatomy-based categorization has been adopted with three classes (Figure 5): the macrovoids that include the lumen of tracheids and of resin canals with radii ranging from 5  $\mu\text{m}$  to ~200  $\mu\text{m}$ ; the microvoids that encompass pit apertures, pit chambers and other small voids with radii from 5 nm to ~5  $\mu\text{m}$ ; and the nanovoids that comprise the cell wall porosity with radii < 5 nm [91,95].

Based on the obtained histograms, it is apparent that the pore size distribution among the archaeological wood and the reference *P. brutia* and *P. halepensis* differs considerably (Figure 5). The porosity of reference samples is mainly represented by microvoids, and to a much lesser extent by macrovoids and nanovoids. In contrast, in archaeological wood macrovoids prevailed noticeably as the porosity showed to be shifted towards pores > 1  $\mu\text{m}$  (dashed line). This shifting of the archaeological wood porosity was to be anticipated, as both charring [49,96,97] and biodeterioration in the marine environment may increase wood porosity and permeability [20,37,57,68,70,98].

More specifically, the increased porosity in charred wood is considered to have occurred due to pyrolytic process [49,96,97], where the main volume of macrovoids with radii > 5  $\mu\text{m}$  was created (Figure 5).

Similarly, in the semi-charred material the porosity increase may also be due to the heat exposure, as upon thermal modification the porosity augments as a function of temperature [99,100]. Nonetheless, as most of the organic moieties of the semi-charred wood were shown to be preserved [4], the material was still susceptible to biodeterioration by microorganisms, and it is very likely that its porosity was further increased during burial. Information on thermally modified wood performance against marine fungi and bacteria is scarce [17,101]; however, there are some studies demonstrating that thermal

modification could make wood more resistant to terrestrial soft rot fungi [42,43]. This could probably explain why the porosity of the semi-charred wood was lower compared to the uncharred material.

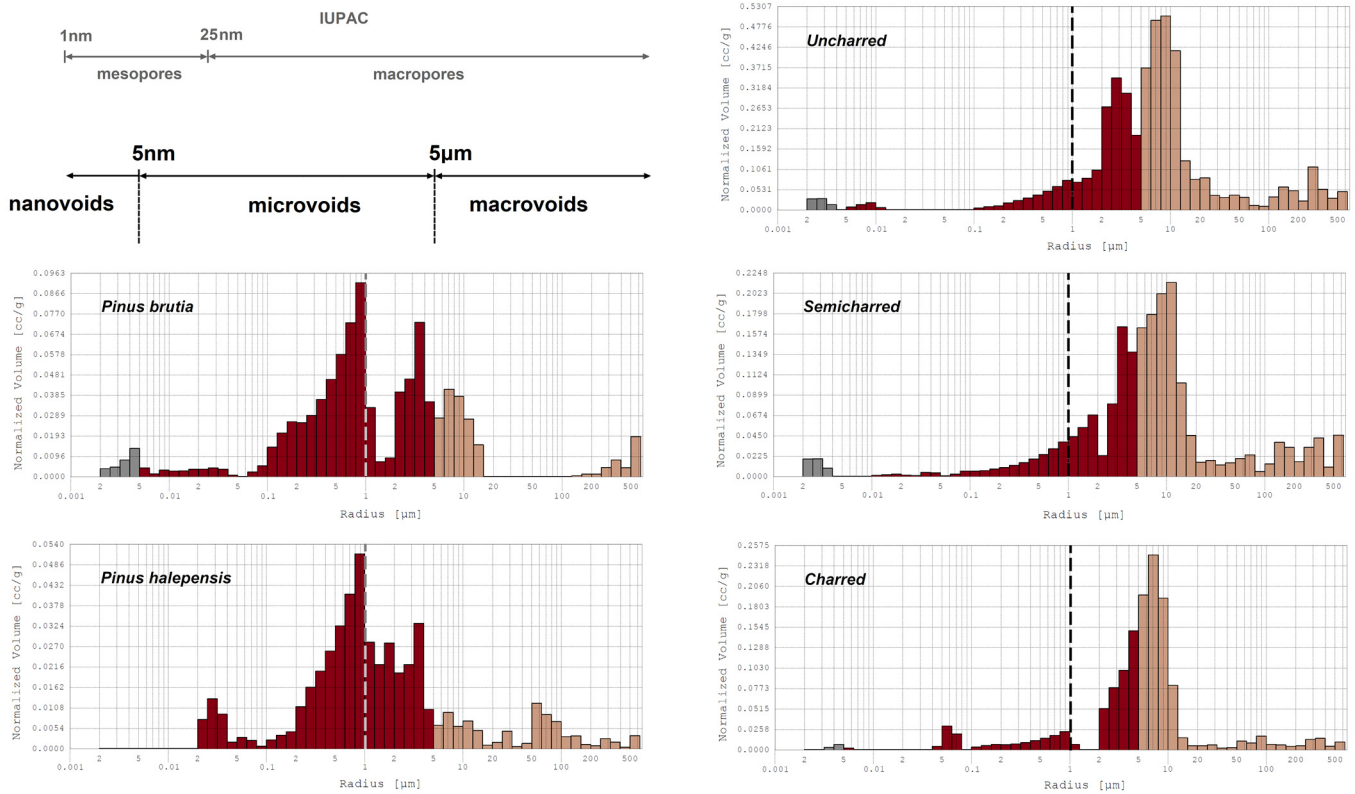


**Figure 5.** Histograms of intruded pore volume as a function of the pore radius of controls (*P. brutia* and *P. halepensis*) and archaeological wood (uncharred, semi-charred and charred).

Lastly, uncharred material presented the highest porosity recorded. As mentioned earlier, this was principally due to biodeterioration, as evident from SEM examination. Furthermore, its porosity was slightly higher than the semi-charred material and much higher in comparison to the charred wood, which had the smallest number of large pores, located mostly at the narrow range of 5 to 15  $\mu\text{m}$ .

Porosity differences among the three charring conditions were also demonstrated with the pore size distribution curves as a function of the intruded volume (Figure 6). In these curves it became clear that the porosity of all three charring conditions increased compared to the reference samples of *P. halepensis* (0.50 cc/g) and *P. brutia* (0.92 cc/g). Furthermore, differences among the three charring conditions were again evident as the uncharred wood showed the highest intruded Hg volume (4.45 cc/g) compared to the semi-charred (2.05 cc/g) and the charred wood (1.40 cc/g).

The porosity of all three charring conditions, as anticipated, was inversely correlated with the basic density values recorded, as the denser a material, the less likely there will be voids present within.

Based on these results, and the fact that porosity greatly affects the impregnation rate [98] and the polymer retention during wood treatments, especially inside pores with diameters  $> 0.1 \mu\text{m}$  [102], it is expected that uncharred archaeological wood will be permeable and thus it will promote diffusion and allow a successful consolidation. In contrast, it is considered that the charred material will be resistant to diffusion even by low molecular weight polymers.

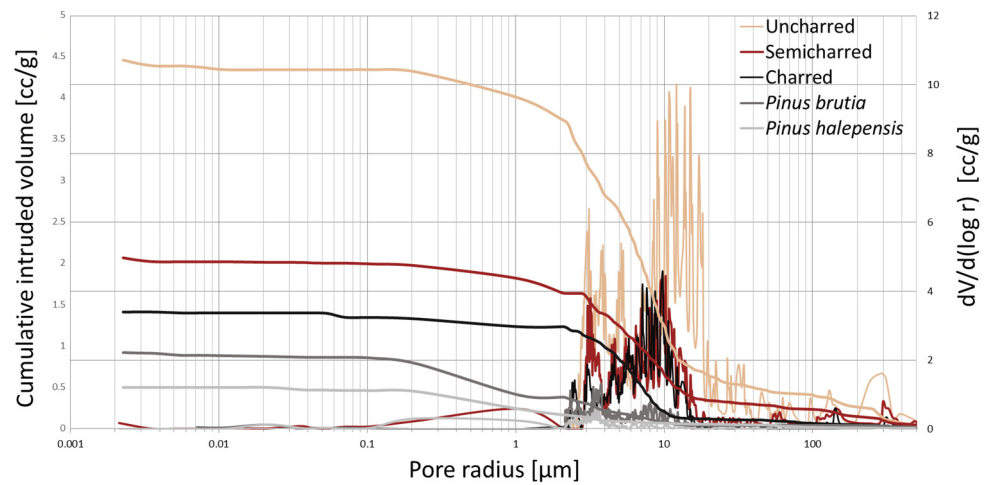


**Figure 6.** Differential pore-size distribution curves and cumulative intrusion curves of controls (*P. brutia* and *P. halepensis*) and the three conditions of the archaeological wood (uncharred, semi-charred and charred).

### 3.3. Mechanical Properties

#### 3.3.1. Janka Hardness Test

Results obtained by employing the modified Janka test on the shipwreck material showed that the hardness of archaeological wood was considerably lower compared to the reference samples of *P. halepensis* and *P. brutia* (Figure 7, Table 2). This was rather justified as low hardness has been reported for deteriorated waterlogged archaeological wood [66] and because thermal exposure can also reduce hardness [24,27,73,77,86–88,103].

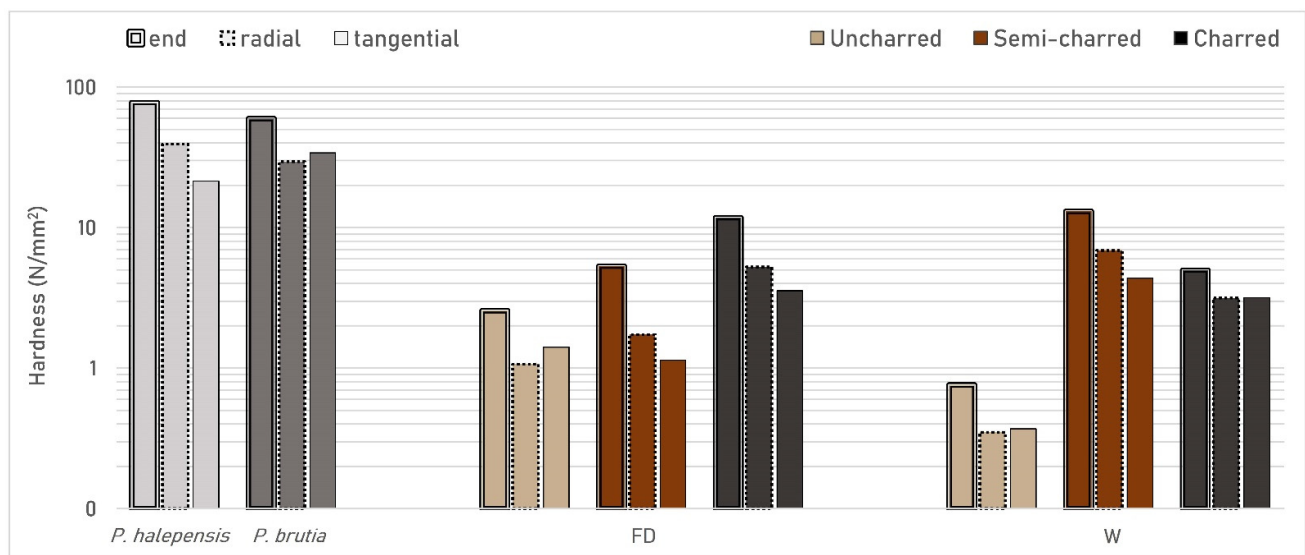


**Figure 7.** End and side (radial and tangential) hardness of the archaeological wood at the freeze-dried (FD) and at the waterlogged (W) state in comparison to the hardness of sound *P. brutia* and *P. halepensis*, of which earlywood-latewood values were averaged.

**Table 2.** Hardness values obtained with the modified Janka test. Values for sound *P. brutia* and *P. halepensis* are the average of four replicates. For the archaeological material, two replicates were used (\* a single value due to material's failure). Values in brackets represent standard deviation.

Hardness (N/mm <sup>2</sup> )		End	Radial	Tangential
<i>Pinus halepensis</i>		77.68 (±21.02)	39.33 (±17.10)	21.43 (±6.59)
<i>Pinus brutia</i>		59.76 (±26.02)	29.53 (±16.32)	34.09 (±16.00)
Uncharred	FD	2.57 (±0.87)	1.07 (±0.26)	1.41 (±0.07)
	W	0.76 (±0.18)	0.35 (±0.02)	0.37 (±0.00)
Semi-charred	FD	5.32 (±1.02)	1.73 (±0.13)	1.14 (±0.20)
	W	13.06 (±3.18)	6.86 (±4.09)	4.37 (±0.04)
Charred	FD	11.76 *	5.25 (±1.44)	3.55 (±0.01)
	W	4.98 (±3.46)	3.16 (±1.15)	3.17 (±1.07)

The hardness values obtained among the three charring conditions varied as well (Figure 7). At the freeze-dried state, charred wood presented the highest hardness value, uncharred demonstrated the lowest and the semi-charred demonstrated an intermediate hardness. In contrast, at the waterlogged state, the hardness of the semi-charred material was the highest among the three charring conditions, followed by the charred and the uncharred material, which was again the lowest recorded.

The higher hardness of the semi-charred material compared to the charred could be also attributed to the different exposure of the materials to heat (temperature and duration), which may affect greatly the mechanical properties of the wood [73,88]. Wood subjected to thermal modification at temperatures from 180 to 250 °C can demonstrate lower hardness than unheated wood [24,27,73,77,88], and as above 250 °C the material is thermally degraded rather than modified [60], wood exposed to temperatures above 300 °C also presents a conspicuous decrease in hardness [86,87,103].

The hardness values recorded for the semi-charred material deviated between the two states (dry and waterlogged). This can be attributed to the transitional nature of the semi-charred material itself. The resolution of the hardness test applied (~1 mm indentation) could demonstrate small hardness differences in respect to its thermal degradation, and thus, values varied depending on how far the area tested was from the fire front. Thus, it is quite possible that for the freeze-dried sample, measurements were taken towards the uncharred decayed zone, whereas in the waterlogged sample towards the charred zone.

Lastly it should be noted that the high standard deviation values recorded for the reference samples (Table 2) demonstrate differences between earlywood (EW) and latewood (LW) [104–106].

### 3.3.2. Penetrometer

Results obtained with the fruit penetrometer for the three charring conditions are graphically presented in Figure 8. Uncharred wood demonstrated the lowest resistance to penetration (430–699 g), semi-charred wood presented almost a double increase in resistance (903–1156 g), whereas charred wood demonstrated the highest resistance (1147–1452 g). However, it should be noted that although a full-length penetration (2 cm) was attempted, the final penetration depth was not the same for all charring conditions. Uncharred wood allowed a 2 cm depth penetration, the semi-charred a partial penetration (~0.5–1 cm), whereas the charred wood allowed only a superficial penetration (~0–0.3 cm). Hence, results cannot be interpreted as hardness values as in hardness tests either the force [28] or the penetration depth [21,28] must be kept constant.



#### 4. Conclusions

This study demonstrated that the physico-mechanical properties of the Rhodes shipwreck timbers varied greatly among the three charring conditions, and they were correlated to the residual chemistry of the wood.

The uncharred material showed typical physical properties of severely deteriorated waterlogged wood. It presented the highest moisture content and shrinkage and the lowest density among the other conditions. Its low hardness and resistance to penetration along with its increased porosity indicates that remedial conservation with a consolidation agent is required.

Charred wood, in contrast, presented the lowest moisture content and shrinkage and the highest density and resistance to penetration among the three charring conditions. It also showed the lowest porosity, suggesting low permeability and thus resistance to consolidation via diffusion. Nonetheless, based on the negligible shrinkage values, it is anticipated that the material may be safely air-dried without treatment.

The semi-charred wood was shown to be a transitional zone between the charred and the uncharred material, and thus, it predictably demonstrated intermediate values for almost all physico-mechanical properties investigated in respect to uncharred and charred material. Regarding its conservation requirements, it is possible that the material can be air-dried untreated, nonetheless further research is considered necessary due to its transitional nature.

Lastly, it became apparent that the most problematic timbers of the shipwreck are those where all three charring conditions coexist. For these timbers, the consolidation of the inner uncharred core will be rather problematic as the outer charred layer is expected to restrain the diffusion of even low molecular weight consolidants.

**Author Contributions:** Conceptualization, A.P.; methodology, A.P. and E.M.; investigation, E.M.; data curation, A.P., E.M. and N.-A.S.; writing—original draft preparation, A.P. and E.M.; writing—review and editing, A.P. and E.M.; supervision, A.P. All authors have read and agreed to the published version of the manuscript.

**Funding:** This research received no external funding.

**Institutional Review Board Statement:** Not applicable.

**Data Availability Statement:** Not applicable.

**Acknowledgments:** The authors would like to thank G. Koutsouflakis, for providing the archaeological material and A. Karampotsos for his technical support with the SEM.

**Conflicts of Interest:** The authors declare no conflict of interest.

#### References

1. Koutsouflakis, G.; Rieth, E. A Late-12th-Century Byzantine Shipwreck in the Port of Rhodes A Preliminary Report. In *Under the Mediterranean I: Studies in Maritime Archaeology*; Demesticha, S., Blue, L., Eds.; Sidestone Press: Leiden, The Netherlands, 2021; ISBN 9789088909450.
2. Koutsouflakis, G. Three Shipwrecks of the Medieval Era in the Commercial Port of Rhodes. In Proceedings of the Archeological Work in Aegean Islands, Rhodes, Greece, 27 November–1 December 2013; Britachta, K., Triantafyllidis, P., Sarantidis, K., Eds.; General Secretariat of the Aegean and Islands Policy of the Greek Ministry of Culture and Sports: Lesvos, Greece, 2017; pp. 477–500.
3. Mitsi, E.; Pournou, A. Conserving a Charred Medieval Shipwreck: A Preliminary Study. In Proceedings of the 14th ICOM-CC on Wet Organic Archaeological Materials Conference, Portsmouth, UK, 20–24 May 2019.
4. Mitsi, E.; Boyatzis, S.; Pournou, A. Chemical Characterization of Waterlogged Charred Wood: The Case of a Medieval Shipwreck. *Forests* **2021**, *12*, 1594. [[CrossRef](#)]
5. Mikkola, E. Charring Of Wood Based Materials. *Fire Saf. Sci.* **1991**, *3*, 547–556. [[CrossRef](#)]
6. Guo, Y.; Bustin, R.M. FTIR Spectroscopy and Reflectance of Modern Charcoals and Fungal Decayed Woods: Implications for Studies of Inertinite in Coals. *Int. J. Coal Geol.* **1998**, *37*, 29–53. [[CrossRef](#)]
7. White, R.H.; Dietsenberger, M. Wood Products: Thermal Degradation and Fire. In *Encyclopedia of Materials: Science and Technology*; Pergamon: Oxford, UK, 2001; pp. 9712–9716.



8. Friquin, K.L. Material Properties and External Factors Influencing the Charring Rate of Solid Wood and Glue-Laminated Timber. *Fire Mater.* **2011**, *35*, 303–327. [[CrossRef](#)]
9. Bartlett, A.I.; Hadden, R.M.; Bisby, L.A. A Review of Factors Affecting the Burning Behaviour of Wood for Application to Tall Timber Construction. *Fire Technol.* **2019**, *55*, 1–49. [[CrossRef](#)]
10. Hao, H.; Chow, C.L.; Lau, D. Effect of Heat Flux on Combustion of Different Wood Species. *Fuel* **2020**, *278*, 118325. [[CrossRef](#)]
11. Constantine, M.; Mooney, S.; Hibbert, B.; Marjo, C.; Bird, M.; Cohen, T.; Forbes, M.; Mcbeath, A.; Rich, A.; Stride, J. Using Charcoal, ATR FTIR and Chemometrics to Model the Intensity of Pyrolysis: Exploratory Steps towards Characterising Fire Events. *Sci. Total Environ.* **2021**, *783*, 147052. [[CrossRef](#)]
12. Liu, Q.; Wang, S.R.; Fang, M.X.; Luo, Z.Y.; Cen, K.F.; Chow, W.K. Bench-Scale Studies on Wood Pyrolysis under Different Environments. In Proceedings of the 7th Asia-Oceania Symposium on Fire Science & Technology, Hong Kong, 20–22 September 2007; International Association for Fire Safety Science, Hong Kong Polytechnic University: Hong Kong, 2007; pp. 1–8.
13. Schaffer, E.L. *Charring Rate of Selected Woods—Transverse to Grain*; FPL Research Paper 69; U.S. Department of Agriculture: Madison, WI, USA, 1967; p. 21.
14. White, R.H. Charring Rate of Different Wood Species. Ph.D. Thesis, University of Wisconsin—Madison, Madison, WI, USA, 1988.
15. Babrauskas, V. Charring Rate of Wood as a Tool for Fire Investigations. *Fire Saf. J.* **2005**, *40*, 528–554. [[CrossRef](#)]
16. Stamm, A.J. Thermal Degradation of Wood and Cellulose. *Ind. Eng. Chem.* **1956**, *48*, 413–417. [[CrossRef](#)]
17. Hill, C.A.S. Thermal Modification of Wood. In *Wood Modification: Chemical, Thermal and Other Processes*; John Wiley & Sons: Hoboken, NJ, USA, 2006; pp. 99–127.
18. Meincken, M.; Smit, N.H.; Steinmann, D. Physical Properties of Burnt Timber, with Special Focus on the Drying Performance. *Eur. J. Wood Wood Prod.* **2010**, *68*, 455–461. [[CrossRef](#)]
19. *ASTM D2395-14*; Standard Test Methods for Density and Specific Gravity (Relative Density) of Wood and Wood-Based Materials. ASTM International: West Conshohoken, PA, USA, 2015. [[CrossRef](#)]
20. Grattan, D.W. Waterlogged Wood. In *Conservation of Marine Archaeological Objects*; Pearson, C., Ed.; Butterworth & Co. (Publishers) Ltd.: London, UK, 1987; pp. 55–67.
21. Kollmann, F.F.; Côté, W.A. *Principles of Wood Science and Technology. Vol. I. Solid Wood*; Springer: Berlin/Heidelberg, Germany, 1968; ISBN 9783642879302.
22. Cook, C.; Grattan, D.W. A Method of Calculating the Concentration of PEG for Freeze-Drying Waterlogged Wood. In Proceedings of the 4th ICOM-CC Group on Wet Organic Archaeological Materials Conference, Bremenhaven, Germany, 20–24 August 1990; Hoffmann, P., Ed.; ICOM-CC: Bremenhaven, Germany, 1991; pp. 239–250.
23. Tsoumis, G. *Structure, Properties, Utilization*; Verlag Kessel: Remagen, Germany, 1991; ISBN 0-442-23985-8.
24. Bakar, B.F.A.; Hiziroglu, S.; Tahir, P.M. Properties of Some Thermally Modified Wood Species. *Mater. Des.* **2013**, *43*, 348–355. [[CrossRef](#)]
25. Kesik, H.I.; Korkut, S.; Hiziroglu, S.; Sevik, H. An Evaluation of Properties of Four Heat Treated Wood Species. *Ind. Crops Prod.* **2014**, *60*, 60–65. [[CrossRef](#)]
26. Rautkari, L.; Honkanen, J.; Hill, C.A.S.; Ridley-Ellis, D.; Hughes, M. Mechanical and Physical Properties of Thermally Modified Scots Pine Wood in High Pressure Reactor under Saturated Steam at 120, 150 and 180 °C. *Eur. J. Wood Wood Prod.* **2014**, *72*, 33–41. [[CrossRef](#)]
27. Sedlar, T.; Šefc, B.; Stojnić, S.; Jarc, A.; Perić, I.; Sinković, T. Hardness of Thermally Modified Beech Wood and Hornbeam Wood. *Šumarski List* **2019**, *143*, 425–433. [[CrossRef](#)]
28. Vörös; Németh, R. The History of Wood Hardness Tests. *IOP Conf. Ser. Earth Environ. Sci.* **2020**, *505*, 012020. [[CrossRef](#)]
29. Grekin, M.; Verkasalo, E. Variations in and Models for Brinell Hardness of Scots Pine Wood from Finland and Sweden. *Balt. For.* **2013**, *19*, 128–136.
30. Heräjärvi, H. Variation of Basic Density and Brinell Hardness within Mature Finnish *Betula Pendula* and *B. Pubescens* Stems. *Wood Fiber Sci.* **2004**, *36*, 216–227.
31. *ASTM D143*; Standard Test Methods for Small Clear Specimens of Timber. ASTM International: West Conshohoken, PA, USA, 1994.
32. *ASTM D1037*; Standard Test Methods for Evaluating Properties of Wood-Base Fiber and Particle Panel Materials. ASTM International: West Conshohoken, PA, USA, 1999.
33. Doyle, J.; Walker, J. Indentation Hardness of Wood. *Wood Fiber Sci.* **1985**, *17*, 369–376.
34. Green, D.W.; Begel, M.; Nelson, W. *Janka Hardness Using Nonstandard Specimens*; Res. Note FPL-RN-0303; Forest Products Laboratory USDA Forest Service: Madison, WI, USA, 2006; p. 13.
35. Christensen, B.B. *The Conservation of Waterlogged Wood in the National Museum of Denmark*; National Museum of Denmark: Copenhagen, Denmark, 1970.
36. Hoffmann, P. Chemical Wood Analysis as a Means of Characterizing Archaeological Wood. In Proceedings of the 2nd ICOM-CC Group on Wet Organic Archaeological Materials Conference, Ottawa, Canada, 15–18 September 1981; Grattan, D.W., McCawley, I.C., Eds.; ICOM-CC: Ottawa, Canada, 1982; pp. 73–83.
37. Florian, M.-L.E. Scope and History of Archaeological Wood. In *Archaeological Wood: Properties, Chemistry, and Preservation*; Rowell, R., Barbour, J., Eds.; American Chemical Society: Washington, DC, USA, 1990; pp. 3–32.

38. Panter, I.; Spriggs, J. Condition Assessments and Conservation Strategies for Waterlogged Wood Assemblages. In Proceedings of the 6th ICOM-CC Group on Wet Organic Archaeological Materials Conference, York, UK, 9–13 September 1996; Hoffmann, P., Daley, T., Grant, T., Spriggs, J.A., Eds.; ICOM-CC: Bremerhaven, Germany, 1997; pp. 185–200.
39. Schindelholz, E.; Blanchette, R.; Held, B.; Jurgens, J.; Cook, D.; Drews, M.; Hand, S.; Seifert, B. An Evaluation of Supercritical Drying and PEG/Freeze Drying of Waterlogged Archaeological Wood. In Proceedings of the 10th ICOM-CC Group on Wet Organic Archaeological Materials Conference, Amsterdam, The Netherlands, 11–15 September 2007; Strætkvern, K., Huisman, D.G., Eds.; ICOM CC: Amsterdam, The Netherlands, 2009.
40. Petrou, M.; Pournou, A. Testing the Efficiency of a Fruit Penetrometer to Assess the Condition of Small Waterlogged Wooden Artifacts. In Proceedings of the 13th ICOM-CC Group on Wet Organic Archaeological Materials Conference, Florence, Italy, 16–21 May 2016; Williams, E., Hocker, E., Eds.; ICOM-CC: Florence, Italy, 2018; pp. 47–53.
41. Pournou, A. Wood Deterioration by Aquatic Microorganisms. In *Biodeterioration of Wooden Cultural Heritage: Organisms and Decay Mechanisms in Aquatic and Terrestrial Ecosystems*; Springer International Publishing: Cham, Switzerland, 2020; pp. 177–260, ISBN 978-3-030-46504-9.
42. Li, T.; Cheng, D.L.; Avramidis, S.; Wålinder, M.E.P.; Zhou, D.G. Response of Hygroscopicity to Heat Treatment and Its Relation to Durability of Thermally Modified Wood. *Constr. Build. Mater.* **2017**, *144*, 671–676. [[CrossRef](#)]
43. Gao, J.; Kim, J.S.; Terziev, N.; Cuccui, I.; Daniel, G. Effect of Thermal Modification on the Durability and Decay Patterns of Hardwoods and Softwoods Exposed to Soft Rot Fungi. *Int. Biodeterior. Biodegrad.* **2018**, *127*, 35–45. [[CrossRef](#)]
44. Caple, C.; Murray, W. Characterization of a Waterlogged Charred Wood and Development of a Conservation Treatment. *Stud. Conserv.* **1994**, *39*, 28. [[CrossRef](#)]
45. Cutter, B.E.; Cumbie, B.G.; McGinnes, E.A. SEM and Shrinkage Analyses of Southern Pine Wood Following Pyrolysis. *Wood Sci. Technol.* **1980**, *14*, 115–130. [[CrossRef](#)]
46. Connor, M.A.; Daria, V.; Ward, J. Changes in Wood Structure during the Course of Carbonisation. In *Advances in Thermochemical Biomass Conversion*; Springer: Dordrecht, The Netherlands, 1993; pp. 846–858. [[CrossRef](#)]
47. Tamburini, D.; Cartwright, C.R.; Gasson, P.; Jacqueline, J.; Luizon, C.; Leme, D. Using Analytical Pyrolysis and Scanning Electron Microscopy to Evaluate Charcoal Formation of Four Wood Taxa from the Caatinga of North-East Brazil. *J. Anal. Appl. Pyrolysis J.* **2020**, *151*, 114. [[CrossRef](#)]
48. Triantafyllou, M.; Papachristodoulou, P.; Pournou, A. Wet Charred Wood: A Preliminary Study of the Material and Its Conservation Treatments. *J. Archaeol. Sci.* **2010**, *37*, 2277–2283. [[CrossRef](#)]
49. De Assis, M.R.; Brancheriau, L.; Napoli, A.; Trugilho, P.F. Factors Affecting the Mechanics of Carbonized Wood: Literature Review. *Wood Sci. Technol.* **2016**, *50*, 519–536. [[CrossRef](#)]
50. Li, G.; Gao, L.; Liu, F.; Qiu, M.; Dong, G. Quantitative Studies on Charcoalification: Physical and Chemical Changes of Charring Wood. *Fundam. Res.* **2022**. [[CrossRef](#)]
51. Boocock, D.G.B.; Kosiak, L. A Scanning Electron Microscope Study of Structural Changes during the Liquefaction of Poplar Sticks by Rapid Aqueous Thermolysis. *Can. J. Chem. Eng.* **1988**, *66*, 121–126. [[CrossRef](#)]
52. Glass, S.V.; Zelinka, S.L. Moisture Relations and Physical Properties of Wood. In *Wood Handbook: Wood as an Engineering Material*; U.S. Department of Agriculture, Forest Service, Forest Products Laboratory: Madison, WI, USA, 2010; pp. 1–19.
53. Crivellaro, A.; Schweingruber, F.H. *Atlas of Wood, Bark and Pith Anatomy of Eastern Mediterranean Trees and Shrubs*; Springer: Berlin/Heidelberg, Germany, 2013; ISBN 9783642372346.
54. Tsoumis, G. *Structure, Properties and Utilization of Wood*; Aristotelian University of Thessaloniki: Thessaloniki, Greece, 1983.
55. De Jong, J. Conservation Techniques for Old Waterlogged Wood from Shipwrecks Found in the Netherlands. In *Biodeterioration Investigation Techniques*; Walter, A.H., Ed.; Applied Sciences Publishers: London, UK, 1977; pp. 295–338.
56. McConnachie, G.; Eaton, R.; Jones, M. A Re-Evaluation of the Use of Maximum Moisture Content Data for Assessing the Condition of Waterlogged Archaeological Wood. *E-Preserv. Sci.* **2008**, *5*, 29–35.
57. Broda, M.; Hill, C.A.S. Conservation of Waterlogged Wood—Past, Present and Future Perspectives. *Forests* **2021**, *12*, 1193. [[CrossRef](#)]
58. Endo, K.; Obataya, E.; Zeniya, N.; Matsuo, M. Effects of Heating Humidity on the Physical Properties of Hydrothermally Treated Spruce Wood. *Wood Sci. Technol.* **2016**, *50*, 1161–1179. [[CrossRef](#)]
59. Thybring, E.E.; Fredriksson, M. Wood Modification as a Tool to Understand Moisture in Wood. *Forests* **2021**, *12*, 372. [[CrossRef](#)]
60. Hill, C.; Altgen, M.; Rautkari, L. Thermal Modification of Wood—A Review: Chemical Changes and Hygroscopicity. *J. Mater. Sci.* **2021**, *56*, 6581–6614. [[CrossRef](#)]
61. Obataya, E.; Higashihara, T.; Tomita, B. Hygroscopicity of Heat-Treated Wood, 3: Effect of Steaming on the Hygroscopicity of Wood. *J. Japan Wood Res. Soc.* **2002**, *48*, 348–355.
62. Zhang, J.; You, C. Water Holding Capacity and Absorption Properties of Wood Chars. *Energy Fuels* **2013**, *27*, 2643–2648. [[CrossRef](#)]
63. Kymäläinen, M.; Turunen, H.; Čermák, P.; Hautamäki, S.; Rautkari, L. Sorption-Related Characteristics of Surface Charred Spruce Wood. *Materials* **2018**, *11*, 2083. [[CrossRef](#)]
64. Kymäläinen, M.; Rautkari, L.; Hill, C.A.S. Sorption Behaviour of Torrefied Wood and Charcoal Determined by Dynamic Vapour Sorption. *J. Mater. Sci.* **2015**, *50*, 7673–7680. [[CrossRef](#)]
65. Kymäläinen, M.; Hautamäki, S.; Lillqvist, K.; Segerholm, K.; Rautkari, L. Surface Modification of Solid Wood by Charring. *J. Mater. Sci.* **2017**, *52*, 6111–6119. [[CrossRef](#)]

66. Schniewind, A.P. Physical and Mechanical Properties of Archaeological Wood. In *Archaeological Wood: Properties, Chemistry, and Preservation*; Rowell, R., Barbour, J., Eds.; American Chemical Society: Washington, DC, USA, 1990; pp. 87–109, ISBN 978-0841216235.
67. Esteban, L.G.; de Palacios, P.; García Fernández, F.; Martín, J.A.; Génova, M.; Fernández-Golfín, J.I. Sorption and Thermodynamic Properties of Buried Juvenile *Pinus sylvestris* L. Wood Aged  $1,170 \pm 40$  BP. *Wood Sci. Technol.* **2009**, *43*, 679–690. [[CrossRef](#)]
68. Broda, M.; Curling, S.F.; Spear, M.J.; Hill, C.A.S. Effect of Methyltrimethoxysilane Impregnation on the Cell Wall Porosity and Water Vapour Sorption of Archaeological Waterlogged Oak. *Wood Sci. Technol.* **2019**, *53*, 703–726. [[CrossRef](#)]
69. Han, L.; Guo, J.; Wang, K.; Grönquist, P.; Li, R.; Tian, X.; Yin, Y. Hygroscopicity of Waterlogged Archaeological Wood Deterioration State. *Polymers* **2020**, *12*, 834. [[CrossRef](#)]
70. Cao, H.; Gao, X.; Chen, J.; Xi, G.; Yin, Y.; Guo, J. Changes in Moisture Characteristics of Waterlogged Archaeological Wood Owing to Microbial Degradation. *Forests* **2023**, *14*, 9. [[CrossRef](#)]
71. Hoffmann, P. On the Stabilization of Waterlogged Oak with PEG- Molecular Size versus Degree of Degradation. In Proceedings of the 2nd ICOM Waterlogged Wood Working Group Conference, Grenoble, France, 28–31 August 1984; CETBGE, CENG ORIS: Grenoble, France, 1985; pp. 95–115.
72. Esteves, B.; Domingos, I.; Pereira, H. Improvement of Technological Quality of Eucalypt Wood by Heat Treatment in Air at 170–200 °C. *For. Prod. J.* **2007**, *57*, 47–52.
73. Ates, S.; Akyildiz, M.H.; Ozdemir, H. Effects of Heat Treatment on Calabrian Pine (*Pinus brutia* Ten.) Wood. *BioResources* **2009**, *4*, 1032–1043.
74. Akyildiz, M.; Ates, S. Effect of Heat Treatment on Equilibrium Moisture Content (EMC) of Some Wood Species in Turkey. *Agric. Biol. Sci.* **2008**, *4*, 660–665.
75. Kymäläinen, M.; Havimo, M.; Louhelainen, J. Sorption Properties of Torrefied Wood and Charcoal. *Wood Mater. Sci. Eng.* **2014**, *9*, 170–178. [[CrossRef](#)]
76. Stanzl-Tschegg, S.; Beikircher, W.; Loidl, D. Comparison of Mechanical Properties of Thermally Modified Wood at Growth Ring and Cell Wall Level by Means of Instrumented Indentation Tests. *Holzforschung* **2009**, *63*, 443–448. [[CrossRef](#)]
77. Nhacila, F.; Siteo, E.; Uetimane, E.; Manhica, A.; Egas, A.; Möttönen, V. Effects of Thermal Modification on Physical and Mechanical Properties of Mozambican *Brachystegia Spiciformis* and *Julbernardia Globiflora* Wood. *Eur. J. Wood Wood Prod.* **2020**, *78*, 871–878. [[CrossRef](#)]
78. Chen, W.H.; Lin, B.J.; Colin, B.; Pétrissans, A.; Pétrissans, M. A Study of Hygroscopic Property of Biomass Pretreated by Torrefaction. *Energy Procedia* **2019**, *158*, 32–36. [[CrossRef](#)]
79. Acharjee, T.C.; Coronella, C.J.; Vasquez, V.R. Effect of Thermal Pretreatment on Equilibrium Moisture Content of Lignocellulosic Biomass. *Bioresour. Technol.* **2011**, *102*, 4849–4854. [[CrossRef](#)]
80. Yan, W.; Acharjee, T.C.; Coronella, C.J.; Vásquez, V.R. Thermal Pretreatment of Lignocellulosic Biomass. *Environ. Prog. Sustain. Energy* **2009**, *28*, 435–440. [[CrossRef](#)]
81. Zelinka, S.L.; Altgen, M.; Emmerich, L.; Guigo, N.; Keplinger, T.; Kymäläinen, M.; Thybring, E.E.; Thygesen, L.G. Review of Wood Modification and Wood Functionalization Technologies. *Forests* **2022**, *13*, 1004. [[CrossRef](#)]
82. Kamperidou, V. The Biological Durability of Thermally-and Chemically-Modified Black Pine and Poplarwood against Basidiomycetes and Mold Action. *Forests* **2019**, *10*, 1111. [[CrossRef](#)]
83. Rautkari, L.; Hill, C.A.S.; Curling, S.; Jalaludin, Z.; Ormondroyd, G. What Is the Role of the Accessibility of Wood Hydroxyl Groups in Controlling Moisture Content? *J. Mater. Sci.* **2013**, *48*, 6352–6356. [[CrossRef](#)]
84. Borgin, K.; Tsoumis, G.; Passialis, C. Density and Shrinkage of Old Wood. *Wood Sci. Technol.* **1979**, *13*, 49–57. [[CrossRef](#)]
85. White, R.H.; Schaffer, E.L. Application of CMA Program to Wood Charring. *Fire Technol.* **1978**, *14*, 279–290. [[CrossRef](#)]
86. De Abreu Neto, R.; Guedes Ramalho, F.M.; Ribeiro Costa, L.; Gherardi Hein, P.R. Estimating Hardness and Density of Wood and Charcoal by Near-Infrared Spectroscopy. *Wood Sci. Technol.* **2021**, *55*, 215–230. [[CrossRef](#)]
87. De Abreu Neto, R.; de Assis, A.A.; Ballarin, A.W.; Hein, P.R.G. Effect of Final Temperature on Charcoal Stiffness and Its Correlation with Wood Density and Hardness. *SN Appl. Sci.* **2020**, *2*, 1020. [[CrossRef](#)]
88. Kamperidou, V.; Barboutis, I. Mechanical Strength and Surface Roughness of Thermally Modified Poplar Wood. *Pro Ligno* **2017**, *13*, 107–114.
89. Broda, M.; Mazela, B. Application of Methyltrimethoxysilane to Increase Dimensional Stability of Waterlogged Wood. *J. Cult. Herit.* **2017**, *25*, 149–156. [[CrossRef](#)]
90. Sing, Everett; Haul; Moscou; Pierotti; Rouquerol; Siemieniowska Reporting Physisorption Data for Gas/Solid Systems with Special Reference to the Determination of Surface Area and Porosity. *Pure Appl. Chem.* **1985**, *57*, 603–619. [[CrossRef](#)]
91. Thygesen, L.G.; Tang Engelund, E.; Hoffmeyer, P. Water Sorption in Wood and Modified Wood at High Values of Relative Humidity. Part I: Results for Untreated, Acetylated, and Furfurylated Norway Spruce. *Holzforschung* **2010**, *64*, 315–323. [[CrossRef](#)]
92. Plötze, M.; Niemz, P. Porosity and Pore Size Distribution of Different Wood Types as Determined by Mercury Intrusion Porosimetry. *Eur. J. Wood Wood Prod.* **2011**, *69*, 649–657. [[CrossRef](#)]
93. Zauer, M.; Hempel, S.; Pfriem, A.; Mechtcherine, V.; Wagenführ, A. Investigations of the Pore-Size Distribution of Wood in the Dry and Wet State by Means of Mercury Intrusion Porosimetry. *Wood Sci. Technol.* **2014**, *48*, 1229–1240. [[CrossRef](#)]
94. Vitas, S.; Segmehl, J.S.; Burgert, I.; Cabane, E. Porosity and Pore Size Distribution of Native and Delignified Beech Wood Determined by Mercury Intrusion Porosimetry. *Materials* **2019**, *12*, 416. [[CrossRef](#)] [[PubMed](#)]

95. Yin, J.; Song, K.; Lu, Y.; Zhao, G.; Yin, Y. Comparison of Changes in Micropores and Mesopores in the Wood Cell Walls of Sapwood and Heartwood. *Wood Sci. Technol.* **2015**, *49*, 987–1001. [[CrossRef](#)]
96. Rutherford, D.W.; Werhaw, R.L.; Cox, L.G. *Changes in Composition and Porosity Occurring During the Thermal Degradation of Wood and Wood Components*; USGS: Reston, VA, USA, 2005.
97. Grioui, N.; Halouani, K.; Zoulalian, A.; Halouani, F. Experimental Study of Thermal Effect on Olive Wood Porous Structure during Carbonization. *Maderas Cienc. Tecnol.* **2007**, *9*, 15–28. [[CrossRef](#)]
98. Thanh, N.D.; Wakiya, S.; Matsuda, K.; Ngoc, B.D.; Sugiyama, J.; Kohdzuma, Y. Diffusion of Chemicals into Archaeological Waterlogged Hardwoods Obtained from the Thang Long Imperial Citadel Site, Vietnam. *J. Wood Sci.* **2018**, *64*, 836–844. [[CrossRef](#)]
99. Pfriem, A.; Zauer, M.; Wagenführ, A. Alteration of the Pore Structure of Spruce (*Picea abies* (L.) Karst.) and Maple (*Acer pseudoplatanus* L.) Due to Thermal Treatment as Determined by Helium Pycnometry and Mercury Intrusion Porosimetry. *Holzforschung* **2009**, *63*, 94–98. [[CrossRef](#)]
100. Jang, E.S.; Kang, C.W. Changes in Gas Permeability and Pore Structure of Wood under Heat Treating Temperature Conditions. *J. Wood Sci.* **2019**, *65*, 37. [[CrossRef](#)]
101. Godinho, D.; de Oliveira Araújo, S.; Quilhó, T.; Diamantino, T.; Gominho, J. Thermally Modified Wood Exposed to Different Weathering Conditions: A Review. *Forests* **2021**, *12*, 1400. [[CrossRef](#)]
102. Ding, W.D.; Koubaa, A.; Chaala, A.; Belem, T.; Krause, C. Relationship between Wood Porosity, Wood Density and Methyl Methacrylate Impregnation Rate. *Wood Mater. Sci. Eng.* **2008**, *3*, 62–70. [[CrossRef](#)]
103. De Abreu Neto, R.; de Assis, A.A.; Ballarin, A.W.; Hein, P.R.G. Dynamic Hardness of Charcoal Varies According to the Final Temperature of Carbonization. *Energy Fuels* **2018**, *32*, 9659–9665. [[CrossRef](#)]
104. Hirata, S.; Ohta, M.; Honma, Y. Hardness Distribution on Wood Surface. *J. Wood Sci.* **2001**, *47*, 1–7. [[CrossRef](#)]
105. Peng, H.; Jiang, J.; Zhan, T.; Lu, J. Influence of Density and Equilibrium Moisture Content on the Hardness Anisotropy of Wood. *For. Prod. J.* **2016**, *66*, 443–452. [[CrossRef](#)]
106. Wimmer, R.; Lucas, B.N.; Tsui, T.Y.; Oliver, W.C. Longitudinal Hardness and Young's Modulus of Spruce Tracheid Secondary Walls Using Nanoindentation Technique. *Wood Sci. Technol.* **1997**, *31*, 131–141. [[CrossRef](#)]
107. Gregory, D.; Jensen, P.; Matthiesen, H.; Strætkvern, K. The Correlation between Bulk Density and Shock Resistance of Waterlogged Archaeological Wood Using the Pilodyn. *Stud. Conserv.* **2007**, *52*, 289–298. [[CrossRef](#)]

**Disclaimer/Publisher's Note:** The statements, opinions and data contained in all publications are solely those of the individual author(s) and contributor(s) and not of MDPI and/or the editor(s). MDPI and/or the editor(s) disclaim responsibility for any injury to people or property resulting from any ideas, methods, instructions or products referred to in the content.